The Development of a Systematic Experimental Method for Damage Identification

by

Yu Liu

Thesis submitted to the Faculty of the
Virginia Polytechnic Institute and State University
in partial fulfillment of the requirements for the degree of

MASTER OF SCIENCE

in

Mechanical Engineering

APPROVED:

Dr. Alfred L. Wicks, Chairman

Dr. Larry D. Mitchell

Dr. Robert L. West

December 1993
Blacksburg, Virginia

The Development of a Systematic Experimental Method for Damage Identification

by

Yu Liu

Committee Chairman: Dr. Alfred L. Wicks
Mechanical Engineering

(ABSTRACT)

The diagnostics of slight damage are extremely significant for providing the early warning damage information for in-service structures. This thesis presents the development of a systematic experimental method to identify structural damage by the experimental techniques. Three carbon fabric squared composite plates were used as the research objects. Two of them with light crack damage that can be classified as fiber breaking and matrix cracking were supposed to be identified through the dynamic experimental techniques. The tests of the frequency response functions (FRFs) of the investigated objects were conducted first to provide a general understanding of the dynamic properties of the material and the structures. Then the tests of the velocity fields at some specified frequencies are performed to acquire dynamic response data of the objects for the study purposes.

A systematic method to process the experimental data has been developed first in this thesis. The best regressive mathematical models for the test velocity fields are built based on the linear polynomial regression procedures and statistical analysis. To perform damage identification, the correlation coefficient (CC) and spatial correlation coefficient (SCC) techniques based on the best-fitted models and the curvature models were used. Finally, the student t' statistical tests were applied to decide whether the two compared data sets are significantly different in statistical sense.

ACKNOWLEDGMENTS

I would like to express my sincere thanks and gratitude to Dr. Alfred L. Wicks for his instruction, guidance and support during this work. His kindness, patience and constant encouragement on the research as well as on the improvement of my English are deeply appreciated. Sincere gratitude is also extended to Dr. Larry D. Mitchell and Dr. Robert L. West, Jr. for their reviewing this thesis, suggestions that make it a better technical product and serving on my committee. I wish to thanks Dr. Raymond H. Myers for his instruction and suggestions in statistics analysis.

I would also like to thank all those at Modal Lab who provide helps and support during this period. Special thanks go to Xiandi Zeng, William X. Li, Jose C. L. Dominguez, David H. Kiel, and Mike Neumann for their helps in many ways.

I would like to specially thank my husband, Junping, for his love, support and help through the most difficult times.

Finally, I have heartfelt thanks to my parents for their love, support, understanding and sacrifice that have enabled me to pursue my goals throughout my life.

TABLE OF CONTENTS

LIST OF FIGURES

LIST OF TABLES

Nomenclature

Roman Characters

E	Modulus of elasticity
f	Cyclical frequency in Hz
l, L	Length, Index
h	Thickness
$MAC(p,x)$	The value of modal assurance criterion between data sets p and x
V''	Curvature of displacement at the beam's cross-section
M	Bending moment
I	The second moment of the cross-sectional area
v_i	Displacement at point i
v''_{xx}, v''_{yy}, v''_{xy}	The *2nd* partial derivatives of the velocity field with respect to x, y and xy
k, j	Index
i	$\sqrt{-1}$, Index
$H(f)$	Frequency response function
$h(\tau)$	Unit impulse response function
s	Laplace variable
t	Time variable
$X(f)$, $Y(f)$	Fourier transforms of $x(t)$ and $y(t)$
$x(t)$, $y(t)$	Time dependent variables
$V(f)$, $A(f)$	Fourier transforms of velocity and accelerance
$G_{xx}(f)$	One-side autospectrum of signal x
$G_{yy}(f)$	One-side autospectrum of signal x
$G_{xy}(f)$	One-side cross-spectrum of between signal x and y
$X(x)$, $Y(y)$	GLP regression models in x coordinates and y coordinates
$w(x,y)$	Velocity field of plates
$w_d(x,y)$	Deterministic part of velocity field data of plates
$w_r(x,y)$	Random part of velocity field data of plates
n, m	Numbers of polynomial order in $X(x)$ and $Y(y)$
r, q	Numbers of regression variable, scanned points
p	Numbers of subset regression variable
a's, b's	Regression coefficients in $X(x)$ and $Y(y)$
x's, y's, z's	Regression variables
$E\{\ \}$	Expectation of { }
s_{ε}^2, s_{ρ}^2	Estimated sample variances of data set and SCC samples
$s_{\hat{\beta}_k}$	Standard error of $\hat{\beta}_k$
$\wedge$	Estimated values

ff	The highest computed order
P	Coordinates matrix of plates
e_i	Residual
qq, pp, rr	Error allowance values
$dSSE$	Diagonal relative difference
$dySSE$	Relative difference in polynomial Y
$dxSSE$	Relative difference in polynomial X
nd, nx, ny	Cutoff orders in diagonal, x and y polynomials
$\overline{w_l(x,y)}$	Sample mean of velocity field of plates
d_l	PRESS residual
R^2	Coefficient of multiple determination
H_0, H_1	Null hypothesis and Alternative hypothesis
$t_{T.S.}$	Value of student-t statistical test
F^*	Value of partial F statistical test
X, Y	Data sets X and Y
x_j, y_j	The j^{th} data point in vector data sets X and Y
A, B	Index of plate numbering
c, d	Index numbers of experiments
x_{kj}, y_{kj}	The k^{th} row and j^{th} column data point in matrix data sets
Q, R	The row and column numbers of subareas
$\rho^2_{AcBd,f}(k_0, j_0)$	Sample of spatial correlation coefficient square
$\overline{\rho}^2_{AcBd,f}$	Sample mean of spatial correlation coefficient squares
u, v	The displacements parallel to the plate plane and normal to each other
$\frac{\partial[\ ]}{\partial(\ )}, \frac{\partial^2[\ ]}{\partial(\ )^2}$	The 1*st* and 2*nd* partial derivatives of [ ] with respect to ( )
$w_{,x}, w_{,y}$	The 1*st* partial derivatives of the displacement field with respect to x and y
$w_{,xx}, w_{,yy}, w_{,xy}$	The 2*nd* partial derivatives of the velocity field with respect to x, y and xy
t', $t'_{T.S.}$	Symbol of t' statistical test and the value of t' statistical test

Greek Characters

ω	Angular frequency in [rad/s]
ρ	Density
$(\phi_x)_j$, $(\phi_p)_j$	The j^{th} values of mode shapes p and
$\varepsilon_x, \varepsilon_y, \varepsilon_z$	The normal strains in x, y and z directions
$\gamma_{xy}, \gamma_{yz}, \gamma_{zx}$	The shear strain in x-y plane, y-z plane and z-x plane

$\frac{\Delta\omega_k}{\omega_k}$	Ratio of the k^{th} mode frequency variation
τ	Time displacement
$\phi(f)$	Phase factor
$\gamma_{xy}^2(f)$	Coherence function between signals x and y
β's	Regression parameters
ε	Random variable
σ_ε^2	Variance
α	Significant level
ρ_{xy}^2	Correlation coefficient square
μ_{ij}	The mean of SCC between sample i and j

CHAPTER I

INTRODUCTION

1.1 Motivation

Many structures and materials are subjected to some kind of dynamic forcing functions while they are in-service. Also these structures and materials may contain flaws caused by manufacturing defects, by impact or by the in-service damage that is initiated during service. Flaws may significantly reduce the load-bearing capabilities of the structure, and may alter the mechanical characteristics (such as stiffness and strains) as well as the behavior of the structure. Eventually the flaws could lead to the failure of the structure as the flaws may grow. Therefore, it is imperative to identify whether flaws are present in structures and materials. This may be achieved by detecting the small changes in dynamic properties while they are in-service. Furthermore, if flaws exist, it would be useful to identify the location.

Owing to the significance of the problems, numerous techniques have been developed for the detection and the characterization of defects in structures and materials. Since the techniques to detect vibrations have been greatly improved with high reliability and test precision (especially in the condition monitoring systems in the aerospace and industries), considerable effort has been undertaken to find an effective way in identifying the flaws in structures by vibrational methods. However, there is no effective way to detect small damage to structures. The major difficulty in using vibrational methods is to identify small changes in dynamic properties. The complex natures of defects also increase the difficulties to detect failure by these methods. Therefore, the motivation for this research is to investigate a systematic approach of detecting slight damage in structures based on

vibrational methods and signal processing techniques. If the method is successful, it can provide early warning information to detect and diagnose faults in structures so that the defective components of structures can be exchanged or repaired prior to catastrophic failure.

1.2 Literature Review

This section reviews the general nondestructive evaluation (NDE) methods used in damage identification. It will focus on the relevant publications of dynamic property measurements of NDE methods in the detection structural damage. Also, the problems and limitations of each method are pointed out.

1.2.1 General NDE approaches used in damage identification

NDE techniques are the most common and most popular methods in structural damage detection. Nondestructive evaluations are the means by which materials and structures may be interrogated without disruption or impairment of their serviceability [1]. By using appropriate NDE techniques, internal properties or hidden flaws in structures may be revealed or inferred.

Many NDE methods may be used to detect the flaws in structures and materials, which include the methods of nondynamic property measurements and dynamic property measurements. In nondynamic property measurement methods, acoustic emission (AE), ultrasonic testing, and radiography methods are some of the most commonly used ones and hence they are briefly reviewed in this section.

Acoustic Emission (AE) or stress wave emission is the method based on the detection of elastic surface stress waves, which are caused by the rapid release of energy from localized sources within materials [2]. By the use of sensors, the sounds generated by crack initiation or growth can be detected to find the locations of the emission centers. However, the size of cracks and other defects can not be identified with the method. For the stabilized cracks without their initiation or growing, AE techniques have little ability to identify damages. In this case, stimuli should be applied to a structure and then the method can only be used to monitor behavior of materials and structures. The method can not be used in some unemissive materials to detect the damage locations.

A radiography method is based on a two-dimensional shadow display or picture of the intensity distribution of x-rays or gamma rays that have passed through an object. The object attenuates radiation according to its mass, material type and size of the presented defect. Thus, an intensity distribution of radiation that varies with the flaw distribution is created [2]. This method provides a visual image of discontinuities in solid materials and a permanent record of inspection results. Due to the use of a silver-coated film and radiation, the radiography is expensive and a health hazard. The major limitation of the method is the requirement of accessing the opposite side of a test object [2]. But, the opposite side is not always available in practical structures.

On the basis of the use of ultrasonic waves having a frequency higher than the hearing range of the normal human ears (> 20 kHz) [2], ultrasonic energy has been used in materials and structures for flaw detection and material property determinations. By using electronically controlled pulses introduced into a material from an outer surface, ultrasonic energy travels within the materials and then reaches an outer boundary. Finally, the

material condition is diagnosed from the characteristic of the received ultrasonic energy. Ultrasonic testing techniques can be classified as ultrasonic imaging techniques, which heavily depend on the computerized data analysis and display, i.e., B-scan, C-scan; acoustical holography, and ultrasonic tomography [2]. The ultrasonic technique has rapid testing capabilities and portable instrumentation is available for field testing. Equipment for automatic recording of inspections is available and results in the relative low costs of the inspections. However, the technique requires that material thickness is at least five-wave-lengths thick [3]. Otherwise, the reflections of the front-surface and the back-surface can not be separated in the thin material situations. For example, for steel inspection, when the frequency of the ultrasonic wave is at MHz, it requires the thickness at least 30 mm [3]. It is difficult to use this method for some thin and light weight composite materials. The other problem is that there may be difficulty in coupling energy to rough surfaces and complex shapes with the methods, and in the detection of small tight cracks and cracks like discontinuities due to the flaw images becoming too complex [2].

It should be noticed that the methods mentioned above are not related to the dynamic properties of structures and materials. Therefore, they are not the best ways to detect damages for in-service structures where they are present in motion and can be dominated by dynamic characteristics.

1.2.2 The NDE methods of dynamic property measurements in damage identifications

Damage in a structure alters its dynamic characteristics in some manner. For instance, the modal parameters (damping values, natural frequencies and mode shapes) may be changed

by damage in structures. Because the modal parameters are functions of a structure's physical properties (mass, damping and stiffness), these parameters can be solved from the differential equations of motion of the structure. Therefore, any change in the physical properties will theoretically cause changes in mode parameters. If damage significantly reduces the stiffness or increases the damping values of the structure, the decrease in the natural frequencies and variation of the vibration modes of the structure will also be associated with the reduction in stiffness. Hence, a wide variety of defects and anomalies may be detected by using dynamic property measurement methods.

In industry, vibrational methods are used for dynamic property evaluations that include both resonance frequency and damping techniques. These methods generally involve the measurements of either the natural frequencies of the structures and materials, or the rate of attenuation (or damping) of vibration. This review of the relevant literature surveys several attempts of damage detection in structures by observing the changes of modal parameters analytically and experimentally. The methods include a numerical comparison of the mode vectors by the Modal Assurance Criterion (MAC), the comparisons of the curvature of the mode shapes as well as the shift of the mode frequencies.

The resonance vibration testing can be used to measure some physical quantities of the materials, such as modulus of elasticity, shear modulus, Poisson's ratio, density and flaws or other inhomegeneities [2]. During the test, the test body itself is caused to vibrate as a whole in one of its resonance modes. The resonance will present when the frequency of an applied exciting force matches any mode frequency of vibration of the test object. The lowest mode frequency of the vibration body is usually used in tests due to the convenience of excitation, test setups and data acquisitions in experiments. When the

fundamental mode frequency is obtained, the appropriate modulus may be calculated from the knowledge giving of the dimensions (length l, thickness h, etc.), the density ρ, and the resonance frequency f. For example, the following equation can be used to determine the modulus of elasticity of a square bar after a mode frequency is obtained [2],

$$E = \frac{0.00245 f^2 l^4 \rho}{h^2} \tag{1-1}$$

If the physical parameters and dimensions of a structure are unchanged, by computation and comparison of changes in modulus of elasticity, the changes in the structure or in dynamic properties of the structure may be identified.

The damping testing method is another way used in detecting the origin of defects. The damping resulting from the relaxation and diffusion process is affected by the magnitude of the strain, frequency of vibration, temperature, composition, aging, and so on [2]. Any inhomogeneity may be expected to increase the damping capacity, because energy should be dissipated at the site of the flaws either as a result of stress concentration or of solid friction. By comparing the vibration scan of an identical part with an known reference standard, the information of quenching cracks, fatigue, creep, and plastic deformation may be detected [2]. Then the meaningful accept/reject data can be established by this method. The success of this flaw detection method depends in large on the skill of the measurement with which the testing procedure is conceived and applied. Damping measurements are becoming more common in research laboratories due to their high sensitivity to small concentrations and phase changes in solids, especially in metals and alloys. However, for some materials with light damping properties (for example composite materials), it is difficult to detect small changes with this method experimentally due to the sharp peaks of the mode frequencies of the materials and structures .

In modal analysis techniques, two methods are normally used. One of these is numerical comparison of mode shapes by the computations of the MAC values. The MAC value is a correlation coefficient between the two compared mode shapes. It is usually used to estimate the consistency between measured and predicted mode shapes (i.e., an experiment mode and a theory mode). It provides a measure of the least square deviation of the points from the straight line correlation [4]. The MAC values are bounded between one (1.0) and zero (0.0). For MAC values equal to 1.0, indicates exact consistency between the two comparison data sets. For MAC values equal to zero, it represents no consistent correspondence. In practice, the MAC values will lie between zero (0.0) and one (1.0) and is defined by the following equation:

$$MAC(p,x) = \left| \sum_{j=1}^{n} (\phi_x)_j \cdot (\phi_p)_j^* \right|^2 / \left(\sum_{j=1}^{n} (\phi_x)_j \cdot (\phi_x)_j^* \right) \cdot \left(\sum_{j=1}^{n} (\phi_p)_j \cdot (\phi_p)_j^* \right) \qquad (1\text{-}2)$$

where * represents a complex conjugate, and ϕ_p, ϕ_x are the values of mode shape p and mode shape x in complex numbers, respectively. In fact, this method is useful for all kinds of comparison and any pair of mode shape estimates. For example, MAC values between undamaged and damaged mode shapes may be used to indicate the inconsistent between the original and damaged structures. However, if only using MAC values, the locations of damages can not be identified due to the global information being provided by the mode shape MAC calculation.

West [5] used this method to detect structural changes in an orbiter test specimen by comparing the MAC values between the pre-flight modal data and post-flight modal data. He treated the modal vector as a whole data set first in an attempt to indicate the inconsistent by the calculation of the MAC value. In order to isolate the change to a particular region, he partitioned the total modal vector into subparts that represent a

logical grouping of structural elements. Then the MAC value for each corresponding individual subpart between the pre- and post-flight modal data was calculated. In this research, the modal models were constructed by extracting corresponding quadrature response from FRF at each resonance frequency, while the tri-axial frequency response functions were measured at near 60 different geometry locations in the structure. According to West, the MAC comparison between pre-flight and post-flight 30 missions for each partition of the complete modal vector, respectively, were most inconsistent in areas where damage was found by conventional inspection methods, such as visual inspections. In other words, MAC values are near unit (1.0) in comparing the corresponding undamaged parts and less than 0.7 in comparing the corresponding parts where there was an obvious damage occurred. The posted damage in this research includes the wear of the heat shield bearing surface and fatigue cracks in stiffeners that can also be easily inspected by visualization. That is to say, for the relative large damage or the obviously visualized damage, the method seems to indicate the locations of the damage. But for the light and small unvisual damage, it still left unknown whether and how the method works. However, it should be pointed out that mode shapes are "global" in nature (which is true for most simple structures) and does not give "local" effect information due to the structure local changes, such as damages. Even when there is a tremendous "local" change in structures, the mode shapes still change globally. This implies that the method, in general, may not work to characterize the fault location when the structures are difficulty to be separated into subparts that represent some "local" properties and characteristics. To give a clear answer of these questions, further research needs to be conduct.

A novel analytical method in damage detections based on curvature mode shapes was proposed by Pandey, Biswas and Samman [6]. According to the paper, the curvature at a point in the flexural stiffness of a beam is given by:

$$V'' = \frac{M}{EI} \tag{1-3}$$

where, $'$ is the displacement curvature at the beam's cross-section, M is the bending moment at the section, E is the modulus of elasticity, and I is the second moment of the cross-sectional area. For the structure containing damage, its flexural rigidity (e.g., EI for a beam) is reduced in the damage region. This results in the increase of the magnitude in the curvature at that section of the structure. Hence, the changes in $''$ are "local" in nature. Similarly, a curvature mode shape is the curvature shape or surface of that mode shape theoretically. The curvature mode shape is generally smooth and continuity in the structure's cross-section if the structure is normal and without any material defect and damage. Due to the "local" nature, any change in the curvature mode shapes is located in the region of damage area in the structure. Therefore, the difference in the curvature mode shapes between the unflawed and damaged structure may indicate the location of the damage.

To verify the idea, two finite element models of a damaged cantilever beam and a simply supported damaged beam, respectively, were used to obtain the displacement mode shapes of the beams. The damage is represented by a 50% reduction in the modulus of elasticity E imposed in turn to all 20 elements. By using a central difference approximation, curvature mode shapes were then calculated numerically from the displacement mode shapes. The relationship between the displacements v_{i+1}, v_i, v_{i-1} and the curvature mode shape v_i'' is given by the following central difference equation for i = 1, 2, 3, ..., 20:

$$v_i'' = \frac{v_{i+1} - 2v_i + v_{i-1}}{h^2} \tag{1-4}$$

where h is the length of the elements. The analytical results show that the maximum curvature values in each curvature mode shape occurs in the damaged region. The curvature values in curvature mode shapes tend to decrease dramatically in the elements located away from the damaged area. Meanwhile, the changes in the displacement mode shapes between unflawed and flawed beams were also presented. But the changes do not give any indication in identifying the damaged zone. In conclusion, the changes of the v_i''s in the curvature mode shapes provide an indicator of the local damage effect. Therefore, the curvature mode shapes may be used to detect the damages in structures. To investigate how the method has effects on the different damage levels, the further study was conducted by changing the modulus of elasticity in finite element models. A changing of the modulus of elasticity from 0.1 to 0.9 of the full value in the specified element represents the intensity variations of damage at a particular location. The results from the finite element models exhibit that for the 10% - 20% changes in the modulus of elasticity, this method almost has no capability to indicate the damage effects. For more than 30% changes in the modulus of elasticity of the element, the results start to display that the large curvature appears at the damage zone. As the damage intensity increases, the changes in curvature mode shapes also increase dependently. On the basis of the fact that the curvature is proportional to the bending strain in the beams, i.e., $\varepsilon_x \propto v_{xx}'', \varepsilon_y \propto v_{yy}'', \gamma_{xy} \propto v_{xy}''$, the strain in the damaged area will be altered when damage occurs of the structure. Thus, detecting the changes of the curvature in the structure is theoretically equivalent to identifying the change in strains of the structure, and hence to identify the location of the damage if the changes of the strains are directly due to the damage. However, it should be pointed out that there is a big difference between the investigation of the theoretical models and the experimental models. The theoretical

models do not contain noise while the experimental models are contaminated by some sort of noise. Consequently, one concern of using this method in practice is whether the method will work for the small damage levels, for the test data contaminated by noise, or for the structures that are more than one dimension. The answer still needs some further investigations.

Rizzi, Clevenson and Daniels [7] performed acoustic fatigue detection from changes in curvature mode shapes in carbon/carbon laminated panels. The acoustic fatigue test was performed at the Thermal Acoustic Fatigue Apparatus (TAFA) facility at NASA Langley Research Center. The test object was subjected to the high intensity and band-limited random noise (130-160 dB and 50-200 Hz). The panel was clamped and excited near the resonance frequency of the (3,3) mode with three PZT piezoceramic actuators mounted in the center of each bay. A scanning laser system was used to determine RMS velocity distribution, and accelerometers were used to determine the resonance frequencies. From data acquired by scanning laser vibrometer system, a moving average was used to smooth the data before calculating the second derivatives with respect to the spatial coordinates by using a finite difference approach. During the acoustic fatigue test, several scanning data sets were taken at the initial (undamaged status) and with gross surface delamination (damaged status) at several different stages, respectively. Supposing the curvatures of the panels are directly proportional to their surface strains [6], the presence of large magnitude derivatives could be an indicator of where damage is likely to occur. Then, subtracting the derivatives from the initial (undamaged) derivatives gives an indicator of where the largest difference in derivatives occurred. Finally, the test results obtained by curvature mode shape method in which the data were collected by a scanning vibrometer were compared consistently with that of the visual inspection and the thermograph

measurements. The method provides a good indicator of the locations of the surface delaminations and an effective way to investigate the progress of the surface or near surface's relative large damage by comparing different damage stages. However, it should be noted that an obvious delimitation and surface fiber breakage could be viewed by the visual inspection from the photographs taken at the end of the test. This means that the method works well for the large damage intensity in this case. And questions still rise whether the method works effectively as well for small damage and what is the quantitative value to indicate damage intensity. That is to say, it is still a question that at least how much the numerical differences between undamaged and damaged structures should occur so that the damaged object can be identified.

Wolff and Richardson [8] used a node line method to detect the physical changes in a structure. Node lines are the locus of node points of the mode shapes, i.e., the locus of zero points of the mode shapes. If the closed-form expressions of the mode shapes of a structure can be represented by sine and cosine functions, or hyperbolic sine and cosine functions, then the node lines will have the same expressions as that of the maximum slope or rate of the change of the mode shapes (i.e., the zero points of the second derivatives of the mode shapes with respect to the coordinates). For instance [8], the k^{th} analytical mode shape solution of a pinned-pinned beam is:

$$Mode\ shape_k(x) = \sin(k\pi x / L) \qquad (1\text{-}5)$$

where: L is the length of the beam, and x is the distance along the beam. By definition [8], a mode shape is the spatial description of the amplitude of each resonance. Thus, the node points for the k^{th} mode are at values of x where: $\sin(k\pi x/L) = 0$, or at $x = nL/k$, for k, n = 1, 2, 3 ... respectively. Then the slope of a mode shape (i.e., the first derivative with respect to x) is:

$$Slope\ of\ Mode\ shape_k(x) = k\pi / L\cos(k\pi x / L) \quad (1\text{-}6)$$

The maximum slope of the mode shape will appear at zero points of the second derivative with respect to x. This represents the location of the most sensitivity of the mode shape to the changes in the structure. The maximum slope of the mode shape can be expressed as: $sin(k\pi x/L) = 0$ or $x = nL/k$, for $k = 1, 2, 3$ ..... It is easy to notice that the expression of the maximum slope of the mode shape is the same as that of the node points for the k^{th} mode. Therefore, a node line represents the maximum slope locus of the mode shape. Since a mode shape is not unique in value but only unique in "shape", any change in the relative amplitudes of a mode shape will have its greatest effect at the node points. In other words, any change in a mode shape should cause the movements of the locations of the node lines. Hence, by the investigation on the node lines of the mode shapes in a structure, the greatest change in mode shapes can be found while the structure has a physical change. To demonstrate this effect, an experiment was conducted by using an aluminum flat plate with a rib stiffener bolted along its centerline. By removing the end bolt from six equally spaced bolts in the rib stiffener, the plots of the node lines of the mode shapes show obvious differences between the before and the after end bolt removal. It should be noted here that removing the end bolt in the stiffener will greatly alter the stiffness of the structure and result in a large change in the structure. However, it is not clearly stated in the paper how the changes in node lines are connected with the local effects on changes in the dynamic properties of the structure. It is also unclear what the relationship is between the location of the greatest change in mode shapes and the local effect of the structure changes. Hence, it is still a question how to identify the location of the change in a structure by the method.

The investigation of the changes of the mode frequencies from frequency response functions (FRFs) is another way to reveal the inconsistency between the original and damaged structure [9, 10, 11]. The principles behind this approach are that damages may alter the dynamic characteristics and the behavior of a structure (such as stiffness and the modal frequencies). Since an FRF gives global information of a structure's dynamic characteristics, it is difficult to identify the location of damages by this method.

Tenek Henneke II and Gunzburger [9] proposed an analytical study of composite plate's dynamic behavior wherein damages appear in a form of delaminations. A finite element method based on the three-dimensional theory of linear elasticity was used in the study of the impact on the natural frequencies of the delaminated plates. For cantilever laminated plates ($L \times W$ = 8 in × 4 in) with varied sizes of flaws, the effects on the natural frequencies are monitored. The three different delaminated configurations of the material are used in the study. The computational results not only are similar to the each other but also indicate that the first few natural frequencies of the composite plates are little affected by delaminations even for a large size flaw ($L \times W$ = 4 in × 2.37 in). The effects due to delaminations became noticeable only under higher frequencies (over 250 Hz), i.e., the vibrational mode surfaces of flawed and unflawed plates tend to vibrate out of phase with each other. According to the authors, the method was also successfully compared with experimental observations in the cases mentioned above.

A similar experimental method was performed by West [10]. A random modal test was applied to the failure detection of an orbiter body flap in the study. The orbiter body flap was completely covered with Orbiter Thermal Protective System tiles. By comparison and analysis of FRF's data sets obtained prior to and after environmental tests, the shifts in first

three mode frequencies can be easily observed from FRF's plots. After finishing the failure tests, the structure was disassembled and the inspection on each component was conducted by the manufacturer. The results of the inspection indicates that some kind of damage had occurred, such as galling of spherical bearings, hinge pin damage and shear clip damage. This damage had not been detected by conventional visual (because the damage located inside the structure), x-ray, and ultrasonic inspections before disassembling inspection by the manufacturer. According to the changes in mode frequencies, it may be easy to indicate the presence of internal damages that have altered the dynamic properties in structures, but how to identify the location of the damage is still unsolved. To figure out the position of the damage from the known changes in the mode frequencies is a completely different question. This is because the same shift on a mode frequency may be caused by the identical damages but located at the different positions. In addition, the global mode frequency information does not directly offer the local information concerned the locations of damages. It is obvious that the same method may results in the different answers while the method is used in the different type of damage or material or structures.

AL-Ansary and Azayem [11] developed a theoretical model to predict the fatigue crack damage and its location in a simple shaft-bearing system. On the basis of investigating the changes in mode frequencies, two methods were used to evaluate the modal frequency variations. One is to obtain a direct solution by solving the fourth-order characteristic equation of the shaft-bearing system using the midpoint iterative method. The other is studied by a finite element analysis (FEA). The crack that causes a discontinuity in the slope curve of the shaft was modeled as a torsion spring element. By introducing the boundary conditions or the geometrical factor of the damage, the solutions of mode

frequencies in both methods are directly connected to the damage information. The damage, i.e., the crack, was introduced by a sharp notch in the form of a sector on one side of the shaft. The strength of damage was controlled by changing the ratios of the crack's depth to the shaft's diameter as 0.1, 0.2 and 0.3, respectively. The modal frequencies and mode shapes were determined from both methods for unflawed and damaged shaft-bearing system individually. Finally, the ratios of mode frequency variations for the first three modes (i.e., $\frac{\Delta\omega_k}{\omega_k}$, k = 1, 2, 3, which are relatively small and lie in the 10^{-2} to 10^{-4} levels) were calculated. According to the values of $\frac{\Delta\omega_k}{\omega_k}$, the crack size, location and possible geometry were predicted. The results from both methods are consistent with each other, and can be used in some kind damage detection with specified damaged strength. However, the analysis was studied by using the axial mode of vibration, the validation of the method is limited for one-dimensional structures only. Since each crack contains the two unknowns (size and position) in the close-form models, if the shaft with more than one crack, at least two additional higher modes are required to identify the cracks. Thus, the damage detection becomes more comprehensive and difficult. For this reason, this method is not suitable to the case of large number of cracks. It should be pointed out that the major drawback of the method is to determine the small values of the ratios, $\frac{\Delta\omega_k}{\omega_k}$, experimentally due to the limitations of the frequency resolutions of instruments.

1.2.3 Damages in composite materials

The use of composite material for engineering application, such as for automobiles, transportation systems and aircraft structures, has been expanding rapidly in recent years. However, the failures of the composite products may happen for a variety of reasons. For

example, a poor design or faulty manufacturing processes and in-service damages resulting from mechanical contact (impact, mishandling and overload) or environmental effects (overheat, lighting strike, use of undesirable solvents etc.). The damage behaviors are changed as different kinds of damages introduced, i.e., the different types of damage can affect the strength or stiffness in structures differently. Thus the methods to detect damage are dependent on the type of damages. Therefore, it is necessary to understand the damage type before the damage identification. Typical structural defects/damages include cut, scratches, delaminations, disbonds, surface damage, edge damage, hole elongation and so on [12]. In fiber composite materials, the variety of damage can be classified by fiber breaking, delamination between plies and fiber fracture, and matrix cracking (transverse cracking) [1]. Figure 1.1 gives the configurations of these damage types.

1.3 Objective of research

So far, all the reviewed vibrational methods mentioned above are significant in theoretical analysis or work only for relative strong intensity damages in real structures. Techniques have been developed to detect damage when big changes in structure dynamic properties (stiffness, damping and mode shapes) have been occurred. But, the results of the research that is based on theoretical models may differ from those that is based on the experimental techniques. One possible difference may be due to that the boundary conditions can hardly be completely matched with these in experiments or in practice. This could result in the different outcome between theoretical approaches and experimental approaches to a certain extent. It may cause another possible difference that the acquired data is contaminated by noise in experiments while theoretical models can hardly take account for noise. For these reasons, there is a need to investigate a practical way to detect flaws in

structures based on experimental techniques. By applying current vibrational methods to the experiments, it is significant to conduct the further research in these areas and to develop a systematic method to identify light intensity damage or small changes of dynamic characteristics in structures. This plays an important role in diagnostics of some early damage in structures while other detection methods fail to do so and the access to internal structures is limited. Therefore the purposes of this research are two-folds. One is to develop a systematic method to identify which experimental data set is associated with the undamaged and damaged structure. The other is to develop a systematic method for identifying the location of the damage for the damaged structure. If the method is successful, it can be applied to general experiments in detection of damage by testing dynamic parameters in structures.

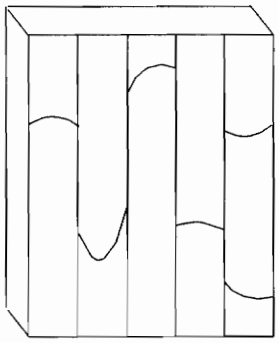

(a). Fiber breaking

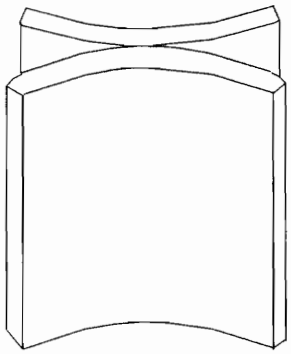

(b). Delamination

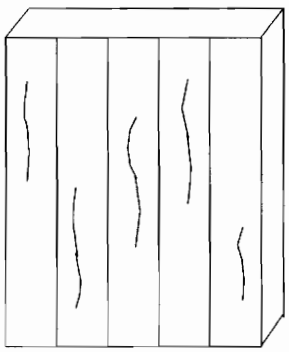

(c). Transverse cracking

Figure 1.1 - Failure types in fiber reinforced composites

CHAPTER II

EXPERIMENTAL APPROACH

2.1 Introduction

This chapter focuses on the description of two experiments. First, the three square composite plates are defined as the objects. The tests of frequency response functions (FRFs) are then conducted to obtain the basic information of the dynamic properties of the material. Meanwhile, the concepts of FRFs and coherence functions are introduced, and also the FRF test setups as well as the test conditions of FRFs are discussed in details. Finally, the dynamic tests of the plates by a VPI laser scanning vibrometer are performed to acquire the velocity fields of the plates. The objective of this experiment is to obtain the velocity data of the plates for further analyses and the identification of the damage in plates.

2.1.1 Definitions of test objects

Three flat square composite plates with the same dimensions (12 in × 12 in × 0.005 in (in thickness)) are used in this research. The plates are all made of identical carbon fiber composite material with the same manufacture process. Therefore, we assume that all the original undamaged plates have the same properties. Because this kind of carbon fiber reinforced epoxy composite has high specific strength and stiffness but light in weight, there is increasing use of the product in structural applications. To identify the flaws in the plates, cracks are introduced as an investigated damage. The cracks in two of the three plates are the same size and same strength level but locate in different positions in the plates. The damage was made by cutting one layer in depth and four inches long at the

plate surfaces. Figure 2.1 shows a sketch of the plates, where Plate No. 1 is a plate without damage, Plate No. 2 is cut at the center, and Plate No. 3 is cut at the edge. The damage in both plates can be classified as fiber breaking and matrix cracking damage type.

2.2 Frequency response functions

2.2.1 Concepts of FRFs and coherence functions

The FRF, $H(f)$, describes dynamic properties of a system in frequency domain. It can be defined as the Fourier transform of a unit impulse response function $h(\tau)$ as follows [13]:

$$H(f) = \int_0^\infty h(\tau) e^{-j2\pi f\tau} d\tau \tag{2-1}$$

The FRF can also be obtained from the transfer function $H(s)$ that describes the dynamic properties of a system in Laplace domain. The "s" in $H(s)$ is a Laplace variable expressed by the complex relation, $(\sigma + j\omega)$. By zeroing the real part of "s", i.e., let $s = j\omega$, the FRF is obtained in the form of $H(j\omega)$. These functions, i.e., $H(f)$, $h(\tau)$ and $H(s)$, can be used to express the same physical system in different aspects. However, the FRF provides some significant and important information about the physical system, such as the distribution of modal frequencies and damping information of a structure. For some complicated structures, it is difficult to procure FRFs theoretically. In this case, the experimental FRF test is an alternative way to obtain an estimate of the FRF. Another form of the FRF can be expressed as the ratio of the Fourier transform of the output $y(t)$, i.e., $Y(f)$, to that of the input $x(t)$, i.e., $X(f)$, of the system, i.e., $H(f) = \dfrac{Y(f)}{X(f)} = |H(f)|e^{-j\phi(f)}$, where the absolute value $|H(f)|$ is the system gain factor and equals the ratio of the output amplitude to the input amplitude; and $\phi(f)$ is the phase factor and equals the phase shift

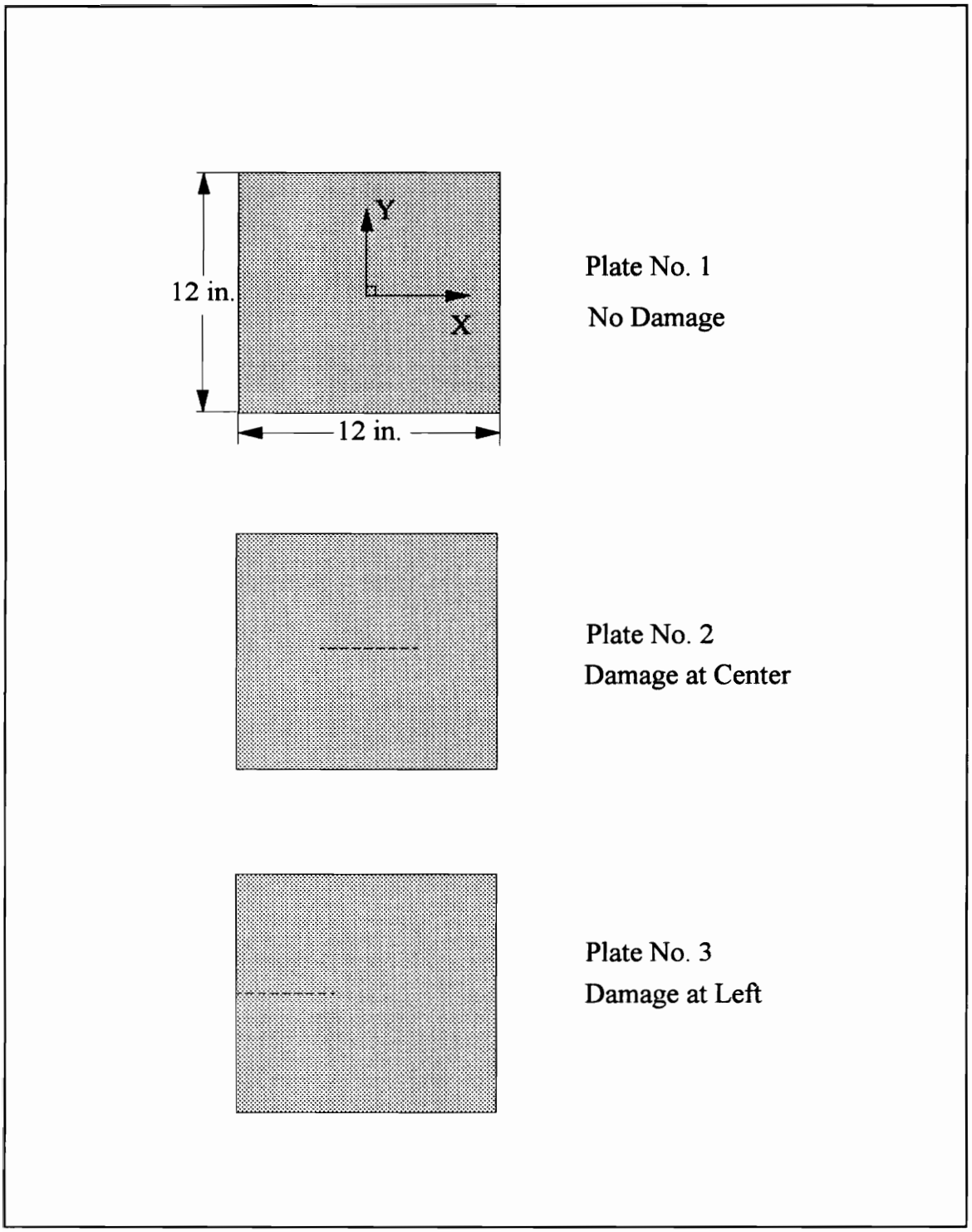

Figure 2.1 - Plate configurations used in the investigation

between the output and input. Therefore the FRF can be experimentally estimated by measuring the output and the input of the system.

Through experiments, the FRF can be measured in the form of compliance, mobility, or accelerance, each of these is defined as follow:

$$\text{Compliance} = \frac{Y(f)}{X(f)} = \frac{\text{Displacement}}{\text{Force}} \quad ;$$

$$\text{Mobility} = \frac{V(f)}{X(f)} = \frac{\text{Velocity}}{\text{Force}} \quad ; \tag{2-2}$$

$$\text{Accelerance} = \frac{A(f)}{X(f)} = \frac{\text{Acceleration}}{\text{Force}} \quad ;$$

Any one of the above expressions can be used to obtain the FRF of the system. For a constant-parameter linear system, the FRF is the function of the frequency only. In this case, the FRF does not vary with either the time or the system excitation force, otherwise, $H(f)$ will be a nonlinear function.

A coherence function γ_{xy}^2 is the measure of the correlation between the input and output in the frequency domain. For all frequencies, the coherence function satisfies: $0 \le \gamma_{xy}^2 \le .0$ and is defined as follows [13]:

$$\gamma_{xy}^2(f) = \frac{|G_{xy}(f)|^2}{G_{xx}(f)G_{yy}(f)} = \frac{G_{xy}(f)G_{xy}(f)^*}{G_{xx}(f)G_{yy}(f)} \tag{2-3}$$

where G's are the one-sided spectra, G_{xx} and G_{yy} are the input and the output autospectra, respectively. The autospectra can be obtained from the following equations:

$$G_{xx}(f) = X^*(f)X(f)$$

and

$$G_{yy}(f) = Y^*(f)Y(f) \tag{2-4}$$

Also, G_{xy} is the cross spectrum and can be obtained as follows:

$$G_{xy}(f) = X^*(f)Y(f) \tag{2-5}$$

where X and Y are the Fourier transforms of the input and the output signals respectively, and * indicates the complex conjugate of the function.

For the ideal case of a constant-parameter linear system with the single input and the single out (SISO) without noise, the γ_{xy}^2 will be unity. If the system output $y(t)$ is completely uncorrelated to the input $x(t)$, the γ_{xy}^2 will equal zero. Since the test system may contain by the input or the output noise, i.e., the uncorrelated content, we can only get the estimates of γ_{xy}^2s and FRFs from experiments. In general, the γ_{xy}^2 lies between unit and zero, it indicates one or more of the following physical situations may exist [13]. (1) extraneous noise is present in the measurements, (2) the system relating $x(t)$ and $y(t)$ is not linear, and (3) $y(t)$ is an output due to an input $x(t)$ as well as to other uncorrelated inputs, such as leakage and resolution bias error.

For a linear system, the [1 - γ_{xy}^2] is a measurement of the mean square value of $y(t)$ not accounted for by $x(t)$ at the frequency f. This can be used to indicate that the content measured in output $y(t)$ is not due to the system input $x(t)$. Therefore, the coherence function could be taken as an indicator of the test quality during the FRF tests.

It should be mentioned that there is a need to take several successive measurements on the FRF tests and to accumulate a running average of the corresponding FRF estimates as well as the coherence functions in the experiments. The purpose of averaging is to reduce the variance of the test random noise on each spectral line in FRFs and in the estimates of the coherence functions.

2.2.2 FRF test system setup

The entire equipment used to obtain the FRFs of the plates is shown in a flow chart in Fig. 2.2. A Zonic 6080/6081Z FFT Analyzer is used to generate an excitation signal, to collect and to analyze the experimental data, and finally, to provide the FRF plots of the tests for the plates. For the composite plates with light damping, a continuous burst random signal with 0-500 Hz frequency range generated by Zonic 6081Z is used as an input signal to excite the plates. The corresponding FRFs with 0-500 Hz frequency range are then obtained. The input signal is amplified first by Harman/Kardon hk770 power amplifier that provides enough signal power to drive an electromagnetic Ling shaker. The shaker is an exciter to provide an excitation force that stimulates the plates into vibration. The actual input force goes through a stinger and into the plates. The stinger is designed to effectively transmit axial loads without bending moments from the shaker to the force transducer. A PCB 208 A03 force transducer mounted on the plates is used to measure the actual force transferred into the plates. A PCB 303A02 accelerometer is used to measure the accelerations of the plates under the excitation force. The outputs of both the force transducer and the accelerometer go into the PCB ICP (Integrated Circuit Power) amplifier and finally into the inputs of the Zonic FFT analyzer to perform the FFT analysis. During the test, all signals, which include the burst random signal from Zonic FFT analyzer, the amplified force signal and the amplified accelerometer signal, were monitored on a Tektronix 2214 oscilloscope. During the tests, the plates were hung from a pipe at the upper corners using nylon monofilament. The pipe with 28 inch in length, 0.9 inch in diameter and 0.006 inch in thickness is suspended from the ceiling using bungee cord (an elastic support), simulating free-free boundary conditions. The details of the test setup is shown in Fig. 2.3 and Fig. 2.4. The test setup was carefully performed so that the

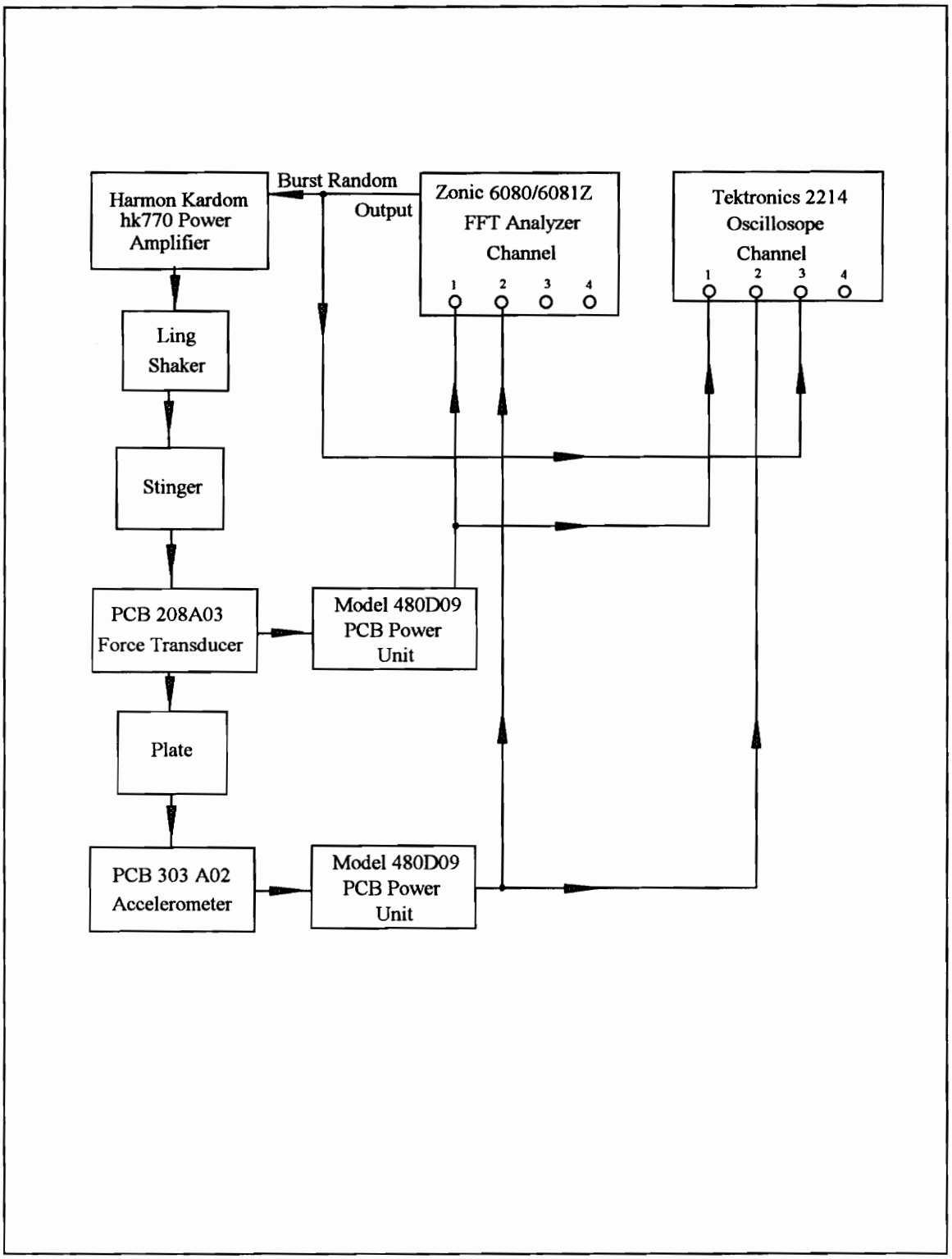

Figure 2.2 - A flow chart of test equipment and system

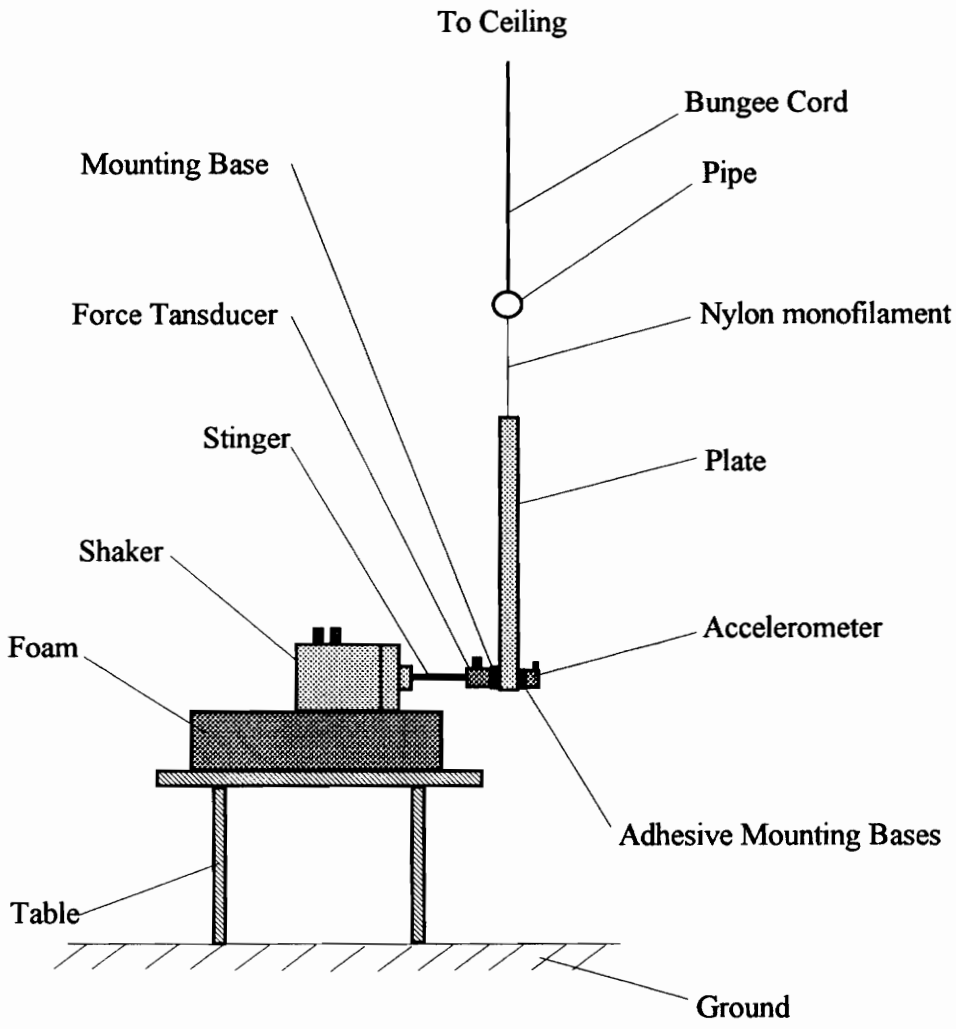

Figure 2.3 - Side view of the FRF test setup

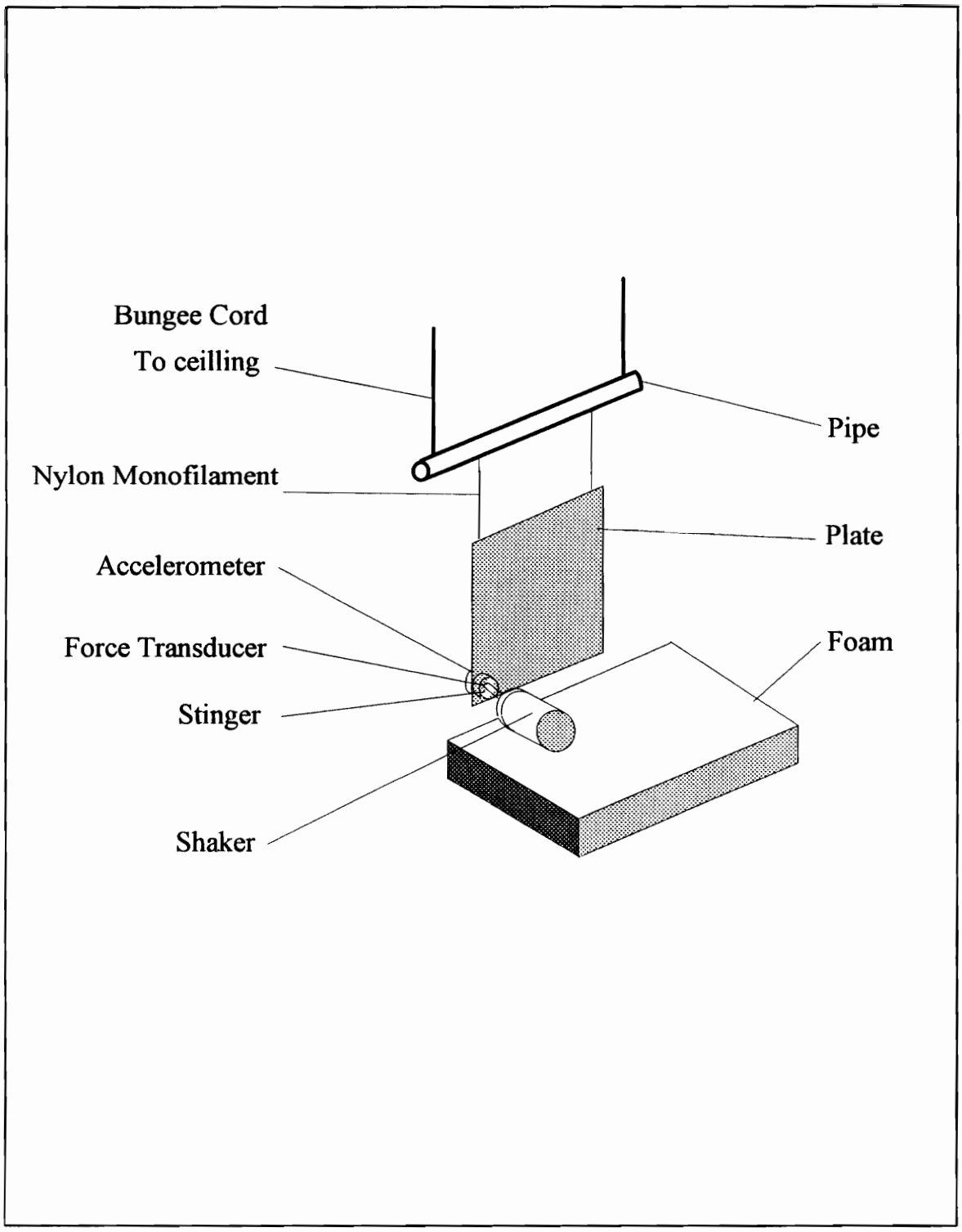

Figure 2.4 - A 3-D view of the plate setup

excitation force is perpendicular to the plate plane. A mounting base is glued at the left bottom of the plates in order to fix the force transducer that is screwed on the base. The accelerometer, which measures the lateral acceleration of the plates, is screwed on a mounting base and waxed onto the plates at the forcing location. Therefore, the configuration of the force transducer and the accelerometer constructs a single-driving point FFT test setup.

2.2.3 Data acquisition conditions

FRF tests were conducted on each plate on several different days under the three different force levels. The varying range of the force magnitudes was decided according to the standard deviations of acquiring velocity fields at natural frequencies without appearing distortional errors. The corresponding output amplitudes of the continuous burst random signal are equal to 0.2, 0.25 and 0.3 volts zero-peak respectively. The burst random signal with 0-1000 Hz frequency range was run first to obtain initial estimates of the FRFs for the plates. Since higher modes are more complicated and more sensitive to small changes in the test setup (i.e., boundary conditions), the signal with 0-500 Hz lower frequency range was used in the FRF tests. The corresponding FRFs plots for all the plates are given latter with the frequency resolutions as 1.25 Hz. An exponential window was used for the transient excitation signal to reduce leakage.

In order to determine a proper burst length, the signals were monitored on an oscilloscope before the FRFs tests. Then the burst lasted time T_1 and the next burst waiting time T_2 were decided. Figure 2.5 gives an illustration of the burst random signal. The T_1 was decided in such a way that the burst signal has enough energy to excite the plates into vibration. The

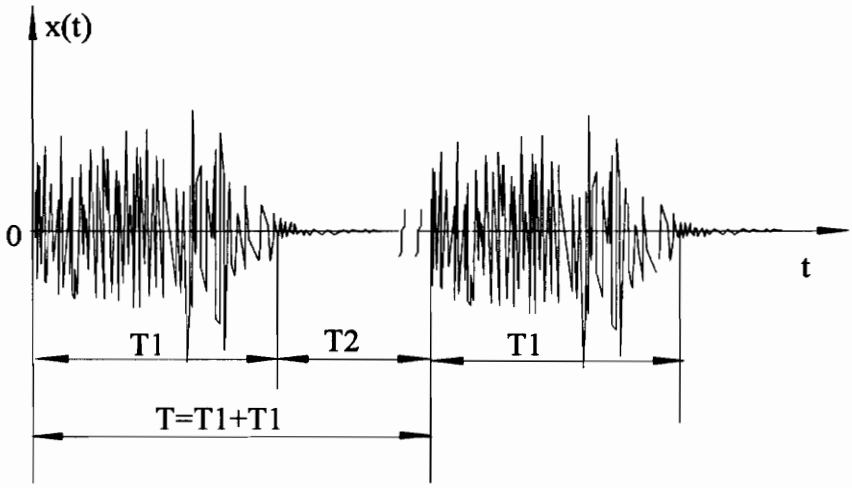

t: Time in second

x(t): Force magnitude

T2: Delay time (sec)

T1: Burst lasted time (sec)

T=T1+T2: The period of the excitation signal (sec)

Figure 2.5 - An illustration of burst random signal

T_2 was decided by considering the damping property of the plates, i.e., the next burst signal should be generated after the response on the last burst signal completely died out. Thus, the last burst has no effect on the next one. Therefore, T_1/T_2 = 0.5 (sec.) / 5.0 (sec.) was determined to satisfy the requirements mentioned above. During the data acquisitions, each FRF was taken 30 averaged times to reduce random errors in the tests. Each peak frequency in FRFs was documented by moving the cursor at corresponding frequency point. Meanwhile, force auto-spectra and coherence functions were also analyzed and plotted, so the changes of the force levels can be observed and the qualities of the tests can be checked.

It should be noticed that all the FRFs tests were conducted at the room temperatures that vary from 75 to 79 ^{o}F. The effects due to the small change in temperature are ignored in this investigation. An attempt to check the stability of the test system's performance was conducted by repeating the same FRF tests. By comparing the plots with those acquired early, it can be concluded that the test system is stable during the test period.

2.2.4 Results of the FRF tests

The FRF plots of magnitudes and phases at different force levels (0.2V, 0.25V, and 0.3V) in the 0-500 Hz frequency range are given in Fig. 2.6-2.8. Each figure gives the FRF plots of the comparisons to the same plate at the three different force levels. Due to single-driven-point FRFs, each mode shows a resonance point and an anti-resonance point too, phases of FRFs jump at each resonance point and drop at each anti-resonance point. Hence, the phase plots appear in alternatively jumping and backing down. The corresponding coherence functions were also been plotting during the tests to check the

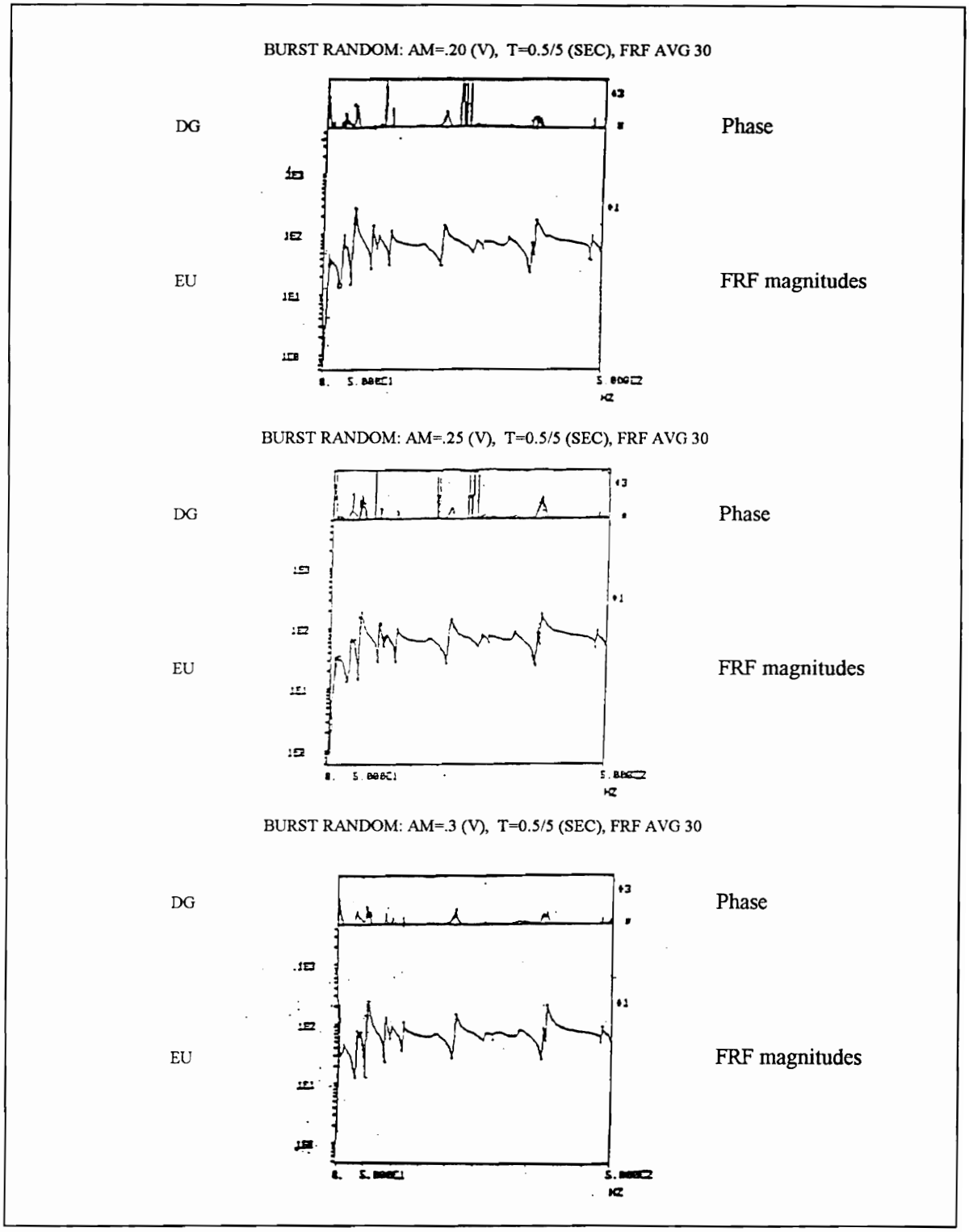

Figure 2.6 - The comparisons of plate No.1's FRF plots at three different force levels

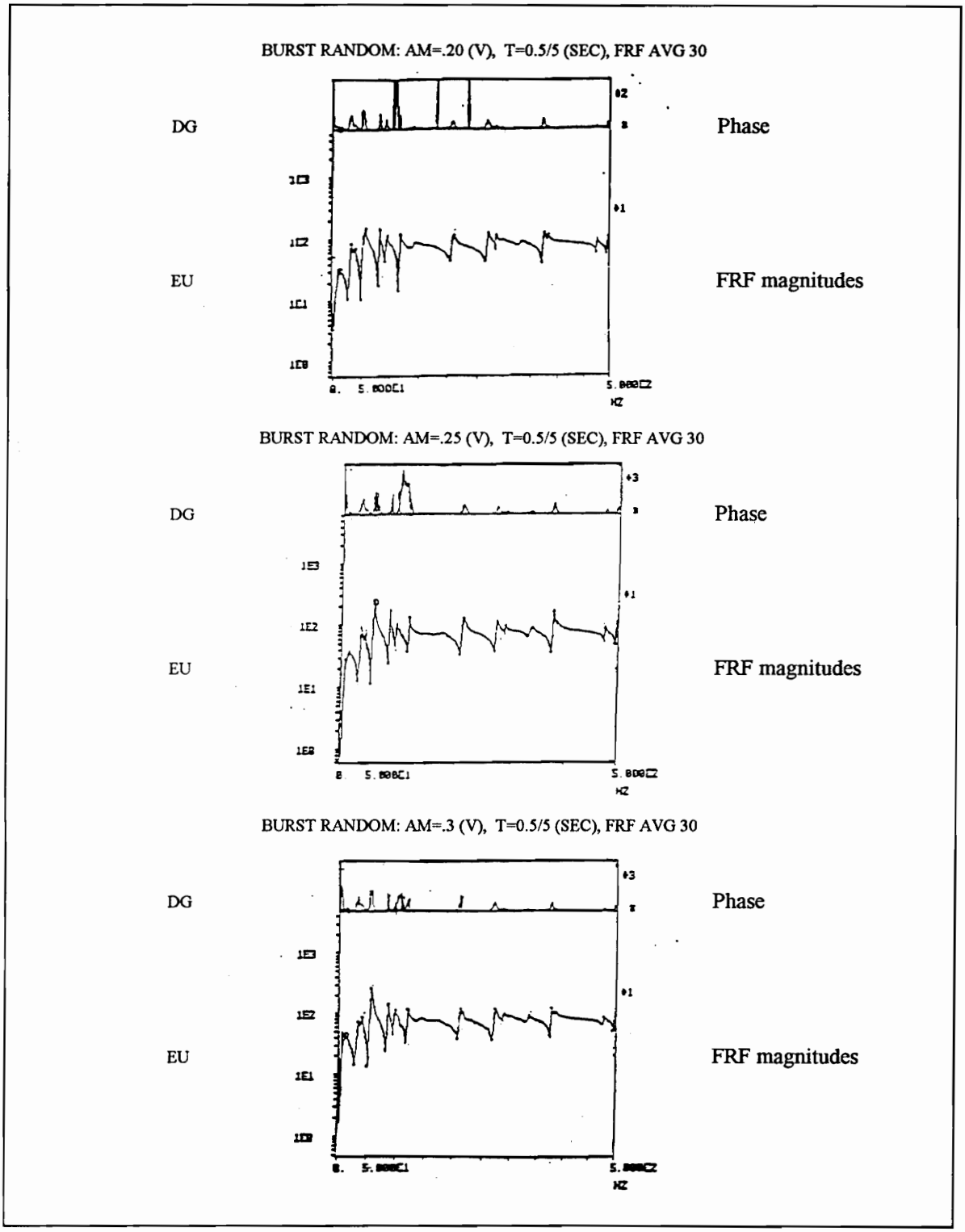

Figure 2.7 - The comparisons of plate No.2's FRF plots at three different force levels

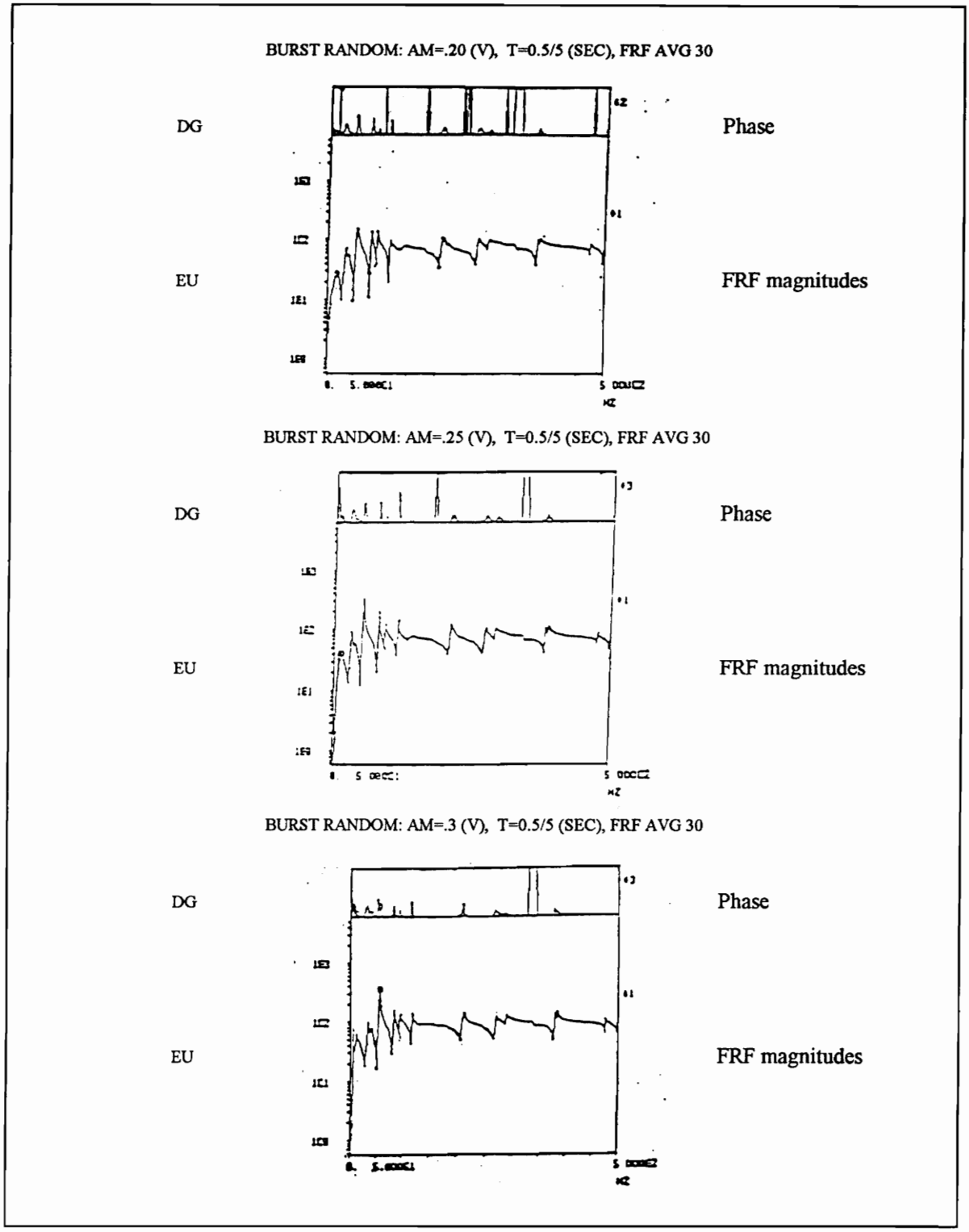

Figure 2.8 - The comparisons of plate No.3's FRF plots at three different force levels

quality of the FRFs. The values of the coherence functions were high enough (close to one) except at the peak frequencies of the FRFs (dropping dramatically). Therefore, the quality of the FRFs are reliable. By comparing the same plate under the different force levels, it can be observed that the shapes of FRFs are similar to each other and the magnitudes of the FRFs stay relatively unchanged. This means that for the force levels applied, the FRFs display a linear relationship. By comparing the different plates under the same force level, it can be observed that some peak frequencies in the FRFs show different values within a specific frequency range. Most of these frequency shifts tends to lower values. For example, a peak frequency of plate No. 1 is at 216 Hz while that of plate No. 2 and No. 3 is near 208 Hz. This is reasonable that the cracks may reduce the stiffness of the plates, hence reduce the natural frequency.

2.3 Velocity field test setup and parameter controls

It is very important that all the tests are conducted under the same test conditions in order to keep the test data consistent. Therefore, there is a requirement to reproduce the same test conditions when the test system is re-setup for repeated tests on the different days. The most important test conditions to be controlled include:

a.) The excitation signal and actual input force:

An attempt was made to keep the corresponding force that is actually input to the plates consistent by measuring the magnitudes of the input force through the digital oscilloscope in a VI on the Macintosh computer.

b.) The plate setup (free-free boundary conditions):

In order to control the boundary conditions of the hanging plates, the height to hang the plates was kept consistently. Moreover, a level was used to check that the plates were hung up in the vertical plane and on a level. The same shaker, foam and stinger were used over all the repeated tests.

c.) The temperature varied within some range:

The temperature is something that can not be strictly controlled but can be roughly adjusted within the specific range. For example, temperature varied from 75° to 79° Fahrenheit by adjusting an air-conditioner. Since the effects due to the small changes in temperature are very small, we can assume that the characteristics of the plates and equipment are unchanged during the test periods.

d.) The distance between the plates and the laser head and the height of the laser head:

The distance and the height were fixed so that the same laser scanning angle and the same laser scanning intensity was maintained over all the tests.

The test equipment system for the velocity fields is similar to that in the FRF tests but a VPI scanning laser vibrometer is used to measure the velocity responses of the plates instead of the accelerometer in FRF tests. The VPI scanning laser vibrometer system includes a VPI laser head and a Macintosh computer. It provides an automatic measurement of the vibrating surface velocities. High sensitivity and a high spatial resolution without the loading effects of accelerometers can be achieved. The Macintosh computer was used to control the data acquisitions instead of the Zonic 6080/6081 FFT analyzer as in FRF tests. The equipment system is illustrated in Fig. 2.9 with a flow diagram of the data acquisition system. A side view of the velocity test setup is given in

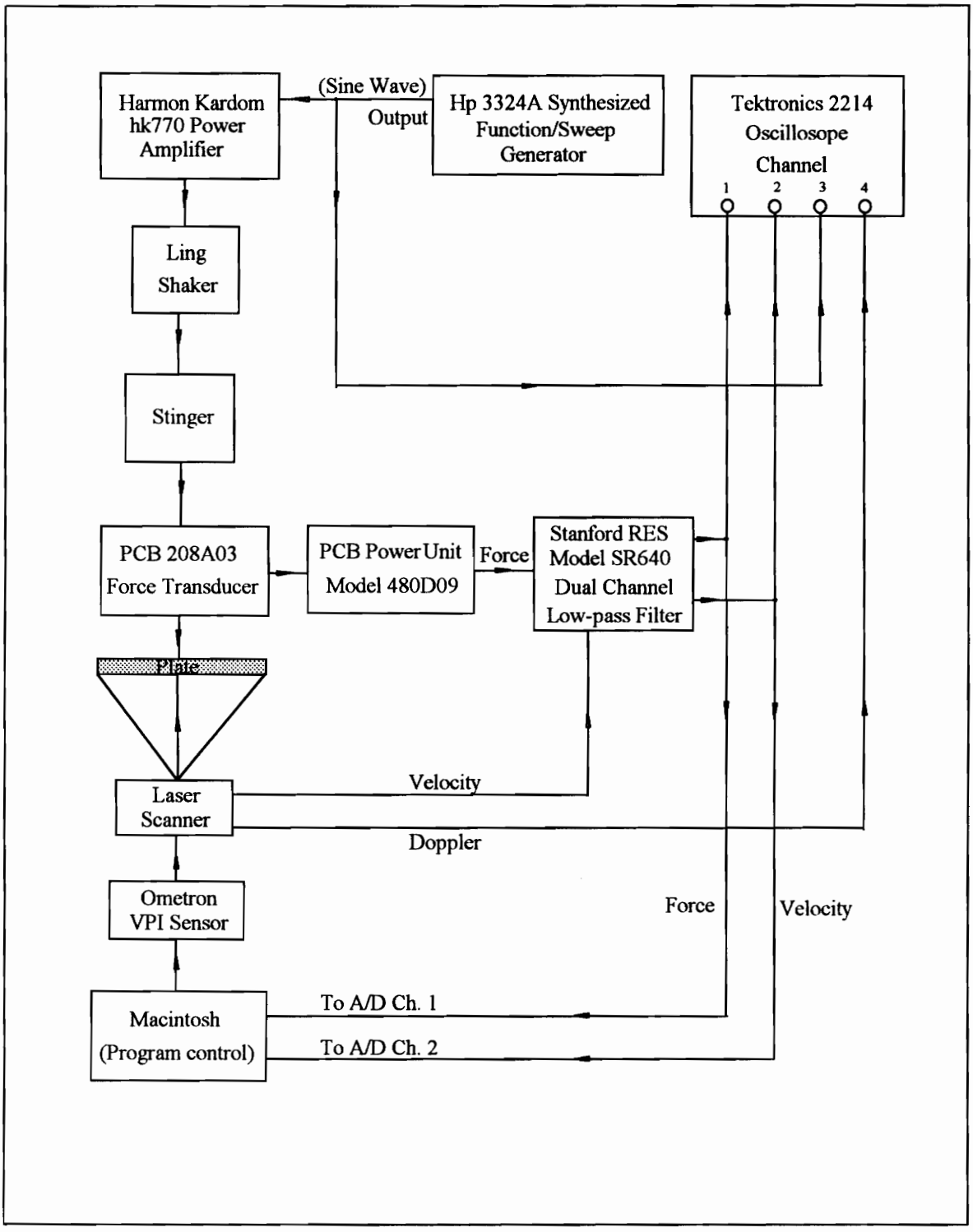

Figure 2.9 - A flow diagram of the velocity test equipment system

Fig. 2.10. The plates were forced with specific single frequencies. A sinusoidal wave is generated by the HP3324 Synthesized Function/Sweep Generations. The velocity response of the plates in real and imaginary form is then measured by the VPI scanning laser system. The input force and the output velocity signals are run to Dual-Channel filters. The Dual-Channel filters are used to prevent the frequencies above the Nyquist frequency from folding into the range investigated and to remove noise. Therefore, the cut-off frequencies of the filters were set at twice of the excitation frequencies. Finally, the input and output signals are acquired simultaneously by Macintosh computer. A dynamic image program in Macintosh provides an automatic control of the VPI sensor to scan two dimensional areas and to measure the velocities over the areas. During the tests, a Tektronix 2214 oscilloscope is used to monitor the laser Doppler signals, the velocity responses of the plates, and the actual input force.

The scanning area of the plates is divided into thirty by thirty points. This results in a total of nine hundred scanned points for each plate to be gathered. The data points are spaced at equal scanned angles. The maximum scanned angles in x and y directions, which are $\pm \theta_{x\max} = 2.7^\circ = \pm \theta_{y\max}$, are relative small to the distance between the plates and the laser head (d = 129 in), hence the data points are considered as approximately equal space along the x and y directions. The order in which the points were scanned by the laser is illustrated in Fig. 2.11.

Each scanned point in the data file contains the following information:

(1). Point number

(2). Point location in X direction, θ_x

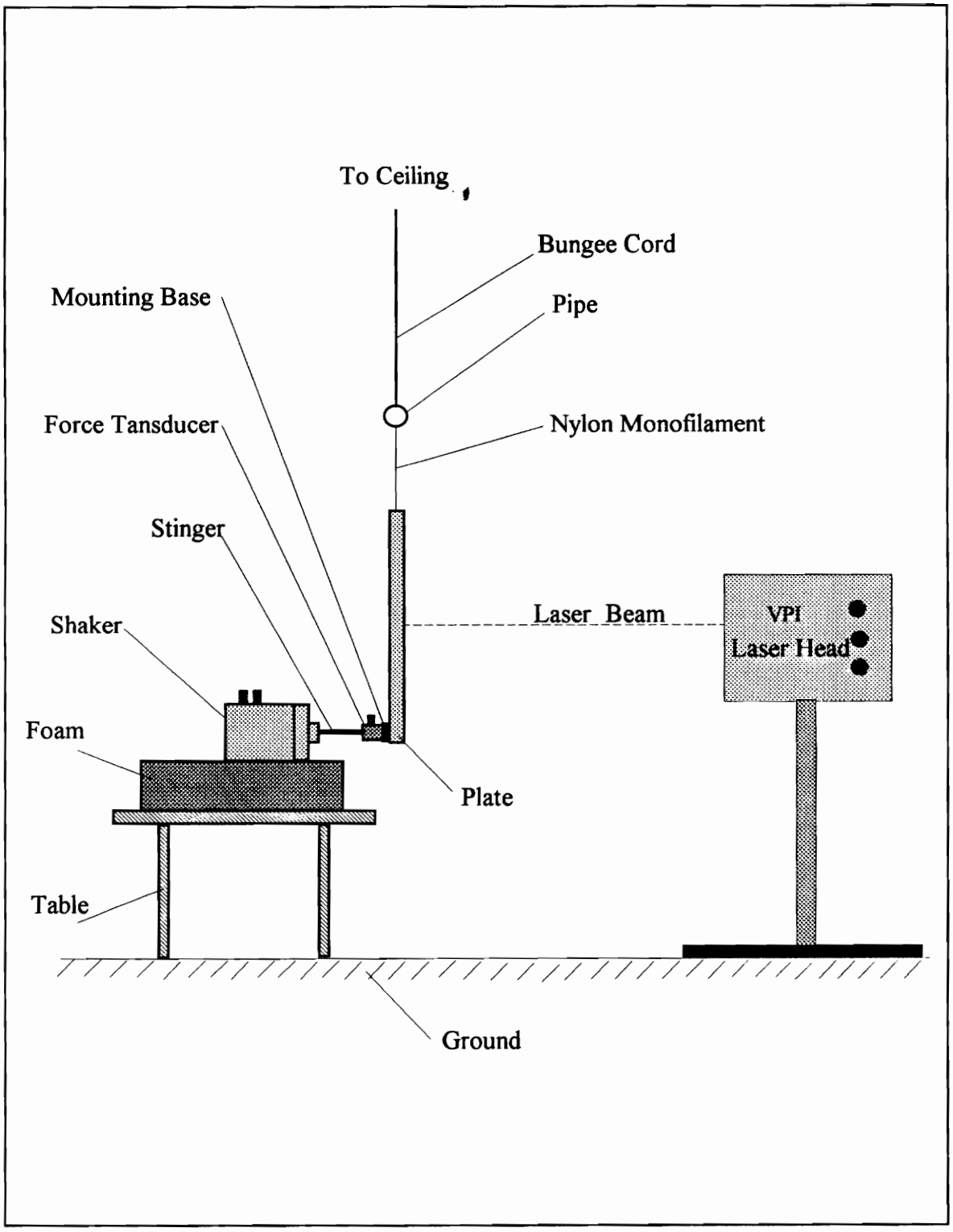

Figure 2.10 - Side view of the velocity test setup

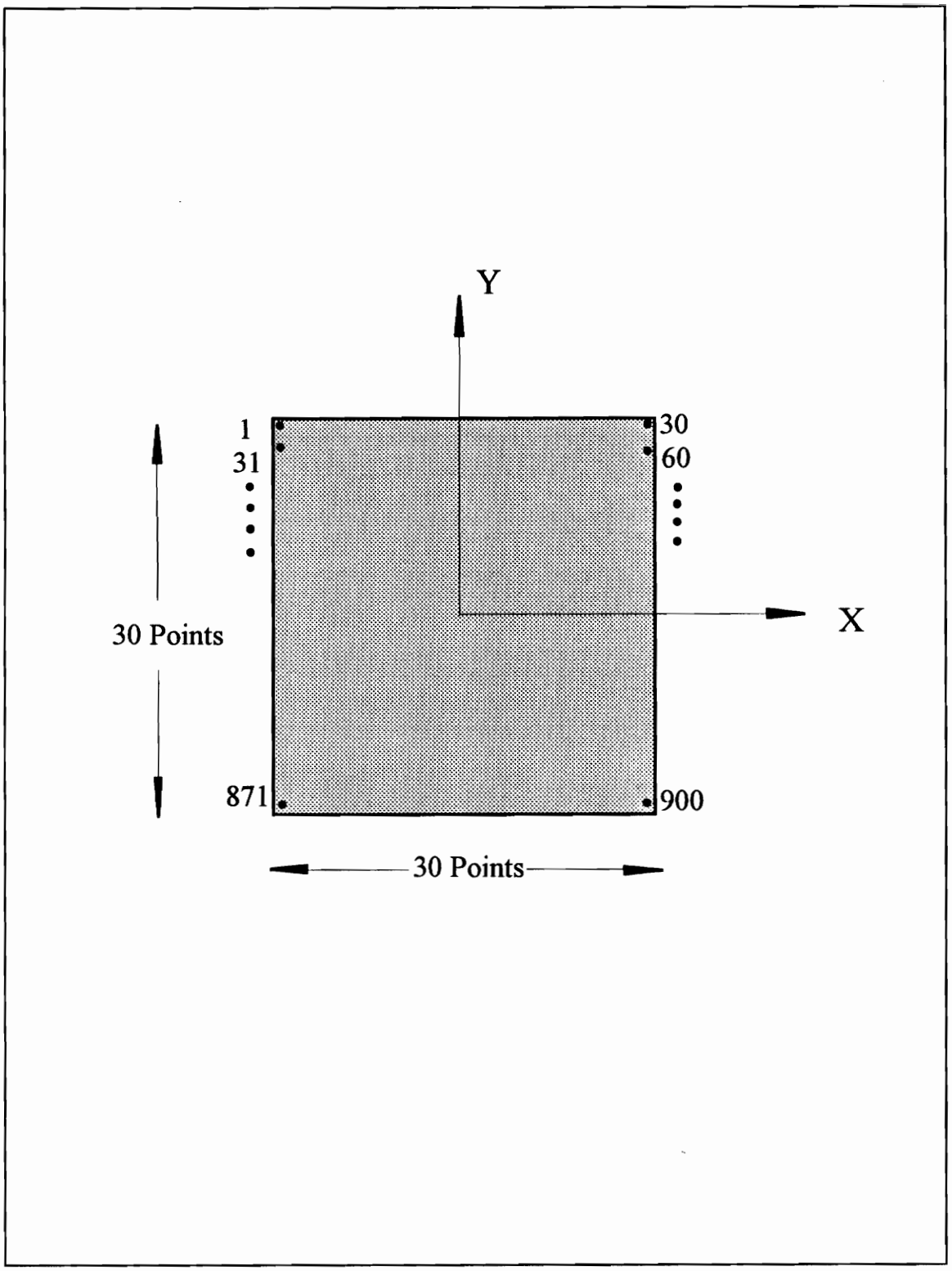

Figure 2.11 - Plate and associated data point numbering system

(3). Point location in Y direction, θ_y

(4). The magnitude of the excitation force

(5). The real part of point velocity

(6). The imaginary part of point velocity

(7). The standard deviations of the data acquisitions

2.4 Experimental procedures and data acquisition of the plates

During all tests, the same defined laser scanned area was used for all plates to keep a consistent test area. The laser was aimed at the center of the plates are the original points on the plates to aim the laser. According to the estimates of FRFs obtained, some special frequencies were chosen to run single-frequency velocity tests. The corresponding velocity fields of the undamaged plate and the damaged plates were investigated for damage identification. In this study, three different frequencies were selected, which are 150 Hz, 208 Hz and 378 Hz frequencies. The selected frequencies can be classified as the ones that are near the peak frequencies of FRFs, which are the 208 Hz and 378 Hz frequencies, and the one that is far away from any natural frequency, which is the 150 Hz frequency. It is not clear whether the comparisons of the mode shapes provide a hint to identify the damaged plates. Therefore, it is necessary not only to conduct tests at the natural frequencies, but also to conduct the tests at the other frequencies. Since the two selected peak frequencies are well separated from others, the approximate corresponding velocity mode shapes can be obtained. Two tests were conducted consecutively within the same test setup time on the same day for each plate to check the static property of the test system. To investigate the consistency of the repeated test data undertaken on different

days, the tests were repeated three times for each plate on the different days while the test system was reset up under the same test conditions.

CHAPTER III

REGRESSION ANALYSIS AND SURFACE FITTING MODELS

3.1 Introduction

The experimental data is typically contaminated by uncorrelated content during tests, because there may be the electric noise from equipment and the changing of environmental conditions, and so on. Therefore, data processing is performed to extract the useful information from the test data as well as separate the uncorrelated content from the test data. Finally, the relationships hidden or implied in the test data can be disclosed. Accordingly, an understanding of the natural properties of the experimental object and a rational interpretation of the test data may be undertaken.

In general, the test data can be split into two parts. One part is the deterministic content, which expresses the relationships between the parameters that may describe the natural properties of a test object. The other part is the random content that represents the uncorrelated content in the test system and is not due to the system inputs. The deterministic content can be estimated analytically and given by mathematical models; while the random content can be extracted from test data by statistical analysis.

Regression analysis [14] is a statistical tool that utilizes the relation between two or more quantitative variables such that these variables can be determined. Regression is usually used when the model is fitted to observational or test data, i.e., finding some mathematical function that relates the two or more data sets. This procedure results in a deterministic relationship between variables with some statistical random error content. In other words, a statistical model that describes the relationship between variables can be constructed in a

statistical sense. Regression analysis is developed in this chapter, which includes building the initial surface fitting models, estimating the quality of the fitted models, and determining the final best fitted models by a set of statistical analysis procedures. As a result, the fitted models that describe the velocity responses of the plates and give an insight about the role of regression variables take place of the velocity test data. To illustrate how the method works, the 208 Hz velocity data sets are used to perform a detail investigation in this chapter.

3.2 Surface fitting methods

In this section, the regression methods used in surface fitting are described in detail. The least squares process is first performed to find the regression coefficients for a general linear polynomial (GLP) regression model. Then the investigations on the polynomial orders against the sum of the square errors (SSE) of the regression model are conducted to find the order of the GLP regression model for the velocity field of the plates at different frequencies. Once the basic initial models are developed, all possible regressions and the forward stepwise statistics are used to find the best regression models with the best combinations of the statistical parameters that are used to build the models. Finally, the residual analysis is carried out for checking the model assumptions and making sure that the final models are appropriate and correct.

3.2.1 GLP models and the least square regression method

3.2.1.1 GLP models

On the basis of the fact that the response data of velocity fields are over the two dimensional plate surfaces, the functions of velocity fields can always be characterized by

the two independent dimensional variables x and y over the plate surfaces mathematically. Hence, the velocity fields of the plates can ideally be expressed by the spatial coordinates functions that are determined by these two independent variables (x,y) as $w(x,y)$. That is to say, we may be able to choose functions $X(x)$ and $Y(y)$ for product solution $w(x,y)$ as follows:

$$w(x,y) = X(x)Y(y) \tag{3-1}$$

where $w(x,y)$ is the velocity, $X(x)$ and $Y(y)$ are functions of independent coordinate variables x and y respectively. This procedure allows us to decompose the responses of the velocity fields into two independent variables along with the two dimensional directions of the plates.

Once $w(x,y)$ is separated into two independent variables x in $X(x)$ and y in $Y(y)$, it is possible to build regression models by using the polynomial regression in both X and Y functions, respectively. The polynomial regression is a particular case of the general linear regressions as well as the most important and general kind of curvilinear response models that are usually considered for describing the relationship between the independent variables. Figure 3.1 gives a good example to illustrate that some complex response surfaces can be well represented by the GLP regression model when there are two independent variables. This kind of curvilinear response model is also the most frequently used one in practice [15], because of its ease in handling as a special case of the general linear regression model. When the GLP model is applied in $w(x,y) = X(x)Y(y)$, it results in the following equation:

$$w(x,y) = X(x)Y(y) =$$
$$(a_0 + a_1x + a_2x^2 + a_3x^3 + \ldots + a_nx^n + \varepsilon_x)(b_0 + b_1y + b_2y^2 + b_3y^3 + \ldots + b_my^m + \varepsilon_y) \tag{3-2}$$

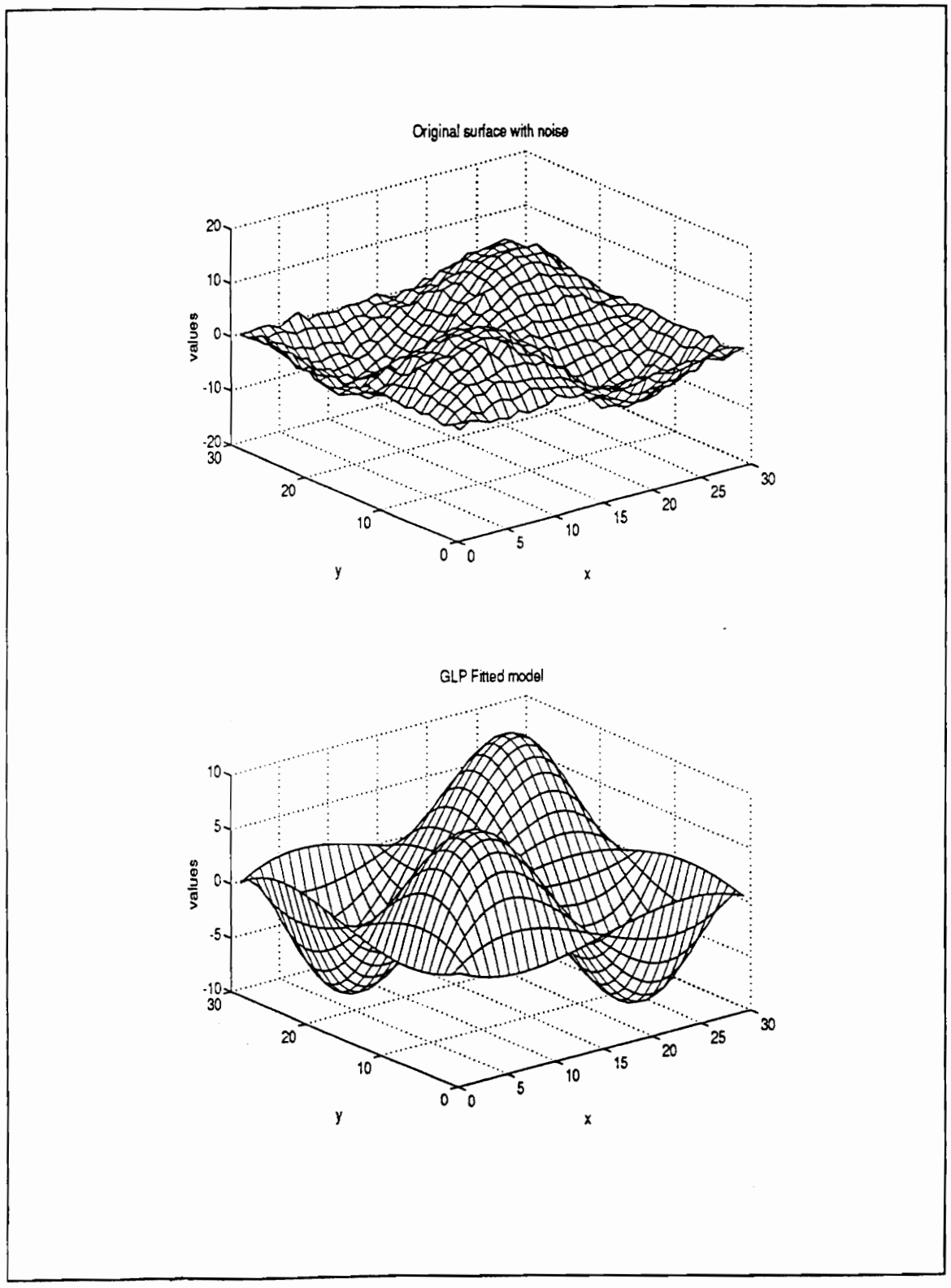

Fig. 3.1 - An example of GLP model in fitting a 3-D complex surface

where $X(x)$ is a GLP regression model with n^{th} order in variable x, and $Y(y)$ is a GLP regression model with m^{th} order in variable y. the $X(x)$ and $Y(y)$ can be expressed as follow, correspondingly,

$$X(x) = a_0 + a_1 x + a_2 x^2 + a_3 x^3 + \ldots + a_n x^n + \varepsilon_x \quad (3\text{-}3)$$

$$Y(y) = b_0 + b_1 y + b_2 y^2 + b_3 y^3 + \ldots + b_m y^m + \varepsilon_y \quad (3\text{-}4)$$

where a's and b's in Eq. (3-3) and (3-4) are the regression parameters or coefficients. x^i and y^j are the regression variables, where $i = 1, 2, \ldots, n; j = 1, 2, \ldots, m$. ε_x and ε_y are the random errors with mean $E\{\varepsilon_x\} = E\{\varepsilon_y\} = 0$ and variance $\sigma^2\{\varepsilon_x\} = \sigma_x^2$, $\sigma^2\{\varepsilon_y\} = \sigma_y^2$, Since the random errors are uncorrelated to the X or Y and each other [14], the covariance will equal zero, i.e., $cov\{\varepsilon_x, \varepsilon_y\} = cov\{\varepsilon_{x_i}, \varepsilon_{x_j}\} = cov\{\varepsilon_{y_i}, \varepsilon_{y_j}\} = 0$, where $i \neq j$. It should be noted that the equations (3-3) and (3-4) are "linear" in the parameters a's or b's. This is why the model is called linear regression.

The orders in X and Y polynomials n and m can be determined by the investigation of the sum of the square errors/residuals (SSE) of the regression models against the order of the regression polynomials. This can provide a first helpful guideline to select the suitable initial regression models. First, we start to fit the data in both X and Y at low orders, then increase the orders, progressively, to higher orders. Meanwhile, the SSE for each order increased model is calculated. The orders are plotted against SSE to show graphically how the fitting quality is improved as the orders increased. In general that the SSE decreases as the number of parameters increases in the regression models, because some higher order terms [16] that significantly contribute to reduce the SSE have been included in the models. As more regression variables are added to already well fitted models, the SSE will tend to stabilize and approach the true value of variance σ^2 since all important variables

have been included in the model. It is important to find where the curve flattens out and the addition of extra parameters makes little improvement to the fit. Figure 3.2-3.4 give 3-D plots of SSEs vs the orders in X and Y polynomials of the regression models for the plates at the three different frequencies, 150 Hz, 208 Hz and 378 Hz as the orders increasing to a specified value. It can be observed that as the orders increase both in X and Y polynomials, the SSEs tend to be stable when the orders are higher than some values, and further increasing the orders do not significantly improve the fitted quality. These specific order numbers will be found as cutoff numbers of the polynomial later.

Expanding $X(x)$ and $Y(y)$ polynomials in Eq. (3-2) gives:

$$\begin{aligned} w(x,y) = {} & a_0b_0 + a_0b_1y + a_0b_2y^2 + \ldots + a_0b_my^m + a_1b_0x + a_1b_1xy + a_1b_2xy^2 + \ldots + a_1b_mxy^m \\ & + a_2b_0x^2 + a_2b_1x^2y + a_2b_2x^2y^2 + \ldots + a_2b_mx^2y^m + \ldots \\ & + a_nb_0x^n + a_nb_1x^ny + a_nb_2x^ny^2 + \ldots + a_nb_mx^ny^m \\ & + \varepsilon_xY(y) + \varepsilon_yX(x) \end{aligned} \tag{3-5}$$

To simplify Eq. (3-5), let the products of a's and b's equal parameters β's like this: $a_ib_j = \beta_k$, where i = 0,1, 2, 3, ..., n; j = 0, 1, 2, 3, ..., m; k = 1, 2, 3, ..., (n+1)(m+1); for example, $\beta_0 = a_0b_0$, $\beta_{m+4} = a_1b_2$, $\beta_{2m+4} = a_2b_1$, etc. Let the random error terms equal ε, i.e., $\varepsilon = \varepsilon_xY(y) + \varepsilon_yX(x)$. Substituting β's and ε into Eq. (3-5) results in a GLP regression model in two independent variables x and y with interaction effects as follows:

$$\begin{aligned} w(x,y) = {} & \beta_1 + \beta_2y + \beta_3y^2 + \ldots + \beta_{m+1}y^m + \beta_{(m+1)+1}x + \beta_{(m+1)+2}xy + \beta_{(m+1)+3}xy^2 + \ldots + \beta_{2(m+1)}xy^m \\ & + \beta_{2(m+1)+1}x^2 + \beta_{2(m+1)+2}x^2y + \beta_{2(m+1)+3}x^2y^2 + \ldots + \beta_{3(m+1)}x^2y^m + \ldots \\ & + \beta_{n(m+1)+1}x^n + \beta_{n(m+1)+2}x^ny + \beta_{n(m+1)+3}x^ny^2 + \ldots + \beta_{(m+1)(n+1)}x^ny^m + \varepsilon \end{aligned} \tag{3-6}$$

The regression model Eq. (3-6) indicates that the velocity response data of the plates, i.e., $w(x, y)$, itself is a random variable because there is an uncorrelated random content ε.

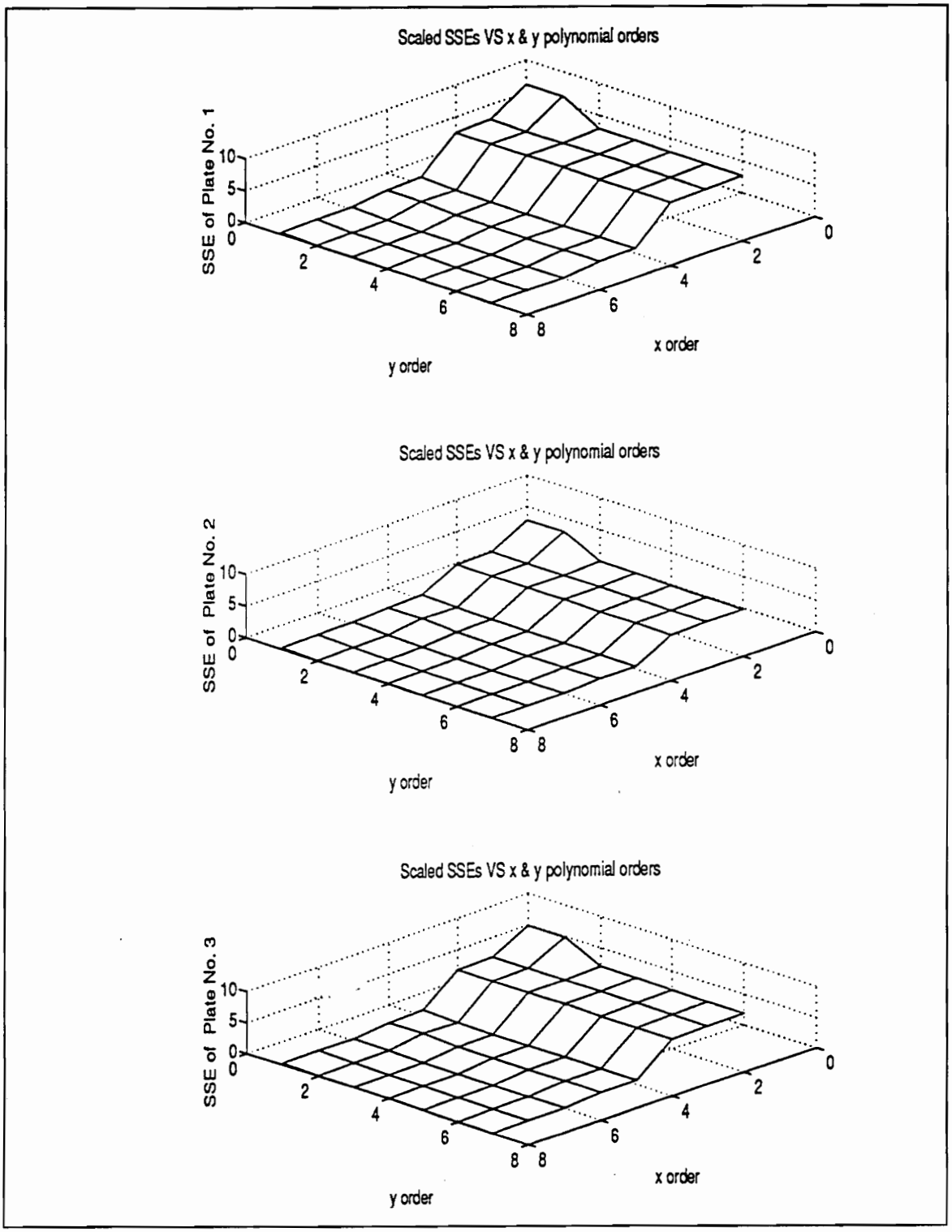

Figure 3.2 - 3-D plots of SSEs vs regression orders in x and y polynomials at 150 Hz

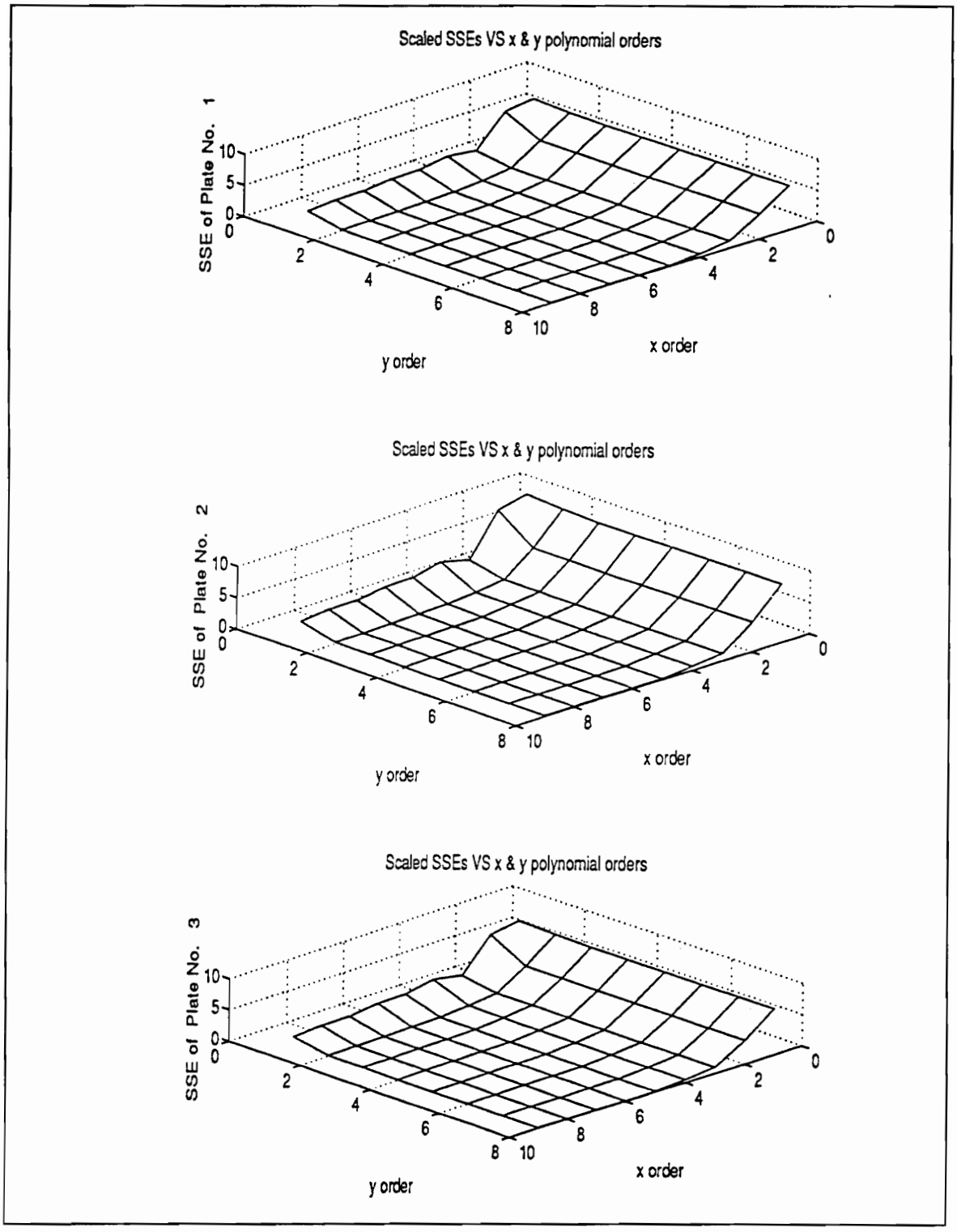

Figure 3.3 - 3-D plots of SSEs vs regression orders in x and y polynomials at the 208 Hz

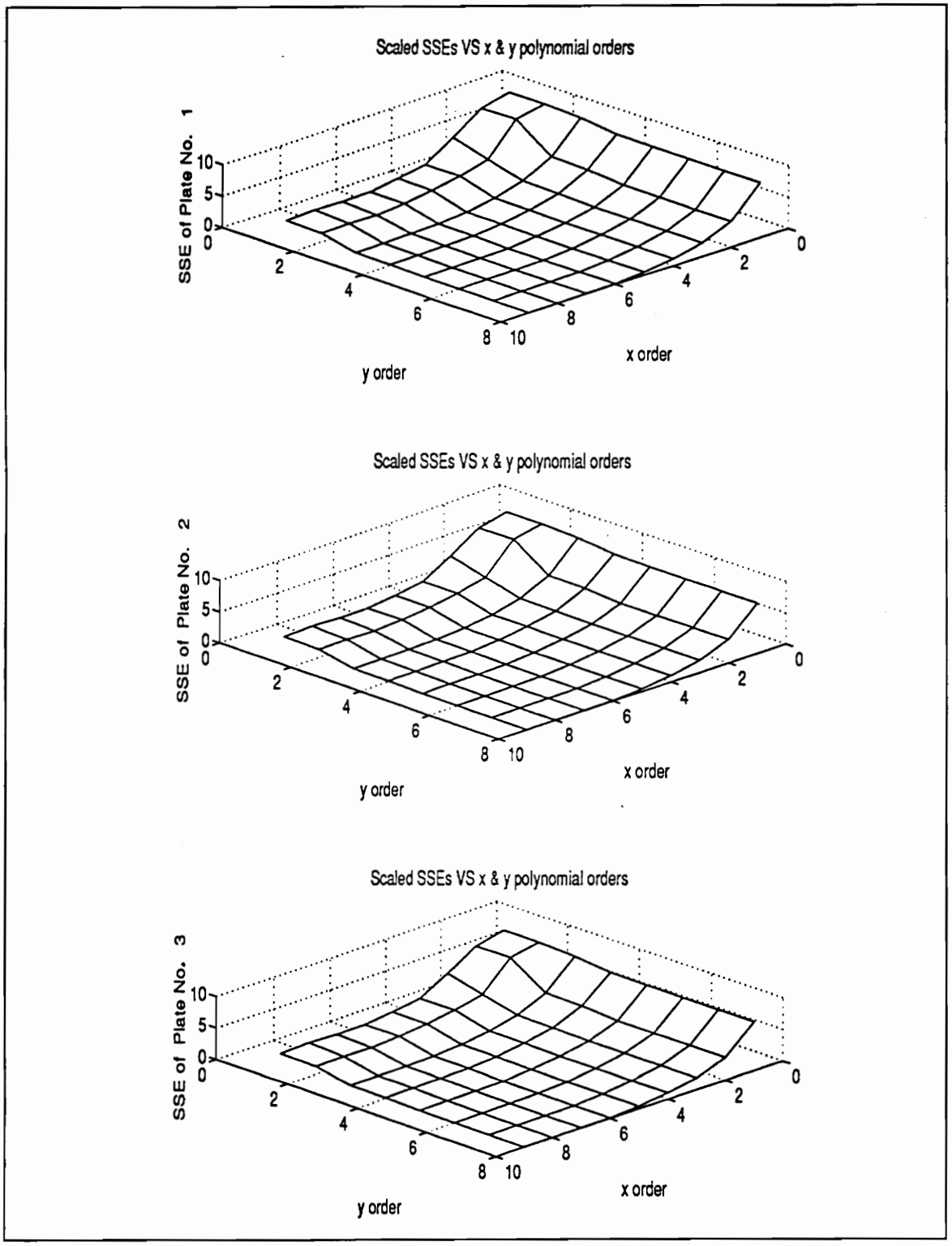

Figure 3.4 - 3-D plots of SSEs vs regression orders in x and y polynomials at 378 Hz

Therefore, the $w(x, y)$ can be split into a deterministic term expressed by Eq. (3-7) and a random term expressed by Eq. (3-8) respectively as follow:

$$\begin{aligned} w_d(x,y) = {} & \beta_1 + \beta_2 y + \beta_3 y^2 + \ldots + \beta_{m+1} y^m + \beta_{(m+1)+1} x + \beta_{(m+1)+2} xy + \beta_{(m+1)+3} xy^2 + \ldots + \beta_{2(m+1)} xy^m \\ & + \beta_{2(m+1)+1} x^2 + \beta_{2(m+1)+2} x^2 y + \beta_{2(m+1)+3} x^2 y^2 + \ldots + \beta_{3(m+1)} x^2 y^m + \ldots \\ & + \beta_{n(m+1)+1} x^n + \beta_{n(m+1)+2} x^n y + \beta_{n(m+1)+3} x^n y^2 + \ldots + \beta_{(m+1)(n+1)} x^n y^m \end{aligned} \tag{3-7}$$

$$w_r(x,y) = \varepsilon \tag{3-8}$$

Equation (3-7) represents the mean of probability distribution $w(x,y)$, i.e., $w_d(x,y) = E\{w(x,y)\}$; Consequently, the velocity fields can also be represented by:

$$w(x,y) = w_d(x,y) + w_r(x,y) \tag{3-9}$$

In order to compare with the typical general linear regression model, we define: $z_k = x^i y^j$, where i , j and k defined as before. Thus the Eq. (3-6) can be alternatively expressed by a typical GLP regression model with an equivalent form as follows:

$$\begin{aligned} w_l(x,y) = {} & \beta_1 + \beta_2 z_{l,1} + \beta_3 z_{l,2} + \ldots + \beta_{m+1} z_{l,m} \\ & + \beta_{(m+1)+1} z_{l,(m+1)+1} + \beta_{(m+1)+2} z_{l,(m+1)+2} + \beta_{(m+1)+3} z_{l,(m+1)+3} + \ldots + \beta_{2(m+1)} z_{l,2(m+1)} \\ & + \beta_{2(m+1)+1} z_{l,2(m+1)+1} + \beta_{2(m+1)+2} z_{l,2(m+1)+2} + \beta_{2(m+1)+3} z_{l,2(m+1)+3} + \ldots + \beta_{3(m+1)} z_{l,3(m+1)} + \ldots \\ & + \beta_{n(m+1)+1} z_{l,n(m+1)+1} + \beta_{n(m+1)+2} z_{l,n(m+1)+2} + \beta_{n(m+1)+3} z_{l,n(m+1)+3} + \ldots + \beta_{(m+1)(n+1)} z_{l,(m+1)(n+1)} + \varepsilon_l \end{aligned} \tag{3-10}$$

Here, the regression coefficient β_k indicates the change in the mean response per unit increase in the corresponding variable z_k while other z's are held constant, where l = 1, 2, 3, ..., 900, is the number of scanned points. According to the conditions of Eq. (3-3) and (3-4), the random error ε is independent to each other with mean zero. Hence, there are $E\{\varepsilon\} = E\{\varepsilon_x Y(y) + \varepsilon_y X(x)\} = 0$ and equal variance σ_ε^2 as well as zero covariance.

3.2.1.2 Least squares method

After the regression models selected, i.e., GLP model, the unknown regression coefficients β's should be estimated. The least square estimate is widely applicable for estimating the coefficients in regressions. This procedure consists of minimizing the sum of the squares of the difference between the fitted and the observed values of the dependent variables, i.e., the β's are determined based on minimizing the SSE. Before the least square process is performed, some basic assumptions on the GLP model (3-10) should be introduced. The least square process is based on the following assumptions: (1) Zero expectation: $E(\varepsilon_l)=0$ for all l. (2) Constant variance: $V(\varepsilon_l)=\sigma_\varepsilon^2$ for all l. (3) ε_l is normally distributed. (4) The ε_l are independent. Now, Let the fitted model to be as follows:

$$\begin{aligned}\hat{w}_l(x,y) = {} & \hat{\beta}_1+\hat{\beta}_2 z_{l,1}+\hat{\beta}_3 z_{l,2}+\ldots+\hat{\beta}_{m+1} z_{l,m} \\ & +\hat{\beta}_{(m+1)+1} z_{l,(m+1)+1}+\hat{\beta}_{(m+1)+2} z_{l,(m+1)+2}+\hat{\beta}_{(m+1)+3} z_{l,(m+1)+3}+\ldots+\hat{\beta}_{2(m+1)} z_{l,2(m+1)} \\ & +\hat{\beta}_{2(m+1)+1} z_{l,2(m+1)+1}+\hat{\beta}_{2(m+1)+2} z_{l,2(m+1)+2}+\hat{\beta}_{2(m+1)+3} z_{l,2(m+1)+3}+\ldots+\hat{\beta}_{3(m+1)} z_{l,3(m+1)}+\ldots \\ & +\hat{\beta}_{n(m+1)+1} z_{l,n(m+1)+1}+\hat{\beta}_{n(m+1)+2} z_{l,n(m+1)+2}+\hat{\beta}_{n(m+1)+3} z_{l,n(m+1)+3}+\ldots+\hat{\beta}_{(m+1)(n+1)} z_{l,(m+1)(n+1)}\end{aligned} \tag{3-11}$$

where the hats "∧" denote the estimated values. For example, $\hat{w}_l(x,y)$ denotes the fitted or estimated values, $\hat{\beta}$'s denote the least squares estimates of the unknown regression coefficients in the regression model. The $\hat{\beta}$'s are determined such that the sum of the squares of deviations of experimental points from corresponding points on the fitted model is minimized, i.e., let the sum of residual square or the sum of squared error (SSE):

$$SSE=\sum_{l=1}^{q}\left\{w_l(x,y)-\hat{w}_l(x,y)\right\}^2 \tag{3-12}$$

is minimized. Under the conditions of regression model Eq. (3-10), the Gauss-Markov theorem states that the least square estimators $\hat{\beta}$'s are unbiased (which is expressed by Eq.

(3-13) and have minimum variance among all unbiased linear estimators, i.e., the least square estimators are more precise than any of these other estimators [14].

$$E\left\{\hat{\beta}_k\right\} = \beta_k \tag{3-13}$$

where $k = 1, 2, 3, ..., (n+1)(m+1)$.

To obtain the solutions of the least squares estimators $\hat{\beta}$'s, we rewrite the regression model Eq. (3-6) in matrix form. By using matrix operations, the solution procedures are simplified. To represent Eq. (3-6) in matrix form, we define the following vectors and matrices: first, let $r = (n+1)(m+1)$, n and m are the highest orders in x and y polynomials, respectively; $q = 900$ is the total scanned points; and index numbers: $1 \le l \le 900$, $1 \le i \le r$, $1 \le j \le m$, $1 \le k \le r$. Then let:

$$\underset{q\times 1}{\mathbf{W}} = \begin{bmatrix} w_1 \\ w_2 \\ \square \\ w_l \\ \square \\ w_q \end{bmatrix}; \quad \underset{q\times 1}{\hat{\mathbf{W}}} = \begin{bmatrix} \hat{w}_1 \\ \hat{w}_2 \\ \square \\ \hat{w}_l \\ \square \\ \hat{w}_q \end{bmatrix}; \quad \underset{r\times 1}{\beta} = \begin{bmatrix} \beta_1 \\ \beta_2 \\ \square \\ \beta_k \\ \square \\ \beta_r \end{bmatrix}; \quad \underset{r\times 1}{\hat{\beta}} = \begin{bmatrix} \hat{\beta}_1 \\ \hat{\beta}_2 \\ \square \\ \hat{\beta}_k \\ \square \\ \hat{\beta}_r \end{bmatrix}; \quad \underset{q\times 1}{\varepsilon} = \begin{bmatrix} \varepsilon_1 \\ \varepsilon_2 \\ \square \\ \varepsilon_l \\ \square \\ \varepsilon_q \end{bmatrix}; \tag{3-14}$$

and

$$\underset{q\times r}{P} = \left[\{1\} \quad \{y\} \quad \{y^2\} \quad \ldots \quad \{y^m\} \quad \{x\} \quad \{xy\} \quad \{xy^2\} \quad \ldots \quad \{xy^m\} \quad \ldots \{x^i\} \right.$$
$$\left. \{x^i y\} \quad \{x^i y^2\} \quad \ldots \quad \{x^i y^m\} \quad \ldots \quad \{x^n\} \quad \{x^n y\} \quad \{x^n y^2\} \quad \ldots \quad \{x^n y^m\}\right] \tag{3-15}$$

where

W is a q dimensional vector of the scanned velocity response data of the plate;

β is an unknown r dimensional vector of the true regression parameters;

P is a known $q \times r$ matrix of two coordinates x and y of the plate scanned points, each column in P is a $q \times 1 = 900 \times 1$ column vector, which is given in Eq. (3-16);

ε is a q dimensional vector of uncorrelated random variables with zero expectation and equal variance as well zero covariance;

$\hat{}$ is the estimated regression vector for the response data of velocity field of the plates;

$\hat{\beta}$ is a least square estimated vector of the regression parameters β's and represents the estimated change in $\hat{w}(z)$ for a one-unit increase in z_k, while holding the other zs constant in model (3-11);

I is an identity $q \times 1$ column vector.

Each vector in Eq. (3-15) is given as follows:

$$\underset{q\times 1}{\{y^j\}} = \begin{Bmatrix} y_1^j \\ y_2^j \\ \square \\ y_q^j \end{Bmatrix}; \qquad \underset{q\times 1}{\{x\}} = \begin{Bmatrix} x_1 \\ x_2 \\ \square \\ x_q \end{Bmatrix}; \qquad \underset{q\times 1}{\{xy^j\}} = \begin{Bmatrix} xy_1^j \\ xy_2^j \\ \square \\ xy_q^j \end{Bmatrix}; \qquad \underset{q\times 1}{\{x^i\}} = \begin{Bmatrix} x_1^i \\ x_2^i \\ \square \\ x_q^i \end{Bmatrix};$$

$$\underset{q\times 1}{\{x^i y^j\}} = \begin{Bmatrix} x^i y_1^j \\ x^i y_2^j \\ \square \\ x^i y_q^j \end{Bmatrix}; \qquad \underset{q\times 1}{\{x^n\}} = \begin{Bmatrix} x_1^n \\ x_2^n \\ \square \\ x_q^n \end{Bmatrix}; \qquad \underset{q\times 1}{\{x^n y^j\}} = \begin{Bmatrix} x^n y_1^j \\ x^n y_2^j \\ \square \\ x^n y_q^j \end{Bmatrix}; \qquad (3\text{-}16)$$

where j =1, 2, ..., m; Finally, in matrix form, the general regression model Eq. (3-6) becomes:

$$\underset{q\times 1}{W} = \underset{q\times r}{P}\,\underset{r\times 1}{\beta} + \underset{q\times 1}{\varepsilon} \qquad (3\text{-}17)$$

The least square estimators $\hat{\beta}$'s can be obtained by the following matrix operations:

$$\underset{q\times 1}{\hat{\beta}} = (P'P)_{q\times q}^{-1}(P'W)_{q\times 1} = A_{q\times q}^{-1}g_{q\times 1} \tag{3-18}$$

where $A = P'P$ is $q\times q$ symmetric matrix, named variance-covariance matrix, and $g = P'W$ is a $q\times 1$ vector.

Once the regression parameters $\hat{\beta}$'s are determined, the initial possible regression model for the velocity response surfaces of the plates is obtained. This model can be used to find the final best models that are used in further analysis and express the analytical mathematical models of the plates.

Consequently, the fitted values are represented by: $\underset{q\times 1}{\hat{W}} = \underset{q\times r}{P}\,\underset{r\times 1}{\hat{\beta}}$ (3-19)

and the residual vector can be expressed by: $\underset{q\times 1}{e} = \begin{bmatrix} e_1 \\ e_2 \\ \square \\ e_l \\ \square \\ e_q \end{bmatrix} = W - \hat{W} = W - P\hat{\beta}$; (3-20)

Then the sum of squared error is:

$$SSE = \sum_{l=1}^{900} e_l^2 = e'e = (W - P\hat{\beta})'(W - P\hat{\beta}) \tag{3-21}$$

In order to find the reasonable order numbers for the initial GLP models, there are three steps used to find the possible cutoff orders as the orders are increased to a specified value *ff* (where *ff* is the highest specified computed order) both in x and y polynomials. Therefore, a square SSE matrix is formed with *ff*-row and *ff*-column for each plate at this time. The ratio of the current diagonal SSE term, $SSE(k,k)$, to the maximum SSE term,

$SSE(1,1)$, dd, is computed to check whether a general requirement of an acceptable relative SSE error, rr, is met. At this stage, the dd, value is calculated as:

$$dd = \frac{SSE(k,k)}{SSE(1,1)} \tag{3-22}$$

where SSE(i,j) is a two-dimensional SSE matrix with x order i and y order j; i,j = 1, 2, ..., ff. SSE(k,k) is the current diagonal term of the SSE matrix. If the dd is less than the specified value rr, an acceptable relative SSE error, we will accept the current diagonal fitting order, k, in both x and y polynomials. For example, for rr = 0.05 = 5%, as the k increases, we accept the diagonal order, k, at least the dd decreases to 5% of the maximum SSE value, i.e., $dd < 0.05$. Then, the cutoff diagonal order could be determined so that the further increasing the orders between the successive diagonal order terms will meet the diagonal acceptable requirement at this time. The relative difference in successive diagonal order term, $dSSE(k,k)$, is developed to investigate the tendency of the variation in the SSEs and used to find the cutoff diagonal order as the orders are increased. The $dSSE(k,k)$ is computed as follows:

$$dSSE(k,k) = \frac{SSE(k-1,k-1) - SSE(k,k)}{SSE(k-1,k-1)} \tag{3-23}$$

If $dSSE(k,k)$ is less than pp, the specified acceptable value, the further decrease in $dSSE(k,k)$ will be considered insignificant, then the cutoff orders both in x and y polynomials equal k. Since the velocity fields may not be perfectly symmetric in both x and y direction, the cutoff orders in both x and y direction may be different. Therefore, the third step is to find the possible cutoff orders for x and y polynomials, respectively. At this stage, the relative difference in successive increasing orders in x and y, $dxSSE(i)$ and $dySSE(i)$, respectively, are computed to determine the corresponding cutoff orders as the iterative variable i decreases one at a step from k to 2 as follow:

in x direction: $$dxSSE\,(i) = \frac{SSE\,(i-1,k) - SSE\,(i,k)}{SSE\,(i,k)} \tag{2-24}$$

in y direction: $$dySSE\,(i) = \frac{SSE\,(k,i-1) - SSE\,(k,i)}{SSE\,(k,i)} \tag{2-25}$$

If the $dxSSE\,(i)$ or $dySSE\,(i)$ is less than a specified value qq, the further increasing in the order will not significantly reduce the SSE at this time. Then the cutoff order is set to equal the current fitted order for x or y respectively.

Table 3.1 lists the results of the cutoff orders, where *nd* for the diagonal term, *nx* for the x polynomial and the *ny* for the y polynomial in each plate at the calculated frequencies. Here the specified values are the followings: rr = 0.10, pp = .25 and qq = .25. Once the cutoff orders are obtained, the initial GLP models are hence determined with the numbers of the total regression terms as $(nx+1)(ny+1)$.

Table 3.1 The initial GLP orders

	Plate No.1	Plate No. 2	Plate No. 3
Freq. Hz	*nd nx ny*	*nd nx ny*	*nd nx ny*
150	5 5 4	5 5 3	5 5 4
208	6 7 5	6 7 5	6 7 5
378	7 8 4	7 8 4	7 8 4

A Matlab program carries out all the above procedures, performs the data transformation and finds the least square estimators of the GLP regression models. The program consists of three parts. The first part is used for data transformations. The velocity data should be transformed into the matrix or vector forms that are available to Matlab codes to conduct

data processing and plots graphs. The second part performs the regression fit for the all models that are built by performing the regression on all possible combinations of x and y's polynomial orders as the orders are increased to specified *ff* value. At the same time, the possible cutoff orders in x and y polynomials and in the diagonal order terms are given based on the specified criteria. The third part of the program is used to perform the 3-D graphic plots of the results. Figure 3.5 gives a flow chart of this Matlab program.

3.2.2 Find the best regression models

Once the regression estimators $\hat{\beta}$'s are computed from the q independent random test data, $w(z)$'s, by the least square process, the initial full model with r regression variables, z_1, z_2, ..., z_r, are, therefore, established in the form of Eq. (3-11). The number of regression variables r in the full model may be relatively large. It is possible that not all of these z's significantly contribute to the $\hat{w}(x,y)$'s because some of these variables may be highly intercorrelated. We wish to find the dominant regression variables and screen out some insignificant independent variables that add little to the building of the best model. The number of regression variables or the order of the regression model can be reduced in the final best model. If the regression variables can be appropriately combined or pooled together to form a subset or a reduced model with p regression variables, z's, where $1 \leq p \leq r$, it is possible to find the best or the most significant subset within the r regression. If each model is simplified and modified, it will save the computational time and the computer memory in further analysis on the regression models. The slight difference existing in the test data between the different plates may be displayed this way. Since we have no intuition about which regression variables and what kinds of pooled regression variables are most significant for the best model, we will use a computer with suitable

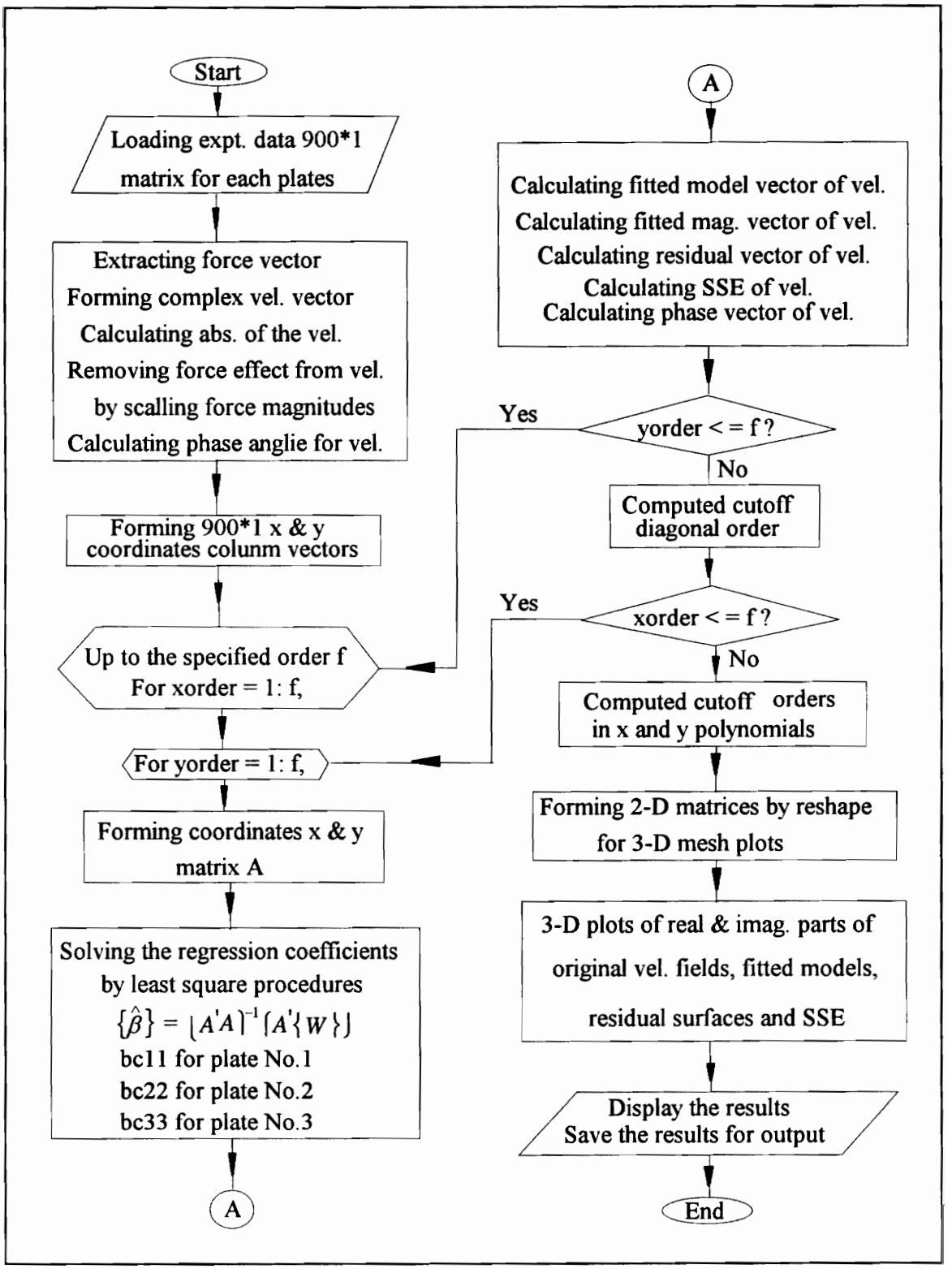

Figure 3.5 - A flow chart of the Matlab program of finding initial models

software, for example, SAS (Statistical Analysis System) software in the mainframe system and the S-plus software in UNIX system, to run a large number of regression models efficiently and to find the final best fitting models for all plates at the investigated frequencies.

The all-possible-regression and the forward stepwise regression are the two most useful statistical procedures for selecting the best regression model. These approaches should only be attempted when we have access to a computer with suitable software. The forward stepwise statistic is the most widely used automatic search methods. It was developed to economize on computational effort, as compared with the all-possible-regression approach, while arriving at the "best' subset of independent variables. The basicdifference between the automatic search procedures and the all-possible-regression approach is that the automatic search procedures end with the identification of a *single* regression model as the "best." In contrast, with the all-possible-regression approach, *several* regression models can be identified as "good" for final consideration [14]. There is no absolute criterion to make the selection of the final best model. The final choice depends on the uses and purposes of building the models. Therefore, we apply both approaches simultaneously to find a few "good" subset regression models for final consideration as well as a *single* best regression model from the different procedures. These will help us reach the final best regression model by using and balancing several criteria as well as by making a double check in selecting the final best models.

3.2.2.1 The all-possible-regression

The all-possible-regression is used to identify a group of regression models that are "good" according to a specified criterion so that a detail examination can be made of these

models and lead to the selection of the final regression model to be employed. The all-possible- regression requires fitting every possible regression equation associated with every possible combination of the independent variables. For r independent variables, the all-possible- regression produces information on all 2^r candidate models. Before running the all-possible-regression, we need to specify what criterion should be used in building the "good" models and in selecting the best-fitting model. Since the purpose of regression models is to find the final best fitted regression models, which can truly describe the velocity fields, and to manipulate the models for analytical purposes, a precise estimation of the regression coefficients $\hat{\beta}$'s and the small prediction error are emphasized here. Therefore, the three criteria: MSE s_ε^2, C_p and the prediction sum of squares of error (PRESS) are specified for running the all-possible-regression.

(1). MSE s_ε^2 criterion

The first and the simplest criterion for selecting the "good" regression models from a set of all possible regression equations is to use an estimate of the error variance s_ε^2, or the mean square error (MSE) [17], where the MSE is defined by:

$$s_\varepsilon^2 = \text{MSE} = \text{SSE}/(q\text{-r}) = \frac{\sum_{l=1}^{q}\left\{w_l(x,y) - \hat{w}_l(x,y)\right\}^2}{q-r} \tag{3-26}$$

where the SSE is given by Eq. (3-12) and written again, i.e.,

$$\text{SSE} = \sum_{l=1}^{q}[w_l(x,y) - \hat{w}_l(x,y)]^2$$

The concept of SSE comes from partitioning the total sum of squares. The total sum of squares (TSS) about the mean represents the total variability in the velocity response data

$w(x, y)$s with (q-1) degree of freedom (d.o.f.), which is the number of independent quantities to enter the expressions. The TSS is given by:

$$\mathrm{TSS} = \sum_{l=1}^{q} [w_l(x,y) - \overline{W}_l(x,y)]^2 \tag{3-27}$$

where the sample mean $\overline{W_l}(x,y)$ is given by:

$$\overline{W}_l(x,y) = \frac{1}{q}\sum_{l=1}^{q} w_l(x,y) \tag{3-28}$$

The TSS can be partitioned into the variability explained by the fitted model, which is expressed by the sum of square of the regression (SSR) with (r-1) d.o.f. and the variability unexplained by the fitted model, which is expressed by the sum of square of error (SSE) with (q-r) d.o.f.. The SSR and SSE are given by the Eq. (3-29) and (3-12), respectively.

$$\mathrm{SSR} = \sum_{l=1}^{q} [\hat{w}_l(x,y) - \overline{w}_l(x,y)]^2 \tag{3-29}$$

Therefore, a fundamental identity to describe the relationship of TSS, SSR and SSE is TSS = SSR + SSE. If the TSS, SSR and SSE are divided by the corresponding d.o.f., the mean square total (MST), the mean square of the regression (MSR) and the mean square of the error (MSE) of the regression are obtained, correspondingly. In general, for a given data set, the larger MSR, the smaller MSE, the better the model fit the data. On the base of the fact that the MSE is used in the most statistical tests and inferences about model parameters, it is reasonable to apply MSE s_ε^2 criterion to find a few subsets for which MSE's are at the minimum or so close to the minimum that adding more variables is not worthwhile [18]. Taking a data set of plate No. 1 at the 208 Hz as an example, the MSE and SSE for the initial full model with the number of the regression variables being (7+1)*(5+1) being 48 are 0.00106 and 0.8994 (with d.o.f.error = 851), respectively. The MSE and SSE for the final selected model with the number of the regression variables

being 31 are 0.00114 and 0.9911 (with d.o.f. error = 868), respectively. The two MSEs are very close to each other. Therefore, it is very clear that adding more regression variables into the final selected model is insignificant to the improvement of the regression quality.

(2). C_p criterion/statistic

C_p is a importance criterion to judge the goodness of fitting and is simple. It reaches a balance between the overfitting (i.e., too much variance) and the underfitting (i.e., bias exist). If we choose a model that leaves out one or more "important" independent variables, the additional variability in the $w(x, y)$ that would be accounted for with these variables becomes part of the estimated error variance [17]. On the other hand, if we choose a model that contains one or more "extraneous" regression variables, our model is overfitting. The C_p statistic balances the problem of over- and under-fitting, and arrives at a choice of the best-balance-fitting subset regression equation. The C_p statistic is defined as:

$$C_p = \frac{SSE_p}{s_\varepsilon^2} - (n-2p) = p + \frac{(s_p^2 - s_\varepsilon^2)(n-p)}{s_\varepsilon^2} \qquad (3\text{-}30)$$

where SSE_r is the sum of squares of error for the reduced model with p parameters (include β_0); s_ε^2 is the MSE for the full regression model with the largest number of regression variables r, where $r = n$; and s_p^2 is the MSE for the reduced model with p variables, it is given by: $s_p^2 = MSE_p = \frac{SSE_p}{n-p}$. The p in Eq. (3-30) is an indicator of the overfit caused by too many regression variables that the additional variability becomes random error and increase the C_p value in the regression model. The $s_p^2 - s_\varepsilon^2$ in Eq. (3-30) is an indicator of the underfit that comes from too few regression variables and forms bias error in the regression model. Theory suggests [17] that a "good" model should have $C_p \cong$

p. It means that the bias error is very small in the model, where C_p can be under p or over p's value. Using the C_p criterion, we compute C_p value for each reduced regression equation and try to identify the best balance subset of z's in Eq. (3-11) for which (1) the C_p values is small for better model and (2) the C_p value is near p. Therefore the small C_p is obtained only if the model reach at the balance.

(3). PRESS statistic

The PRESS statistic is used to indicate the goodness of the prediction of the regression models. It is based on the PRESS residuals [14], i.e., $d_l = w_l(x,y) - \hat{w}_{l,-l}(x,y)$, where $\hat{w}_{l,-l}(x,y)$, l = 1, 2, ..., q, is the predicted value for the l^{th} data based on the fitted regression model that *did not* use the l^{th} velocity response $w_l(x,y)$. Therefore $\hat{w}_{l,-l}(x,y)$ and $w_l(x,y)$ are independent to each other, and d_l indicates the pure predicted error when $\hat{w}_{l,-l}(x,y)$ is used as predicted value. For each fitted regression model, there are q PRESS residuals. The PRESS is defined as the sum of the PRESS residuals, i.e.,

$$\text{PRESS} = \sum_{l=1}^{q} d_l^2 = \sum_{l=1}^{q} [w_l(x,y) - \hat{w}_{l,-l}(x,y)]^2 \qquad (3\text{-}31)$$

The models with small PRESS values indicate that the models fit the data well in the sense of having small prediction error. Hence, the model with minimum PRESS value is the best-balance-fitting prediction model. Even though we are not going to use the regression models to predict future values that are not at the fitted points, we still hope to do further analysis on the regression models, such as calculating the second partial derivatives with respect to the coordinates x and y. Therefore, it is important to obtain the regression models that not only have high precision in the fitted points, but also have smallest predicted error in the points other than the fitted points, i.e., the future prediction points. This is why we perform the PRESS statistic associated with the best model selections.

On the base of the specified criteria, the all-possible regressions are carried out. The procedures are described as follow: First, partition the different initial regression equations into sets involving 1, 2, 3, ..., r variables, and then order the equations within each set according to specified criteria.

Once a set of the "good" fitting model list obtained by the all-possible regressions, we will focus on the several top "good" subsets according to the specified criteria. The final best regression models are then selected according to the specified criteria. The models will also be compared with the best model found by the stepwise regression procedures. Considering the specified criteria, the final best subset of the "good" fitted models would be the model with smallest MSE, the lowest C_p with close to the number of the regression parameters p, and the lowest PRESS value. But it is hardly always the case that each of the criterion points out the same "best" model. Therefore, the balance of the different criteria in evaluating the possible final best subset of the regression variables should be comprehensively considered. Base on this consideration, the top two "good" C_p models are selected to be studied in detail by the other two criteria for the final best model and compared to the corresponding one obtained by the forward stepwise regressions. Table 3.2 lists these models as well as their specified statistical parameters for each plate at the 208 Hz frequency based on the initial models with cutoff X order = 7, cutoff Y order = 5 and the number of the data points = 900. It should be noted, the SAS code can only process the real data sets, so the complex velocity fields are split into real and imaginary to process. The notion "No." in the table is the number of the variables in the model; the notion "R^2" in the table is the coefficient of multiple determination given by the least square fit. If the R^2 is more close to 1, it means the model are better fitted the data. The

Table 3.2(a) - The best C_p models of plate No.1 at 208 Hz

(1)	C_p	R^2	No.	Variables in Model
imag.	45.5752	0.9884	31	X Y X2 XY X2Y XY2 X2Y2 X3 Y3 XY3 X3Y3
real	31.2801	0.9664	31	X3Y1 X3Y2 X4 Y4 XY4 X3Y2 X4Y2 X4Y4 X5 X5Y3 X5Y2 X6 X6Y X6Y2 X6Y3 X6Y4 X7 X7Y X7Y2 X7Y3

ANOVA TABLE

Imag. 1.		D.O.F.	Sum of Squares	Mean Square	F	Prob>F
	Regression	31	51.0223	1.64588	3918.762	0.0001
	Error	868	0.36729	0.00042		
	C Total	899	51.92959			
	PRESS =0.3958					

Real 1.		D.O.F.	Sum of Squares	Mean Square	F	Prob>F
	Regression	31	19.55615	0.55694	674.605	0.0001
	Error	868	0.74384	0.00086		
	C Total	899	20.2999			
	PRESS =0.7056					

(2)	C_p	R^2	No.	Variables in Model
imag.	46.2305	0.9932	31	X Y X2 Y2 XY XY2 X2Y X2Y2 X3 Y3 XY3 X3Y3 X3Y1
real	32.0490	0.9640	31	X3Y2 X4 Y4 XY4 X2Y4 X4Y2 X4Y3 X4Y4 X3Y4 X5 X5Y3 X5Y2 X6 X6Y2 X6Y3 X7 X7Y X7Y2 X7Y3

ANOVA TABLE

Imag. 2.		D.O.F.	Sum of Squares	Mean Square	F	Prob>F
	Regression	31	51.02131	1.64585	4113.601	0.0001
	Error	868	0.34729	0.00040		
	C Total	899	51.36859			
	PRESS =0.3890					

Real 2.		D.O.F.	Sum of Squares	Mean Square	F	Prob>F
	Regression	31	17.26515	0.55694	750.846	0.0001
	Error	868	0.64384	0.00074		
	C Total	899	17.90899			
	PRESS =0.6956					

Table 3.2(b) - The best C(p) models of plate No. 2 at 208 Hz

(1)	C_p	R^2	No.	Variables in Model
imag.	32.0014	0.9890	32	X Y X2 Y2 XY XY2 X2Y X2Y2 X3 Y3 XY3 X2Y3 X3Y
real	38.5775	0.9599	32	X3Y2 X3Y3 Y4 XY4 X2Y4 X4Y4 X5 X5Y4 X5Y3 X5Y2 X5Y X6 X6Y X6Y3 X6Y4 X7 X7Y X7Y3 X7Y4

ANOVA TABLE

Imag. 1.	D.O.F.	Sum of Squares	Mean Square	F	Prob>F
Regression	32	66.72367	2.08511	2439.588	0.0001
Error	867	0.74102	0.00085		
C Total	899	67.46469			
PRESS =0.8184					

Real. 1.	D.O.F.	Sum of Squares	Mean Square	F	Prob>F
Regression	32	18.37867	0.57433	648.072	0.0001
Error	867	0.76835	0.00089		
C Total	899	19.14702			
PRESS =0.6277					

(2)	C_p	R^2	No.	Variables in Model
imag.	33.2384	0.9989	32	X Y Y2 XY X2Y XY2 X2Y2 X3 Y3 XY3 X3Y3
real	39.6895	0.9506	32	X3Y1 X3Y2 X4 Y4 XY4 X3Y2 X4Y2 X4Y4 X5 X5Y X5Y3 X5Y2 X6 X6Y X6Y2 X6Y4 X6Y5 X7 X7Y X7Y2 X7Y3

ANOVA TABLE

Imag. 2.	D.O.F.	Sum of Squares	Mean Square	F	Prob>F
Regression	32	64.38296	2.011968	2186.922	0.0001
Error	867	0.85115	0.00092		
C Total	899	65.22411			
PRESS =0.8105					

Real. 2.	D.O.F.	Sum of Squares	Mean Square	F	Prob>F
Regression	32	17.18936	0.53717	556.749	0.0001
Error	867	0.83651	0.00096		
C Total	899	18.02587			
PRESS =0.8965					

Table 3.2(c) - The best C(p) models of plate No. 3 at 208 Hz

(1)	C_p	R^2	No.	Variables in Mode
imag.	35.1912	0.9953	33	X Y Y2 XY X2Y XY2 X2Y2 X3 Y3 XY3 X3Y3 X3Y1
real	34.9980	0.9599	33	X3Y2 X2Y3 X4 Y4 X4Y4 X3Y2 X4Y2 X2Y4 X4Y4 X5 X5Y X5Y3 X5Y2 X6 X6Y X6Y2 X7 X7Y X7Y2 X7Y3 X7Y4

ANOVA TABLE

Imag. 1.	D.O.F.	Sum of Squares	Mean Square	F	Prob>F
Regression	33	55.37871	1.67814	4461.439	0.0001
Error	866	0.32574	0.00038		
C Total	899	55.70445			
PRESS =0.4140					

Real. 1.	D.O.F.	Sum of Squares	Mean Square	F	Prob>F
Regression	33	12.36851	0.37480	635.254	0.0001
Error	866	0.51873	0.00059		
C Total	899	12.88724			
PRESS =0.5832					

---

(2)	C_p	R^2	No.	Variables in Model
imag.	36.3729	0.9950	33	X Y X2 Y2 XY XY2 X2Y2 Y3 XY3 X3Y2 X3Y1 X2Y3
real	33.6990	0.9600	33	X3Y4 X4 Y4 XY4 X4Y2 X2Y4 X4Y3 X4Y4 X5 X5Y4 X5Y3 X5Y2 X5Y X6 X6Y X6Y2 X6Y4 X7 X7Y X7Y2 X7Y4

ANOVA TABLE

Imag. 2.	D.O.F.	Sum of Squares	Mean Square	F	Prob>F
Regression	33	55.27272	1.67493	5260.189	0.0001
Error	866	0.27575	0.00032		
C Total	899	55.54847			
PRESS=0.3130					

Real. 2.	D.O.F.	Sum of Squares	Mean Square	F	Prob>F
Regression	33	12.22233	0.37037	630.458	0.0001
Error	866	0.50875	0.00059		
C Total	899	12.73108			
PRESS=0.5498					

notion "X2Y2" in the table represents the regression variable x^2y^2, the number followed the X and Y is the power of the variable.

3.2.2.2 The forward stepwise statistic

Before we perform the forward stepwise statistic, we need mention the basic concepts used in this statistic, i.e., the statistic hypothesis test.

3.2.2.2.1 Statistic hypotheses test on the regression parameters for the deterministic content analysis

Once the regression estimators $\hat{\beta}$'s are computed from the q independent random test data $w(z)$ by the least square process, we need to examine the regression equations or models whether they are appropriate for the fitted data. In the regression process, we assume that the true parameters β's being estimated have specific values β_0's. Now, even if $\beta_k = \beta_{k0}$ for $k = 1, 2, 3, ..., p$, the estimated value $\hat{\beta}$'s will probably not come out exactly equal to β_0's, correspondingly, because there is estimating variability associated with $\hat{\beta}$'s depend on the different data set [13]. We hypothesize $\beta_k = \beta_{k0}$ and desire to know whether the estimated regression coefficients $\hat{\beta}$'s differ from the specific values β_0's correspondingly. If so, how much difference between the $\hat{\beta}$'s and β_0's must occur before the hypothesis should be rejected as being invalid. This situation requires us to perform a statistical test or hypothesis test of significance on the true values of the regression coefficients. This test provides an indicator of the degree of confidence that can be placed in the regressions. For the probability of any noted difference d_k between $\hat{\beta}_k$ and β_{k0} based upon the sampling distribution of $\hat{\beta}$'s, the estimated regression coefficients $\hat{\beta}_k$ falls into the rejection region if the probability of over a given difference d_k is smaller than the specified value α, i.e., p-

value = Prob.$\left\{\left|\hat{\beta}_k - \beta_{k0}\right| > d_k\right\} < \alpha$. In this case, the difference between $\hat{\beta}_k$ and β_{k0} would be considered significant. Thus, the hypothesis that $\beta_k = \beta_{k0}$ would be rejected. Figure 3-6 (a) shows this case. Specially, if $\beta_{k0} = 0$, Prob.$\left\{\left|\hat{\beta}_k\right| > d_k\right\} < \alpha$. On the other hands, if the probability of over a given difference d_k is large, i.e., p-value = Prob.$\left\{\left|\hat{\beta}_k - \beta_{k0}\right| > d_k\right\} > \alpha$, the difference between $\hat{\beta}_k$ and β_{k0} would be accepted as normal statistical variability. Figure 3-6 (b) shows this case. Again, if $\beta_{k0} = 0$, Prob.$\left\{\left|\hat{\beta}_k\right| > d_k\right\} > \alpha$. The hypothesis that $\beta_k = \beta_{k0}$ would be accepted in this case [13]. In our situation, we desire to know whether all or one of estimated regression coefficients significantly differs from zero, i.e., we want to test the hypothesis that the true regression coefficient β_k for $k = 1, 2, 3, ..., p$, differs from zero. In order words, we want to test that the β_k has no power to predict the $\hat{w}(z)$ in the model. Thus we perform two kinds of null hypothesis statistical tests. One is the hypothesis that performs an overall F-test, i.e., to simultaneously test the significance of all regression parameters β's taking together. Meanwhile, the MSE, R^2 and the p-values are obtained by running this test. The purpose of performing this test is to find the "good" reduced models from the full models. Another is the hypothesis that performs a student's t test or a partial F-test on the *individual* regression parameters β_k by using the experimental data $w(z)$'s to test whether the regression parameter $\hat{\beta}_k$ is different enough from the hypothesized value zero, i.e., $\beta_{k0} = 0$ for $k = 1, 2, ..., p$. Here, we perform a hypothesis test that β_k has no power in contribution to the model in order to conclude that the null hypothesis is unlikely to be true. Finally, we will conclude whether and which estimated parameters $\hat{\beta}$'s are significant or not in the model.

The general procedures used in testing a statistical null hypothesis is based on the concept

(a)

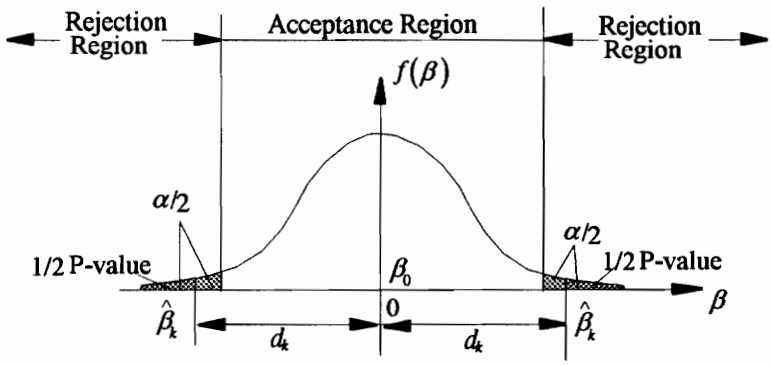

(b)

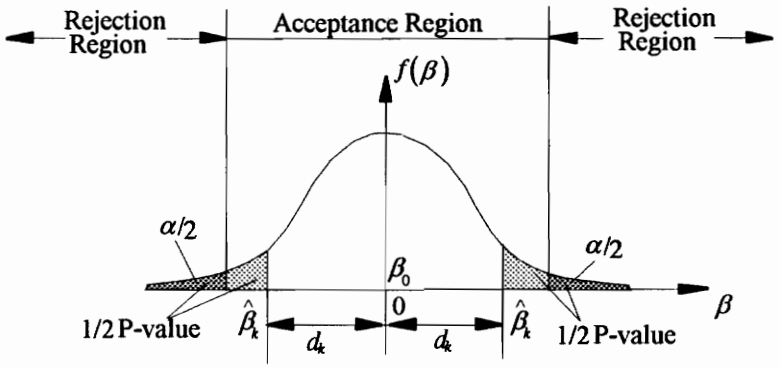

Figure 3.6 - A sketch of the distribution of $\hat{\beta}_k$ (a). An example of $\hat{\beta}_k$ falling into the rejection region; (b). An example of $\hat{\beta}_k$ falling into the acceptance region

of proof by contradiction. The procedures consist the following five steps:

1. State the null hypothesis, H_0, and the alternative hypothesis, H_1.

Two kinds of null hypotheses, i.e., (a) the overall hypothesis and (b). further hypothesis, are stated as follow:

(a). H_0: $\beta_1 = \beta_2 = \beta_3 = ... = \beta_p = 0$; where $1 \le p \le r$.

This is the overall hypothesis to test the significance of the overall regression, i.e., to test whether or not there is a regressive relation between the dependent variable $\hat{w}(z)$ and a set of p regression variables z's by hypothesizing that $w(z)$ is not related to the regression variables z's in such a way as in the model Eq. (3-11). In other words, all p regression variables z's taken together do not explain a significant amount of the dependent variable $\hat{w}(z)$ in the model. So a test on a set of β's that is equal to zero will be performed on the model against alternative hypothesis, which states that the all estimated parameters taken together or the overall regression is significant in this model and given later [17]. The overall hypothesis is used when comparing two regression models and finding the good one.

(b). H_0: $\beta_k = 0$, $k = 1, 2, 3, ..., p$, respectively, where $1 \le p \le r$.

This hypothesis is used to perform a student's t test or partial F-test test of whether a particular regression coefficient β_k equals zero while all β's taken together in the model. It hypothesizes that β_k has no regression power or is insignificant in the model. This hypothesis will be used when selecting a subset of the all regression variables and giving an indicator which regression variable with smallest insignificant power in the model and should being dropped first. By contradicting the null hypothesis and performing the

student's t or F test statistic that is given in detail later, we can easily verify whether the alternative hypothesis holds or not. The two kinds of alternative hypotheses, which argue with the null hypotheses above corresponding, are stated as follow:

For hypothesis (a). H_1: At least one of the β's is nonzero.

For hypothesis (b). H_1: $\beta_k \neq 0$, $k = 1, 2, 3, ..., p$; where $1 \leq p \leq r$.

2. Determine the rejection value or the region under the null hypothesis, e.g., $\pm t_{\alpha/2}$ for the student's t test, by specifying a significance level α. The α value is the weight of the evidence for rejecting the null hypothesis and represents the risk probability that we wrongly reject the H_0 when H_0 is true, (i.e., Prob.$\{reject H_0 \,/\, H_0 true\} = \alpha$). Figure 3-6(a) gives an example of the rejection region for a student's t test. If a test statistic (T.S.) falls into the rejection region, e.g., $|t_{TS}| > t_{\alpha/2}$ for the student's t test, we will reject the null hypothesis H_0 in favor of the alternative hypotheses H_1. It is generally specified for α to have a value such as 0.01, 0.05, 0.025, or 0.01. For example, if we choose α = 0.05, it means that we will be willing to take a 5 % risk to incorrectly reject the H_0 when H_0 is true. An alternative way is to use a p-value of the statistical test. For instance, p-value = Prob.$\{|t| \rangle t_{T.S.}\}$ for a student's t test, and if the p-value = Prob.$\{|t| \rangle t_{T.S.}\} < \alpha$, it means T.S. falls into the rejection region. So we will reject the null hypothesis H_0 and in favor of the alternative hypotheses H_1.

3. Specify the test statistic (T.S.) to be used and its distribution under, H_0.

The decision to accept the null hypothesis H_0 or reject H_0 in favor of the alternative hypothesis H_1 is based on a T.S., or based on the decision maker computed from the experimental fitted data. The purpose of the hypothesis test is to find the appropriate deterministic models for the experimental data and extract the most random content out of

the data. Thus, We assume a random variable ε_l, where l = 1, 2, 3, ..., q, has a normal distribution with an equal variance and mean zero as before. That means the experimental data $w(z)$'s have the same distribution with ε_l. Hence, we can use an overall F-test for hypothesis (a), and a student-t distribution to conduct a two-tailed student's t test or use a partial F-test for hypothesis (b). We state as follows [19]:

For hypothesis (a): $$\frac{MSR_{p-1}}{MSE_{q-p}} \sim \text{F}(p\text{-}1, q\text{-}p) \text{ under } H_0 \qquad (3\text{-}32)$$

The Eq. (3-32) states that under the null hypothesis H_0, the ratio of MSR to MSE, i.e., $\frac{MSR_{p-1}}{MSE_{q-p}}$, follows an F distribution with two parameters (p-1) which is the regression d.o.f. associated with MSR, and (q-p) which is the error d.o.f. associated with MSE. This hypothesis is used when testing whether the model explains a significant portion of variability.

For hypothesis (b): $$\frac{\hat{\beta}_k - 0}{s_{\hat{\beta}_k}} \sim t_{q-p} \text{ under } H_0 \qquad (3\text{-}33)$$

The Eq. (3-33) states that under the null hypothesis H_0, the ratio of $\frac{\hat{\beta}_k - 0}{s_{\hat{\beta}_k}}$ has a t distribution with (q-p) d.o.f. associated with $s_{\hat{\beta}_k}$, where $s_{\hat{\beta}_k}$ is the standard error of $\hat{\beta}_k$ and can be determined by sample standard deviation $\sqrt{s_\varepsilon^2}$ associated with the full model and the variance-covariance matrix A in Eq. (3-18) as follows: $s_{\hat{\beta}_k} = s_\varepsilon \sqrt{a_{k+1,k+1}}$, where $s_\varepsilon^2 = MSE$ given by Eq. (3-26) and $a_{k+1,k+1}$ is the diagonal term of the matrix A given in Eq. (3-18).

4. Compute the value of T.S., t or F.

For hypothesis (a): Since the TSS can be partitioned into SSR and SSE [17], the larger SSR is relative to SSE, the better the model "fits" the data. Therefore, we can form an overall F-test statistic based on the ratio of SSR to SSE. It represents the ratio of the explained variation to the unexplained variation divided by the corresponding d.o.f., i.e.,

$$\text{T.S.} \quad F = \frac{SSR\,/\,regression(d.o.f.)}{SSE\,/\,error(d.o.f.)} = \frac{SSR\,/\,(p-1)}{SSE\,/\,(q-p)} = \frac{MSR_{p-1}}{MSE_{q-p}}$$

with the regression d.o.f. = p-1; the error d.o.f. = q-p.

For hypothesis (b):

T.S. For a student's t-test: $t_{T.S.} = \dfrac{\hat{\beta}_k - 0}{s_{\hat{\beta}_k}} \sim t_{q-p}$

A student's t statistical test about β_k can be equally restated in the term of a partial F statistic, which also test the significant power of β_k while all other β's are taken together in the model and given as follows [14]:

T.S. For a partial F-test: $F^*_{T.S.} = \dfrac{MST_{(1)}(\beta_k\,/\,\beta_1,\ldots,\beta_{k-1},\beta_{k+1},\ldots,\beta_{p-1})}{MSE_{(q-p)}} \sim$ F(1, q-p);

The T.S. for a partial F-test has two parameters, where "1" associated with the regression d.o.f. of β_k, and (q-p) associated with the error d.o.f. of MSE.

It should be noted that a student's t test and a partial F-test are equivalent at: $F = F^*_{T.S.} = t^2_{T.S.} = t^2_{\alpha/2,q-p}$. The results of the tests will be put into the format of an "analysis of variances" and summarized in ANOVA table, which lists the sources of variability, the

sum of squares, their d.o.f., the mean squares and the overall F statistic associated with the hypothesis (a). Table 3.4-3.6 give ANOVA tables of the statistical tests.

5. Draw conclusions concerning rejection of H_0 if the test is significant.

For hypothesis (a):

A large F value of T.S. provides an evidence to reject H_0 in favor of H_1. We reject H_0 in favor of H_1 if $F_{T.S.} > F_{\alpha,dof_1,dof_2} = F_{\alpha,l_1,q-p}$, or the p-value = $\text{Prob.}\{F > F_{T.S.}\} < \alpha$.

For hypothesis (b):

In the student's t test: For d.o.f. = q-r and specified value α, we reject H_0 in favor of H_1 if $|t_{T.S.}| > t_{\alpha/2}$ or if the p-value = $\text{Prob.}\{|t| > t_{T.S.}\} < \alpha$.

In the partial F-test: We reject H_0 in favor of H_1 if $F^*_{T.S.} > F_{\alpha,dof_1,dof_2} = F_{\alpha,l_1,q-p}$, or the p-value = $\text{Prob.}\{F > F^*_{T.S.}\} < \alpha$.

where the values of $F_{\alpha,l_1,q-p}$ and $t_{\alpha/2}$ can be found in any statistical tables on percentage points of the student's t and F distributions when α and $(p\text{-}q)$ are specified.

3.2.2.2.2 The forward stepwise regression procedures

The forward stepwise regression procedures relate to a set of procedures that introduce regression variable in steps, one variable at a time. On the basis of the maximum increase in R^2 or the partial F value for entry a regression variable, it permits reexamination at every step. The first step [15] is to select the regression variable z_a that is the most correlated with $w(z)$, i.e., the z_a with Max. R^2, where $1 \le a \le r$; and fit the data in a simple linear regression model: $\hat{w}(z) = f(z_a)$. Then the program checks if z_a or β_a is significant

by a student's t statistic test (or a partial F statistic test $F_a^* = \frac{MSR(z_a)}{MSE(z_a)}$). If the test is not insignificant, the program terminates with no regression variable z's entering the model and adopts the model $w(x,y) = \overline{w}(x,y)$ as the best, where the $\overline{w}(x,y)$ is the sample mean of the data set; otherwise the program search for the second regression variable to enter the regression model. The next step is to fit all GLP regression models with two regression variables. For each such regression model, the program performs a set of partial F statistic tests and calculates T.S. $F_k^* = \frac{MSR(z_j / z_a)}{MSE(z_j, z_a)}$; where j = 1, 2, ..., a-1, a+1, ..., r-1. The variable z with the largest partial F value is the candidate to enter the model at the second stage. Another way is to check R^2 for all z's not in the regression equation at this stage, the variable z with the largest R^2 is the candidate to enter the model at the second stage. If the partial F test is significant, the second z variable, say z_b, where $1 \leq b \leq r$, is added to the model. Otherwise the program terminates. The third step that is the most important in the stepwise statistic is to examine whether any of the other variables already in the model should be dropped, i.e., the program performs a set of partial F tests again within the model. For our instance only one partial F test at this stage, i.e., $F^* = \frac{MSR(z_a / z_b)}{MSE(z_a, z_b)}$. The regression variable with the smallest partial F value is the candidate for deletion. If the partial F value falls below the specified α level, this variable is dropped from the model. Otherwise, it is retained. Therefore, a regression variable that entered at an early stage may, at a later stage, become wasteful because of its relationship with other regression variables now in the model. To check on this possibility, at each step a partial F-test or student's t test is conducted for every variable presently in the model [19]. After the variable with the smallest insignificant partial F value (if there is such a variable) is removed, the model is refitted with the remaining variables that stay in the model. The partial F tests are conducted similarly, and so on. For forward (entry a

regression variable), the procedures stop when all variables entered are significant (by partial F-test or student's t test on the individual regression parameter β's), i.e., the minimal F-value > F_α (specified F value) and no more regression variable can enter significantly. The summary of the stepwise procedure in Table 3.3 gives a clear example to illustrate these procedures for plate No.1's real velocity fields.

All these statistic processes mentioned above are performed by using the SAS software in IBM-PC mainframe. Appendix I provides a SAS program in doing the processes.

Table 3.4-3.6 list the best models and their statistical parameters given by forward stepwise regressions for the plates at the 208 Hz excitation frequency. In the stepwise procedures, all variables left in the models are significant at the 0.1500 level. No other variable met the 0.1500 significance level for entry into the model at the last step.

3.3 The final best GLP regression models for the velocity fields of the plates

In comparison with the top subset models obtained by the all possible regressions, the numbers of the regression variables in all the final stepwise models are less than that of the top C_p all-possible-regression models with different regression variables in the real and imaginary models for the same plate. The C_p values in the stepwise models are greater than that of the all-possible-regression models, so are the PRESS values. Therefore, the final best models for each plate at the corresponding frequency are determined as the second top C_p models for plate No.1 and No. 3, and the first top C_p model for plate No.2. These final GLP regression models for the velocity fields of the plates at the 208 Hz

Table 3.3 - An example to illustrate the procedures of the stepwise statistics

Summary of stepwise procedure for dependent variable real (SAS1288r data)

Step	Variable Entered	Removed	No. In	Partial R^2	Model R^2	C_p	F	Prob>F
1	XY4		1	0.0460	0.0460	22859.003	43.3215	0.0001
2	X7Y4		2	0.0274	0.0735	22177.635	26.5686	0.0001
3	X7Y		3	0.0843	0.1577	20080.993	89.6573	0.0001
4	XY		4	0.1000	0.2577	17593.392	120.5511	0.0001
5	X2Y4		5	0.0937	0.3514	15262.145	129.1582	0.0001
6	X6Y4		6	0.1121	0.4636	12471.801	186.6747	0.0001
7	Y		7	0.0466	0.5102	11313.425	84.8586	0.0001
8	X4		8	0.0173	0.5274	10885.816	32.5278	0.0001
9	X		9	0.0378	0.5653	9945.4775	77.4729	0.0001
10	X2		10	0.0445	0.6097	8840.6212	101.2484	0.0001
11	X2Y		11	0.1282	0.7379	5649.6654	434.4913	0.0001
12	Y4		12	0.1249	0.8628	2542.2404	807.3378	0.0001
13	X3		13	0.0228	0.8856	1977.0337	176.3914	0.0001
14		X2Y4	12	0.0000	0.8856	1975.5454	0.1591	0.6901
15	X7Y3		13	0.0185	0.9041	1516.6130	170.9721	0.0001
16	XY3		14	0.0158	0.9199	1124.8971	174.6649	0.0001
17	X5Y3		15	0.0063	0.9262	969.6803	75.6278	0.0001
18		X7Y4	14	0.0000	0.9262	968.5124	0.4003	0.5271
19	X7		15	0.0047	0.9309	853.3313	60.1791	0.0001
20		X2	14	0.0001	0.9308	852.7489	0.7280	0.3937
21	X4Y4		15	0.0018	0.9326	810.4348	23.3394	0.0001
22		XY4	14	0.0000	0.9326	808.5408	0.0558	0.8133
23		X6Y4	13	0.0000	0.9326	807.1562	0.3245	0.5691
24	X3Y1		14	0.0018	0.9344	764.1392	24.3799	0.0001
25	X6		15	0.0035	0.9378	680.0535	49.1583	0.0001
26		X4	14	0.0000	0.9378	678.2344	0.1033	0.7480
27	X4Y		15	0.0056	0.9434	541.1913	87.2231	0.0001
28	X2		16	0.0052	0.9486	413.9681	89.1461	0.0001
29	X6Y3		17	0.0011	0.9496	389.7853	18.4188	0.0001
30		X7Y3	16	0.0000	0.9496	388.8493	0.7484	0.3872
31	X5		17	0.0008	0.9504	371.9768	13.4675	0.0003
32		X6	16	0.0000	0.9504	369.9770	0.0002	0.9889
33	X6Y2		17	0.0007	0.9510	355.0255	12.2649	0.0005
34	X7Y3		18	0.0006	0.9516	343.0763	10.1980	0.0015
35	X4Y3		19	0.0009	0.9525	322.9991	16.4226	0.0001

Table 3.4 - The results of the stepwise for plate No.1 at 208 Hz

For imaginary velocity fields:

At the last step 43, variable X5Y entered, R^2 = 0.99366065, C_p = 89.07594145

The variables in model: X Y X2 Y2 XY X2Y XY2 X3 Y3 XY3 X3Y X4 Y4 XY4 X4Y4 X5 X5Y4
(N = 27) X5Y3 X5Y X6Y X6Y2 X6Y3 X7 X7Y X7Y2 X7Y3 X7Y4

ANOVA table (SAS12088I DATA)

	D.O.F.	Sum of Squares	Mean Square	F	Prob>F
Regression	27	51.04294876	1.89047958	5062.28	0.0001
Error	872	0.32564373	0.00037344		
Total	899	51.36859249			

PRESS = 0.9877

For real velocity data:

At the last step35, variable X4Y3 entered, R^2 = 0.952491, C_p = 322.999.

The variables in model: X Y X2 XY X2Y X3 XY3 X3Y Y4 X4Y X4Y3 X4Y4 X5 X5Y3 X6Y2 X6Y3
(N = 19) X7 X7Y X7Y3

ANOVA table (SAS1208R DATA)

	D.O.F	Sum of Squares	Mean Square	F	Prob>F
Regression	19	17.05817241	0.89779855	928.59	0.0001
Error	880	0.85082233	0.00096684		
Total	899	17.90899474			

PRESS= 1.3320

Table 3.5 - The results of the stepwise for plate No.2 at 208 Hz

For imaginary velocity fields:

At the last step 49: variable X6Y3 entered, $R^2 = 0.98819312$ $C_p = 97.92493367$.

The variables in model: X Y X2 Y2 XY XY2 X2Y2 X3 Y3 XY3 X3Y3 X3Y Y4 XY4 X3Y4 X2Y4
(N = 25) X4Y4 X5 X5Y4 X5Y X6Y3 X6Y4 X7 X7Y X7Y4

ANOVA table (SAS2208I DATA)

	D.O.F.	Sum of Squares	Mean Square	F	Prob>F
Regression	25	66.66814636	2.66672585	2926.03	0.0001
Error	874	0.79654741	0.00091138		
Total	899	67.46469377			

PRESS = 0.8612

For real velocity data:

At the last step38, variable X2Y4 entered, $R^2 = 0.95895301$, $C_p = 39.63202712$

The variables in model: X Y X2 Y2 XY X2Y XY2 X3 Y3 XY3 X3Y Y4 XY4 X2Y4 X5 X5Y4 X5Y3
(N = 26) X5Y2 X5Y X6 X6Y X6Y3 X6Y4 X7 X7Y3 X7Y4

ANOVA table (SAS2208R DATA)

	D.O.F.	Sum of Squares	Mean Square	F	Prob>F
Regression	26	18.36442821	0.70632416	787.92	0.0001
Error	873	0.78259184	0.00089644		
Total	899	19.14702004			

PRESS = 0.8329

Table 3.6 - The results of the stepwise for plate No.3 at 208 Hz

Imaginary velocity data:

At the last step 47, variable X4Y2 entered, $R^2 = 0.9950301$, $C_p = 53.60588$

Variables in model: (N=31) X Y X2 Y2 XY X2Y XY2 X2Y2 Y3 XY3 X3Y X3Y2 X3Y4 X4 Y4 XY4 X4Y2 X4Y3 X4Y4 X5 X5Y4 X5Y3 X5Y2 X5Y X6 X6Y2 X7 BX7Y X7Y2 X7Y4

ANOVA table (SAS3208I DATA)

Source	D.O.F.	Sum of Squares	Mean Square	F Value	Prob>F
Model	31	55.27219	1.78297	5601.813	0.0001
Error	868	0.27627	0.00032		
C Total	899	55.54847			

PRESS = 0.3098

For real velocity data:

At the last step35, variable X2Y entered, $R^2 = 0.95145379$, $C_p = 196.42772519$

Variables in model: (N=25) X Y X2 Y2 XY X2Y XY2 X2Y2 Y3 XY3 X3Y X3Y2 X3Y4 X4 Y4 XY4 X4Y2X4Y3 X4Y4 X5 X5Y4 X5Y3 X5Y2 X5Y X6 X6Y2 X7 X7Y X7Y2 X7Y4

ANOVA table (SAS3208R DATA)

Source	D.O.F.	Sum of Squares	Mean Square	F Value	Prob>F
Model	21	12.11303242	0.57681107	819.42	0.0001
Error	878	0.61804563	0.00070392		
C Total	899	12.73107806			

PRESS = 0.8517

frequency are shown by 3-D graphic plots and given in Fig. 3.7-3.9. Each figure contains six 3-D subplots that give the original data plots, the fitted model plots in real and imaginary receptively, and the corresponding residual subplots.

3.4 Residual analysis for checking model assumptions

After the best-fitted models of the velocity data for all plates are obtained, we still need to make sure whether the models are built on the correct assumptions that we stated before. That is to say, we need check the violations of the model assumptions and examine the aptness of models. Residual analysis provides an attempt to discern which assumptions are being violated, and it can be done through graphic analyses or the related statistical tests. The graphic analysis is very clear and easy to explain and be understanding. By performing the residual analysis, we can check whether the models departure from assumptions and make sure there is on any important regression variables omitted from the models.

Recall that our model assumptions on the random error ε_l for the GLP regression model Eq. (3-10), they are stated again as follow:

(1). Zero expectation: $E(\varepsilon_l) = 0$ for all l.

(2). Constant variance: $V(\varepsilon_l) = \sigma_\varepsilon^2$ for all l.

(3). ε_l is normally distributed.

(4). The ε_l is independent.

Considering that the assumptions for our models are written in terms of the random error ε_l, it is reasonable to check the assumptions by using the residuals that are the estimates of the ε_l, i.e., $w_l(z) - \hat{w}_l(z)$.

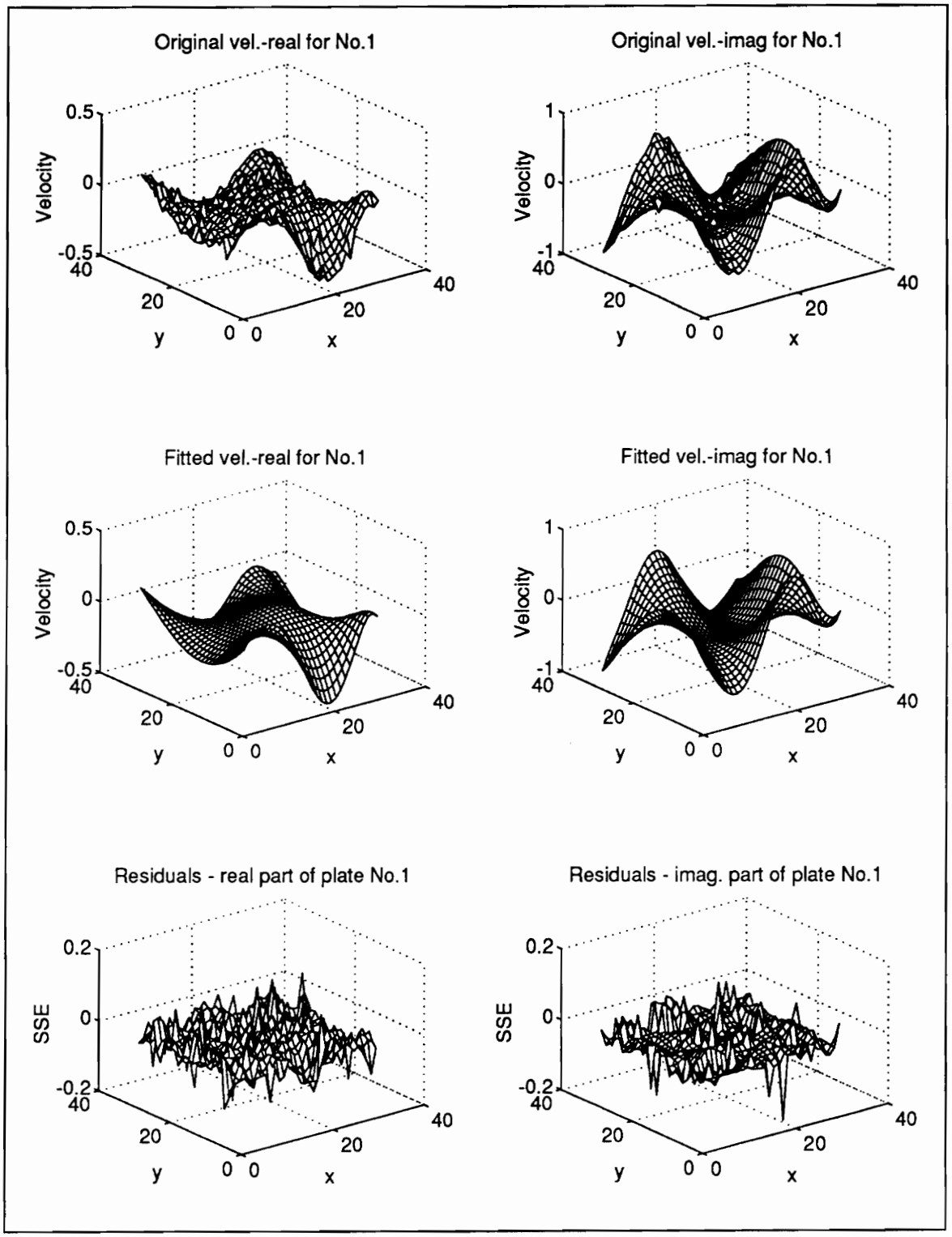

Figure 3.7 - 3-D plots of plate No.1's original data, fitted model and their residuals

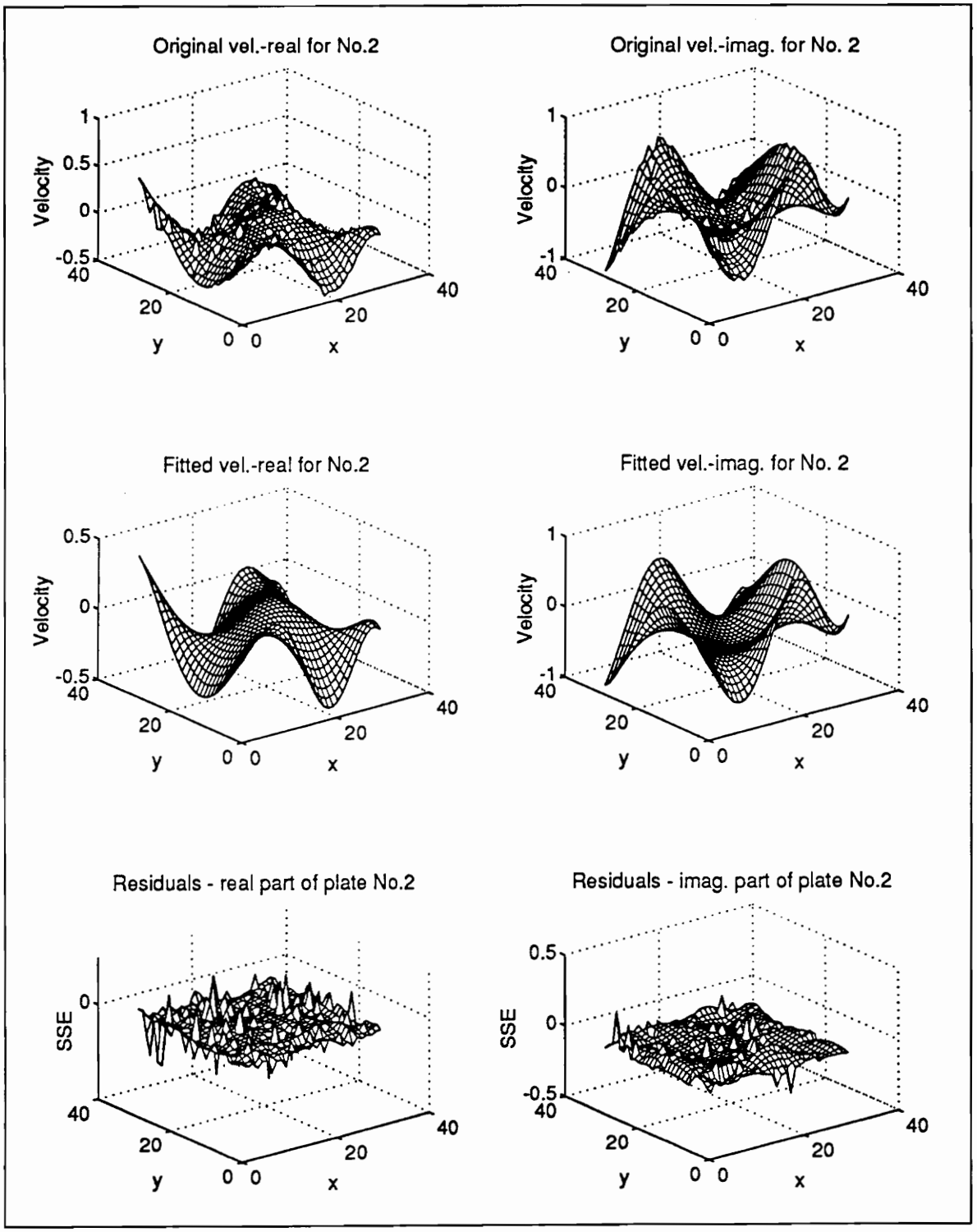

Figure 3.8 - 3-D plots of plate No. 2's original data, final fitted models and their residuals

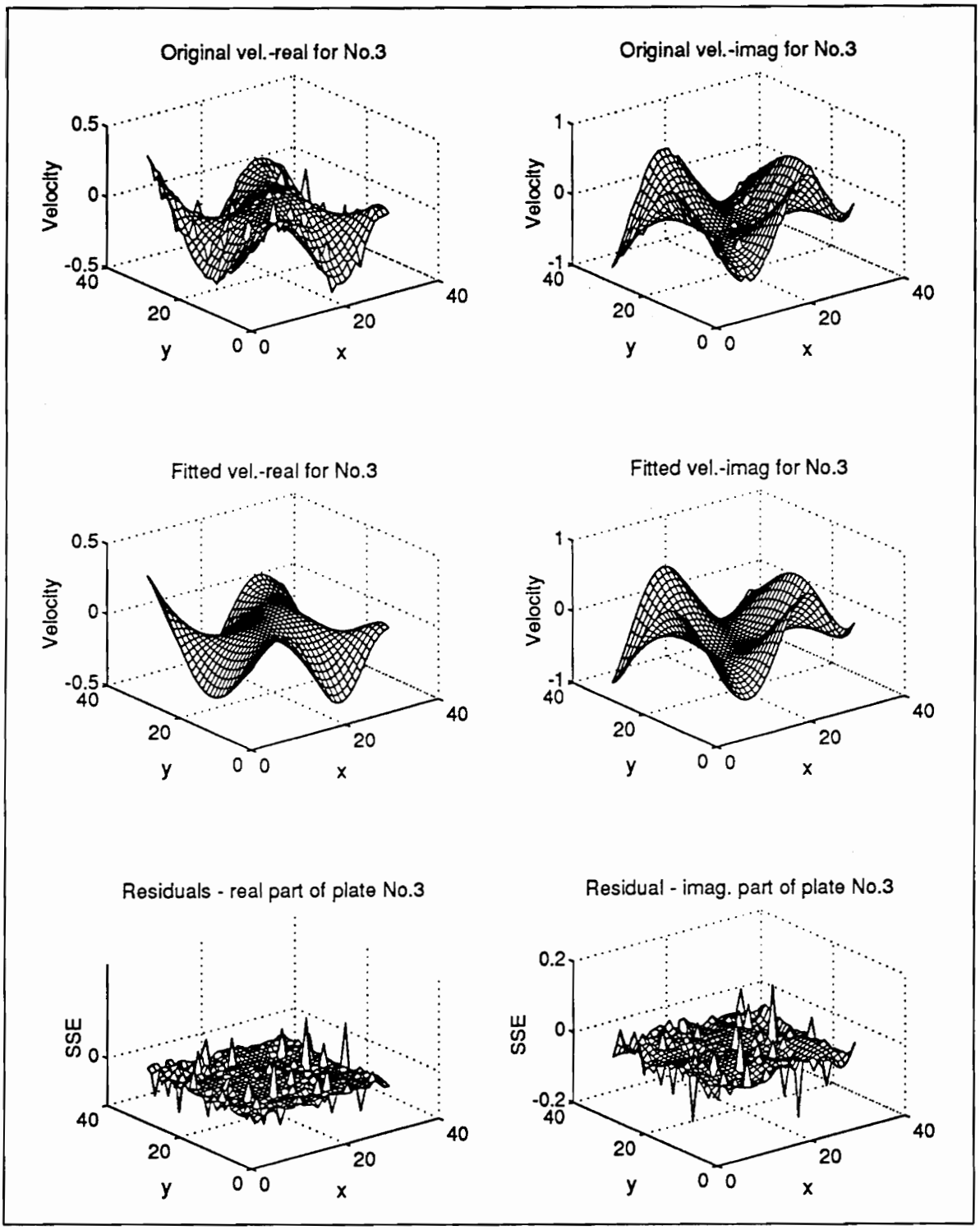

Figure 3.9 - 3-D plots of plate No. 3's original data, final fitted models and their residuals

The zero expectation assumption deals with the model selection. The examination of the assumption provides an indication of whether or not additional regression variables need to be included in the model. If $E(\varepsilon_l) = \Delta_l \neq 0$, it means that some deterministic content is not included in the model and has been put into the ε_l. Therefore, the additional regression variables should be added into the model. The assumption can be inspected by calculating the estimate of the error expectation, $\hat{E}(\varepsilon_l)$, as follows:

$$\hat{E}(\varepsilon_l) = \hat{E}[w_l(z) - \hat{w}_l(z)] = \frac{1}{q}\sum_{l=1}^{q}[w_l(z) - \hat{w}_l(z)] \tag{3-34}$$

where $w_l(z)$ represents velocity test data, $\hat{w}_l(z)$ represents the corresponding fitted velocity values, and l represents the data index number from 1, 2, ..., 900. Table 3.7 gives the computational results of $\hat{E}(\varepsilon_l)$'s for all plates at the 208 Hz. From Table 3.7 it is easily noticed that all $\hat{E}(\varepsilon_l)$ values are relatively small when compared to the velocity data. That means the $\hat{E}(\varepsilon_l)$ can be ignored, i.e., $\hat{E}(\varepsilon_l) \approx 0$. Hence the zero expectation assumption holds.

Table 3.7 - The computational results of $\hat{E}(\varepsilon_l)$ at 208 Hz

	Velocity fields	$\hat{E}(\varepsilon_l)$ $(\times 10^{-16})$
Plate No. 1	Real	-0.3227
	Imag.	0.8234
Plate No. 2	Real	-0.0611
	Imag.	0.9421
Plate No. 3	Real	0.0362
	Imag.	-0.1564

The constant or homogeneous error variance assumption can be examined by plots of residuals against the fitted values, i.e., $w_l(z) - \hat{w}_l(z)$ Vs. $\hat{w}_l(z)$. The equal variance assumption holds if the magnitudes of the residuals are general constant with the magnitudes of the varied fitted values. In contrast, if the magnitudes of the residuals are general increasing or deducting with the magnitudes of the fitted values, this indicates a possible unconstant variance. The reason to check this assumption is that if the assumption is violated, the least square estimates, i.e., the regression parameters $\hat{\beta}$'s, may not be as accurate as expected. Otherwise, another technique, e.g., the weighted least square process, should be applied instead of the least square process. Figure 3.10 gives a SAS plot of residuals against the fitted values yhat = $\hat{w}_l(z)$ of plate No. 1 at the 208 Hz as an example. From the plots it can be observed that the most of the magnitudes of the residuals lie between -0.025 to +0.025. A few residuals distribute beyond this bound. The number of $|residuals| > 0.025$ equals $n_{up} + n_{down} = 9 + 14 = 25$. This takes up approximate 2.7% of the total 900 residuals. Since the number of outliers is relatively small, the magnitudes of the residuals can still be approximately considered unchanged or constant. Therefore, the assumption still holds.

On the bases of the fact that the student's t and F distributions are dependent on the samples that are taken from a normal distribution, once the student's t test or F-test performed, the assumption that ε_l is normally distributed should be held. This assumption can be inspected through a plot of the residuals in the form of a histogram. Any skewness of the plot and outliers (which are the extreme values in regression variable direction) indicate unnormality. Taking plate No. 1 at the 208 Hz data set as checking example, Figure 3.11 gives a plot of the histogram and the plot of the normality statistical test on the model. From the histogram plot it can be easily observed that the distribution of the

Figure 3.10 - A SAS plot of residuals against the fitted values $\hat{w}_l(z)$ = yhat

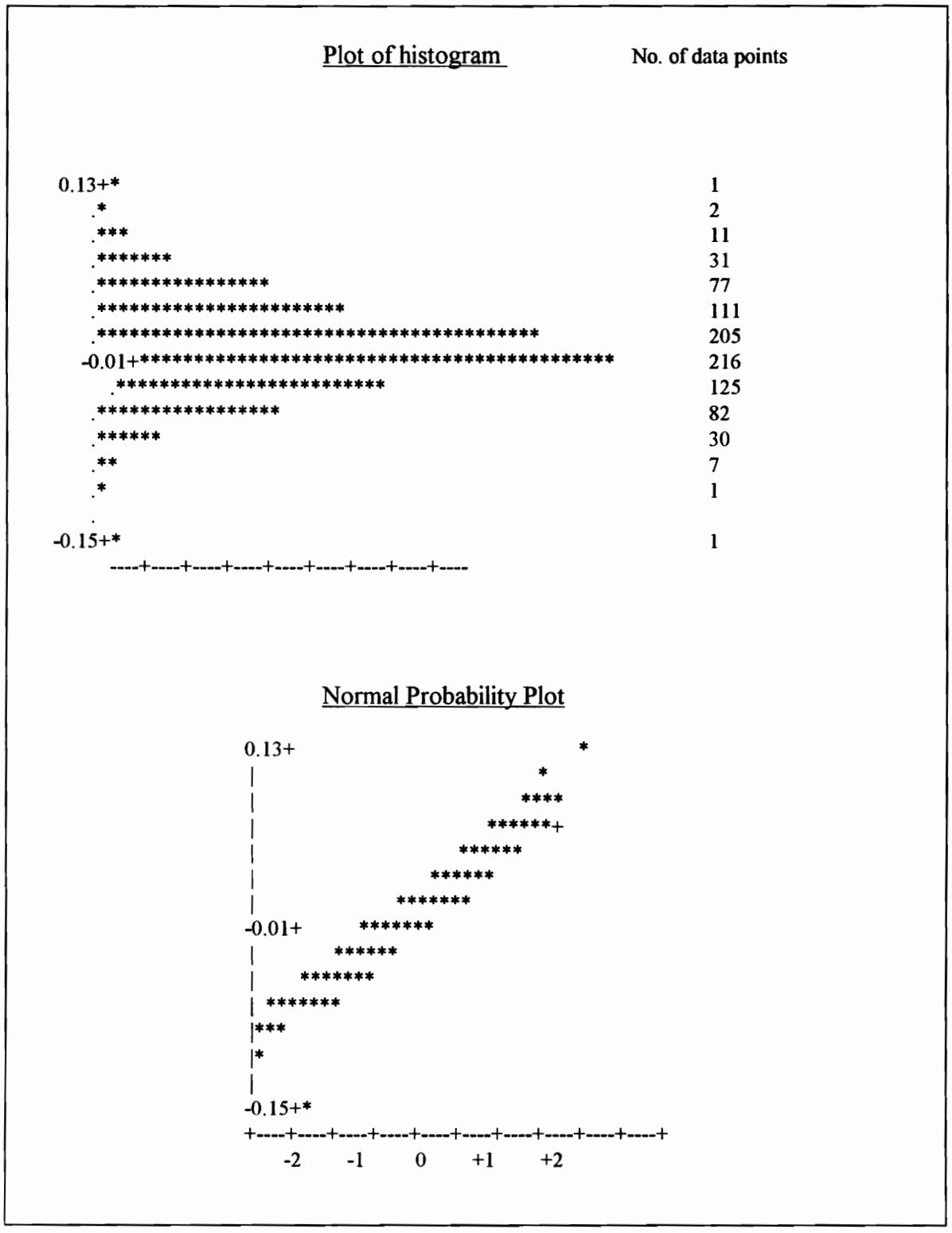

Figure 3.11 - Normality assumption check

residuals is symmetrical on zero and appears in nice normal distribution shape. It suggests that the ε_i is normal. Meanwhile, a normal probability plot is also given to detect the normality. The normal probability plot will be approximately a straight line if the residuals are normal. Both two plots indicates that the assumption holds.

When the data are taken at successive points in time, analysis of residual DFTs can be used to approximately examine whether the ε_is are statistically random. The residuals will be considered as uncorrelated or random in statistical sense if there is no any frequency component that is much larger than others in DFT, no any frequency component that dominates in DFTs. Hence, the residuals are independent. Figure 3.12 gives 3-D plots of residual DFTs for the data taken at the 208 Hz as an example. From the plots it is easily observed that no one frequency dominates in DFT plots. Therefore, the residuals are approximately random and the assumption holds.

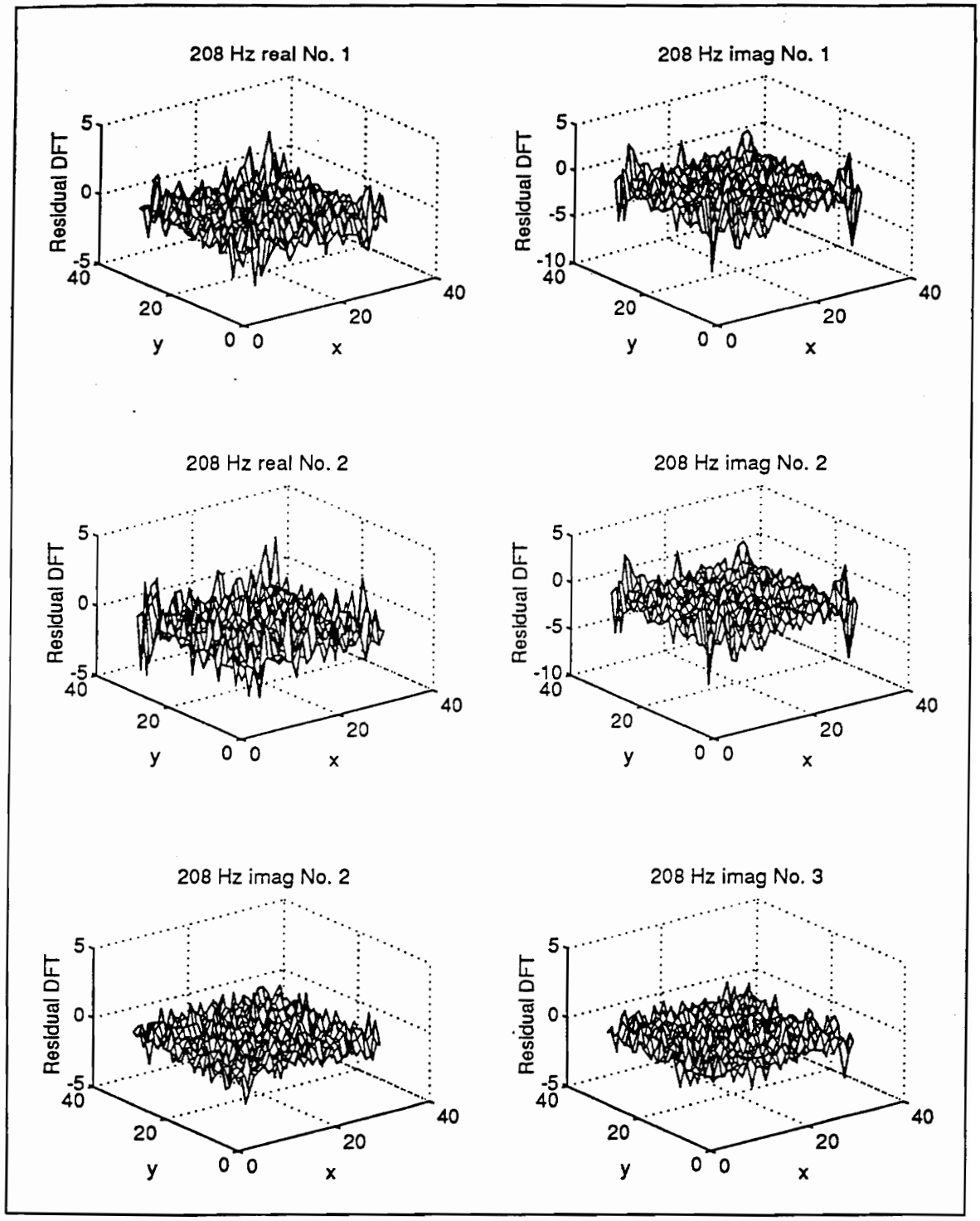

Figure 3.12 - 3-D plots of residual DFTs at 208 Hz

CHAPTER IV

CORRELATION COEFFICIENTS AND DAMAGE DIAGNOSTICS

4.1 Introduction

On the basis of the final best regression models (which represent the velocity fields of the plates), it is possible by further analyses to reveal some useful information hidden in the models. This chapter focuses on developing the methods not only to distinguish differences among the models (which are finally used to recognize the damaged plates) but also to identify the locations of the differences or damages. To conduct further analyses, first, the correlation coefficients between the different plate's fitted models are computed in an attempt to investigate the differences of the fitted models between the known undamaged plate and the other plates. Then the spatial correlation coefficients on the fitted models as well as t' statistical tests on the two means of corresponding SCCs are developed to identify the damaged plates. Once the damaged plates are recognized, the curvature models are developed to display the local effects due to the damage in strain fields of the plates. In order to identify the locations of the damage, the spatial correlation coefficients on the curvature models are calculated to numerically compare the consistency of the corresponding strain fields. The smallest spatial correlation coefficient indicates the location with most inconsistency in the strain fields between the two compared strain fields. Hence, the locations of the largest difference that may be due to the physical damage in the plates is identified. In addition, the consistency of the repeated test data for the same plate under the same test conditions is also investigated in this chapter.

4.2 Definitions of correlation coefficients and spatial correlation coefficients

4.2.1 Definition of correlation coefficients

The correlation coefficient (CC) is a measure of the strength of the relationship between two variables or any two data sets. The CC gives an indicator that quantitatively depicts the degree of consistency between the two variables or the two data sets. If there are two data sets, say X and Y, where $X=[x_1,x_2,...x_n]$ and $Y=[y_1,y_2,...y_n]$, the correlation coefficient square based on the sample data, denoted by ρ_{xy}^2, is defined as:

$$\rho_{xy}^2 = \frac{\left|\sum_{j=1}^{n} x_j \cdot y_j^*\right|^2}{(\sum_{j=1}^{n} x_j \cdot x_j^*)(\sum_{j=1}^{n} y_j \cdot y_j^*)} \tag{4-1}$$

Equation (4-1), especially, provides a measure of the least square deviation of the points from the straight line correlation. The ρ_{xy}^2 values are bounded between one (1.0) and zero (0.0). The CCs between the different plate's fitted models or curvature models indicate the consistency between the different plate's velocity fields or strain fields. So long as the CCs are computed, the differences, if any, between the models can be quantitatively represented. Based on the fact that any damage in the plates could alter their dynamic properties somehow or somewhere (e.g., the stiffness or strain of the plates), the velocity fields of the damaged plate will consequently be changed when compared with that of the undamaged plate. This results in the differences of the two compared velocity fields. Accordingly, the damage identification could be carried out by the recognition of the difference. In order to detect the damaged plates, all plates are supposed with the same physical, dynamic and geometry properties before any of them is damaged.

On the other hand, the CCs between the same plate's fitted models indicate the consistency between the same plate's velocity fields, where the models are established on the repeated test data of the plate under the same test conditions. Analyzing these CC values enables one to investigate how the acquired data from each individual plate is affected when the experiments are repeated under the same test conditions on different days. Hence, the consistency of the repeated test data can be evaluated.

4.2.2 Spatial correlation coefficients

A spatial correlation coefficient (SCC) gives an quantitative comparison of the correlation relationship between the corresponding subareas on the two compared dimensional areas. It plays an important role when the locations of differences between the two compared objects are tried to be found. The critical step to identify the locations of the damage is to found where the differences in the velocity fields between the two different plates appear. Therefore, developing the SCC for the velocity fields is a good procedure to fulfill the purpose. The SCC can be described as the relationship among values of some variables that are attributable to the manner in which the corresponding area units are ordered or arranged on a planar surface [20]. For example, the velocity fields of the plates are a kind of data set that each data point is associated with a particular position in the plates, therefore, the velocity fields are the area units. If the area units are divided into several arranged subareas, the CC between the corresponding two-subarea is called a SCC of the two compared area units. By calculating the SCCs between the different plate's velocity fields or curvature models, the consistency of the velocity fields or the strain fields in the corresponding subareas of the plates can be estimated.

In order to do so, each plate is split into $Q \times R$ equal subareas, each subarea contains $\left(\frac{n}{Q}\right) \times \left(\frac{m}{R}\right)$ scanned points, where n and m are the numbers of the scanned row and column respectively. In this research, each plate is split into $Q \times R = 5 \times 6$ equal subareas (see Fig. 4.1 (a)). Each subarea contains 5-row by 6-column scanned points, i.e., 30 scanned points. The SCC is then calculated in each two-compared-subarea. No matter the velocity data that comes from the same plate by repeating the tests on different days or from the different plates on the same day test, the scanned data of the plates can always form $a \times b$ individual SCCs over the corresponding plates. Each SCC is noted by $\rho_{AcBd,f}(i,j)$, where $i = 1, 2, \ldots, Q$, $j = 1, 2, \ldots, R$ are the row and column index, respectively; A, B =1, 2, 3 are the plate number index, where the corresponding plate definition are given in Fig. 2.1; the integers for c and d are the index numbers of the experiments. Figure 4.1 (b) gives an example of the notations. For $Q \times R = 3 \times 3$, $\rho_{AcBd,f}(i,j) = \rho_{1121,300}(2,3)$ is the SCC of the 2nd row and the 3rd column subareas between plate No. 1's 1st experiment and plate No. 2's 1st experiment at the 150 Hz excitation frequency. For two 2-D data sets X and Y, where $X = [x(i,j)]$ and $Y = [y(i,j)]$, when each 2-D area is split into $Q \times R$ equal subareas, the squared SCC is defined as follows:

$$\rho^2_{AcBd,f}(k_0,j_0) = \frac{\left| \sum_{k=(k_0-1)\times 10+1}^{k_0 \times \left(\frac{a}{n}\right)} \sum_{j=(j_0-1)\times 10+1}^{j_0 \times \left(\frac{b}{m}\right)} x_{kj} \cdot y^*_{kj} \right|^2}{\left(\sum_{k=(k_0-1)\times \left(\frac{a}{n}\right)+1}^{k_0 \times \left(\frac{a}{n}\right)} \sum_{j=(j_0-1)\times \left(\frac{a}{n}\right)+1}^{j_0 \times \left(\frac{a}{n}\right)} x_{kj} \cdot x^*_{kj} \right) \left(\sum_{k=(k_0-1)\times \left(\frac{b}{m}\right)+1}^{k_0 \times \left(\frac{b}{m}\right)} \sum_{j=(j_0-1)\times \left(\frac{b}{m}\right)+1}^{j_0 \times \left(\frac{b}{m}\right)} y_{kj} \cdot y^*_{kj} \right)} \quad (4\text{-}2)$$

The 3rd part of the Matlab program performs the SCC calculations. This is discussed in detail later.

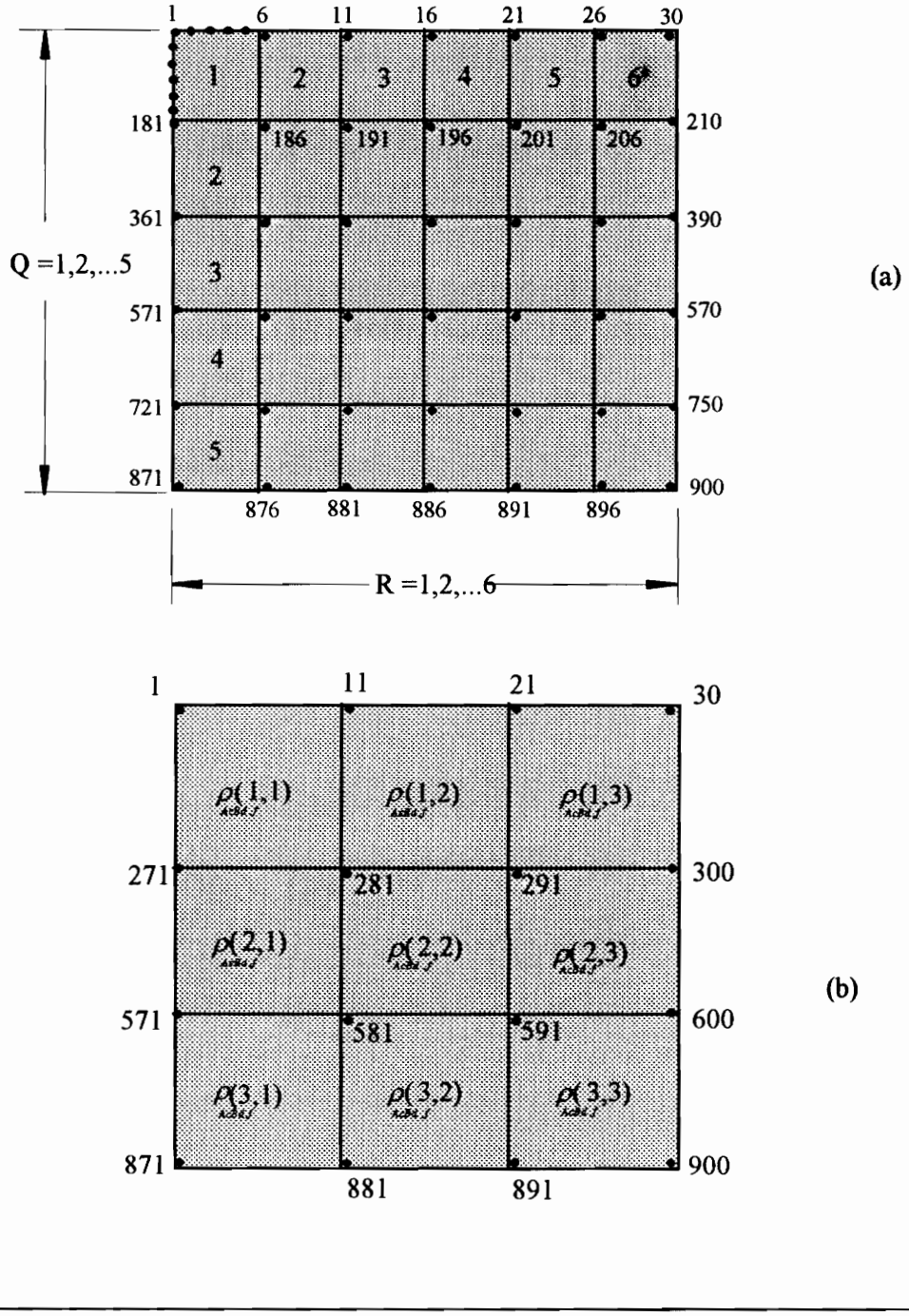

Figure 4.1 - (a). Plate and associated SCC sample areas
(b). Spatial correlation coefficient representation

4.3 Curvature models of the velocity fields of the plates

According to the definition of strain-displacement relations, normal strain is the ratio of change in length to the original length. Shear strain is defined as the amount of change in a right angle [21]. Since the plates are very thin and hung from the ceiling, there is no restraint perpendicularly to the plate plane. The vibration of the plates can be classified as a "plane stress" state in which the normal strain, ε_z, and the shear strains, γ_{yz} or γ_{zx}, can be ignored. Therefore, the two-dimensional strain-displacement relations of the plates can be expressed as follows:

$$\begin{Bmatrix} \varepsilon_x \\ \varepsilon_y \\ \gamma_{xy} \end{Bmatrix} = \begin{bmatrix} \dfrac{\partial}{\partial x} & 0 \\ 0 & \dfrac{\partial}{\partial y} \\ \dfrac{\partial}{\partial y} & \dfrac{\partial}{\partial x} \end{bmatrix} \begin{Bmatrix} u \\ v \end{Bmatrix} = \begin{bmatrix} \dfrac{\partial u}{\partial x} \\ \dfrac{\partial v}{\partial y} \\ \dfrac{\partial u}{\partial y} + \dfrac{\partial v}{\partial x} \end{bmatrix} \tag{4-3}$$

where ε_x and ε_y are the normal strain in x and y direction, respectively; γ_{xy} is the shear strain in the x-y plane; $u = u(x,y)$ and $v = v(x,y)$ are the displacements parallel to the plate plane and normal to each other. According to the small bending deformation theory of thin plates, there is no deformation in the midsurface plane of the plates are assumed, the displacement fields u and v at a distance z from the neutral surface can be expressed in terms of the lateral displacement w as follow:

$$\begin{aligned} u &= u(x,y) = -z\frac{\partial w(x,y)}{\partial x} = -zw_{,x} \\ v &= v(x,y) = -z\frac{\partial w(x,y)}{\partial y} = -zw_{,y} \end{aligned} \tag{4-4}$$

Substituting Eq. (4-4) into (4-3) gives:

$$\begin{Bmatrix} \varepsilon_x \\ \varepsilon_y \\ \gamma_{xy} \end{Bmatrix} = \begin{Bmatrix} -z\dfrac{\partial^2 w}{\partial x^2} \\ -z\dfrac{\partial^2 w}{\partial y^2} \\ -z\dfrac{\partial^2 w}{\partial x \partial y} - z\dfrac{\partial^2 w}{\partial y \partial x} \end{Bmatrix} = \begin{Bmatrix} -zw_{,xx}(x,y) \\ -zw_{,yy}(x,y) \\ -2zw_{,xy}(x,y) \end{Bmatrix} \qquad (4\text{-}5)$$

where the second partial derivative with x, $w_{,xx}$, is the curvature of the displacement field in a plane parallel to the xz-plane. The second partial derivative with y, $w_{,yy}$, is the curvature of the displacement field in a plane parallel to the yz-plane, and the second cross partial derivative with x and y, $w_{,xy}$, is the twist curvature of the displacement field [22].

From Eq. (4-5), it is obvious that the curvatures of the plates are directly related to the corresponding strains of the plates. For a constant distance z, the strains are directly proportional to the corresponding curvatures, any change in the strains will cause the proportional change in the corresponding curvatures. In addition, the curvatures are the functions of the coordinates x and y and relate to the locations of the plates, i.e., they display the local effects of the changes in the strains of the plates. The large difference in curvatures indicates a significant change in the plate's strain field. Therefore, the maximum values in ε_x or ε_y plays an important role to indicate the locations of the changes in structures due to the change in their strain fields. This is why the damage information can theoretically be detected by investigating the changes in the curvatures of the plates. In our cases, the damaged plates are cut somewhere in the x direction, as a result, the normal strain in y direction will increase due to the decrease in the y direction's stiffness of the damaged area for the plates. On the basis of this fact, the curvature models (which are the second partial derivatives with respect to coordinates x or y over the fitted models of the velocity fields) are used to display the local variations of the strain fields due to the

damage in the plates. Finally, the SCCs on the curvature models are computed to identify the locations of the damage.

It should be pointed out that, in this research, the displacement fields in the Eq. (4-5) are replaced by the corresponding velocity fields. In the steady state, the dynamic responses of displacement, velocity and acceleration are only different in constant $i\omega$ and ω^2, where ω is angular frequency, so the curvature mode shapes for velocity and acceleration are also proportional to that on displacement. Considering the specified sinusoidal excitation frequency, the difference between the velocity fields and the displacement fields of the same plate is a constant value in magnitude and phase. For example, if the displacement field of a plate can be expressed as:

$$w(x,y,t) = W(x,y)T(t) = W(x,y) \times A_0(\cos\omega t + i\sin\omega t) = A_0 \cdot W(x,y)e^{i\omega t} \qquad (4\text{-}6)$$

where i is an imaginary unit and equals $\sqrt{-1}$. A_0 and ω are the amplitude and the angular frequency of the excitation force, respectively (ω is in [rad/s] and equals $2\pi f$ in Hz). Substituting the displacement into the velocity expression of the plate results in the following equation:

$$v(x,y,t) = \frac{dw(x,y,t)}{dt} = W(x,y)\frac{dT(t)}{dt} = i\omega A_0 W(x,y)e^{i\omega t} = i\omega w(x,y,t) \qquad (4\text{-}7)$$

Comparing the Eq. (4-6) and (4-7), the only difference between the velocity field and the displacement field is the complex constant $i\omega$. In other words, the velocity fields, $v(x,y,t)$, can be obtained by multiplying the constant ω and turning the displacement field, $x(x,y,t)$, 90° counterclockwise in complex plane. Therefore, the velocity fields are proportional to the displacement fields in magnitudes, but the two fields are 90° out of phase with each other. Taking the velocity field instead of the displacement field in Eq. (4-5) gives:

$$\begin{Bmatrix} \varepsilon_x \\ \varepsilon_y \\ \gamma_{xy} \end{Bmatrix} = \frac{1}{i\omega} \begin{Bmatrix} -zw_{,xx} \\ -zw_{,yy} \\ -2zw_{,xy} \end{Bmatrix} \tag{4-8}$$

where, the physical relationship between the strains and curvatures of the plates still holds.

The second part of the Matlab program computes the curvature models, i.e., the second partial derivatives with respect to x and y of the velocity fields for the plates. The source code will be discussed in section 4.4 D. Figure 4.2 - 4.4 show the computed curvature models of the final regression models for all plates at 208 Hz frequency.

4.4 Calculations of CCs and SCCs of the velocity fields of the plates

The purpose of writing this section is three-fold. First, in an attempt to distinguish which models are associated with the damaged plates and which model is associated with the undamaged plate. Meanwhile, the CCs among the different plate's final models are calculated. When the velocity fitted models between the undamaged and damaged plates are compared, the small CC value could give a clue to recognize the damaged plate. This topic is discussed in Section 4.4.1. Once the damaged plates were identified, the second step is to investigate where the damage has occurred in the plates. For this purpose, the SCCs on the curvature models between the undamaged and damaged plates are calculated. The small values of the SCCs indicate the locations where the corresponding velocity fields are less correlated. This could indicate the locations where the damage appears. At this step, the curvature models based on the final best regression models for each plate are calculated first. And then the corresponding SSCs on these curvature models are calculate. Meanwhile, the SCCs on the final regression models are also computed for constructing

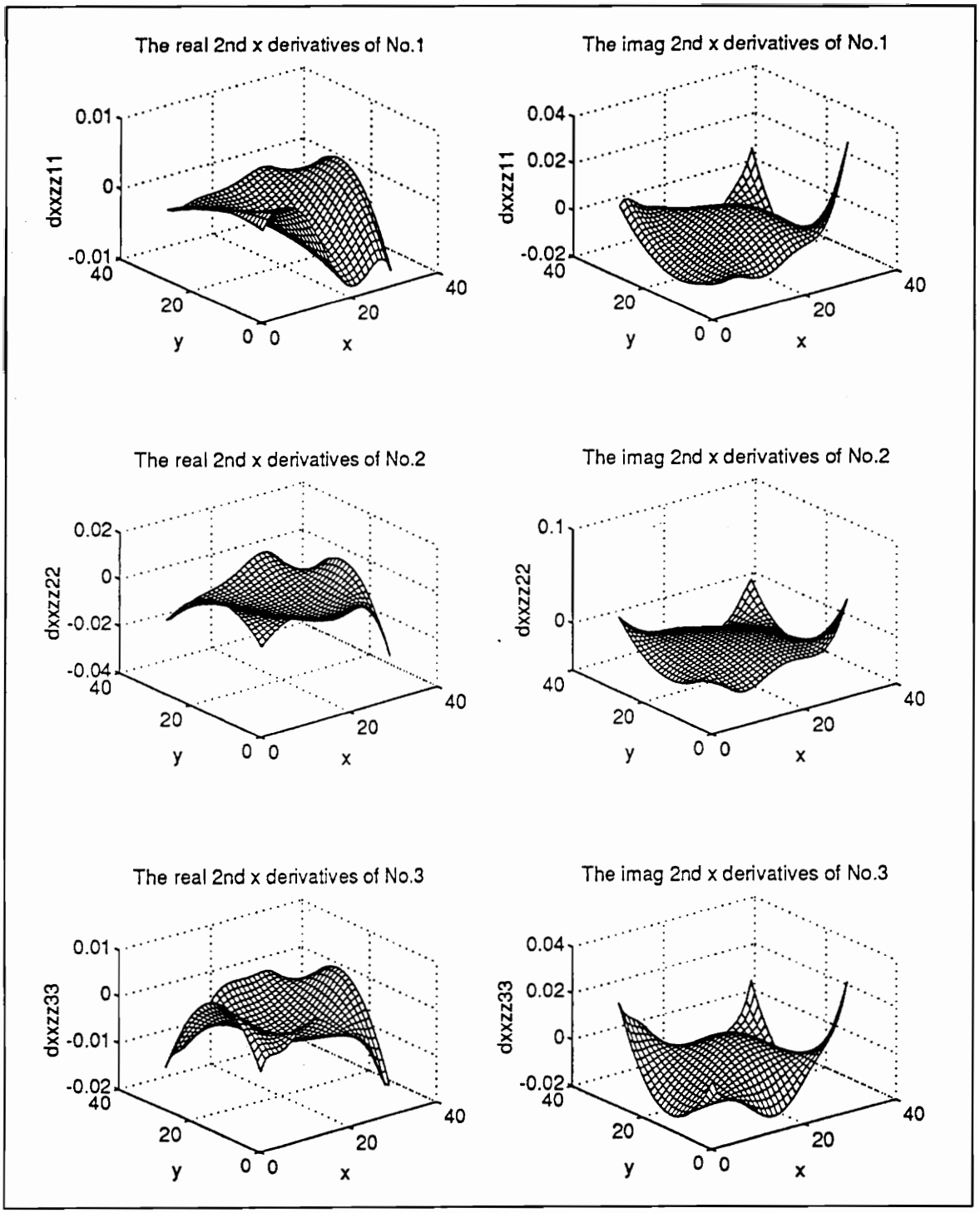

Figure 4.2 - Curvature models in x direction at 208 Hz

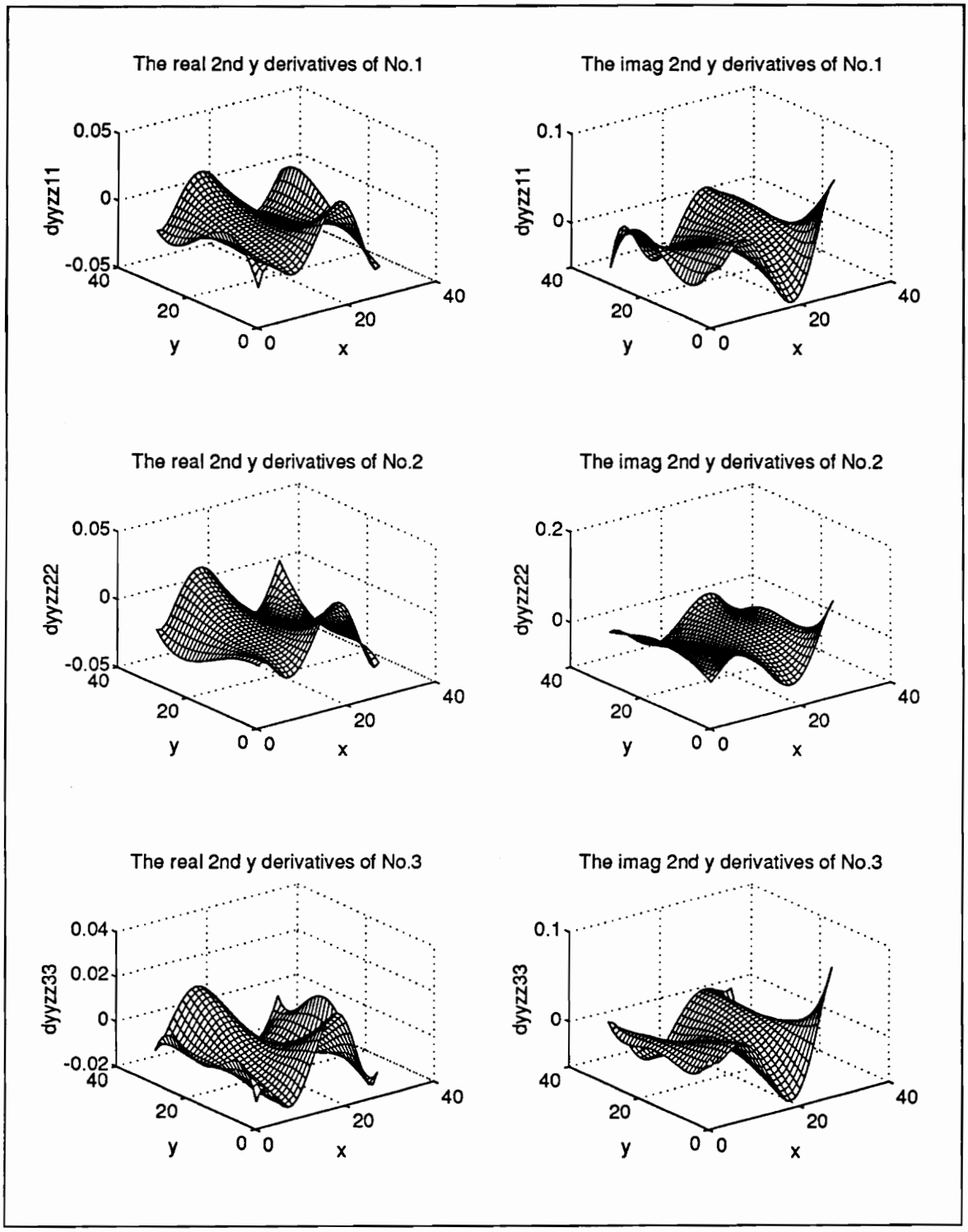

Figure 4.3 - Curvature models in y direction at 208 Hz

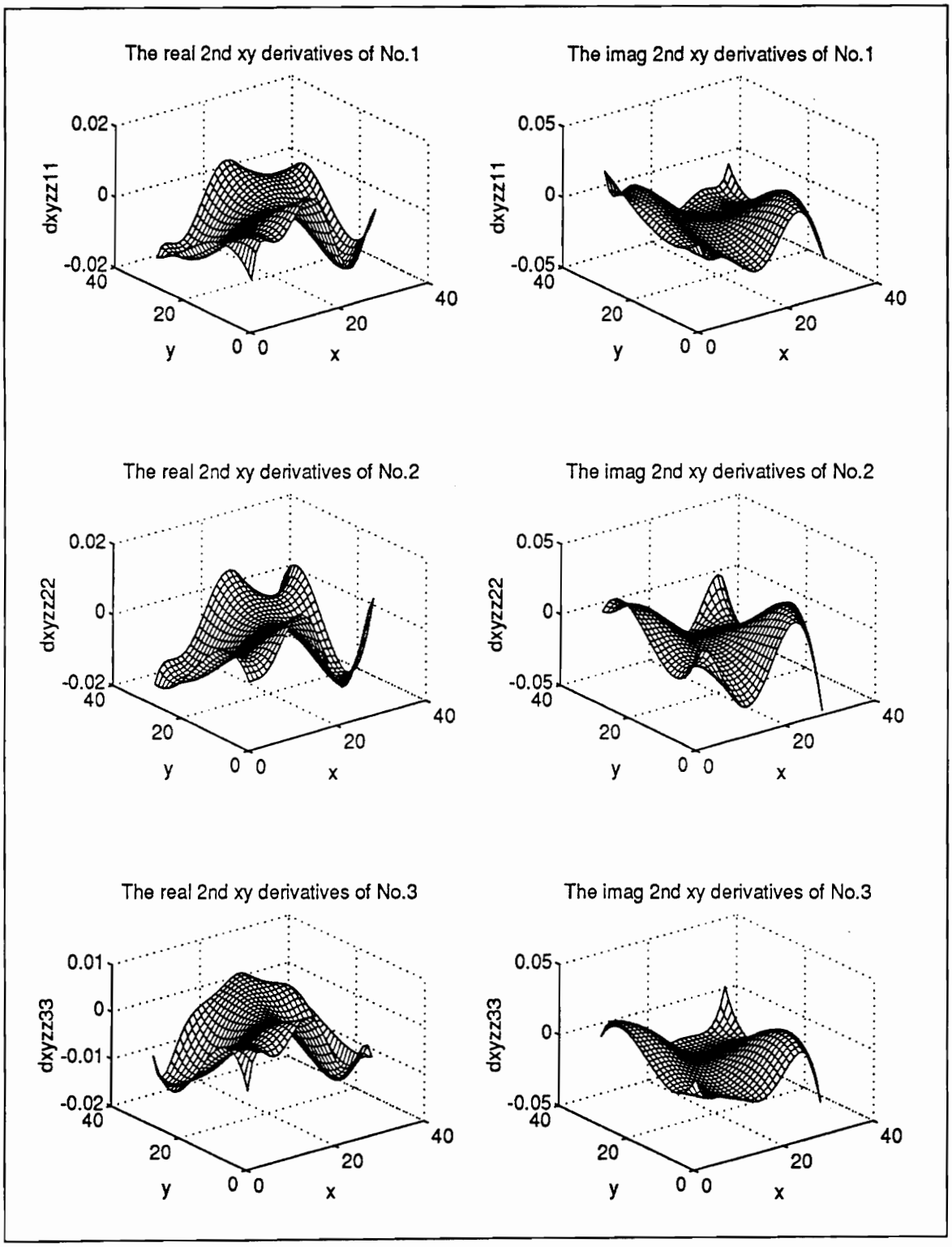

Figure 4.4 - Twist curvature models in x-y direction at 208 Hz

the samples for t' statistical tests on the two means of the SSCs. This topic will be presented in Section 4.4.2. Last, the CCs of the same plate's regression models (which are built on the velocity data that are taken from the repeated tests on the different days) are calculated. These CC values are used to evaluate the consistency of the test data when the experiments are repeatedly taken under the same test conditions for the same plate. If the models are high correlated to each other, we can conclude that the data acquired from the repeated experiments under the same test conditions are equivalent, and hence have the same characteristics. It means that the test data are comparable to each other, any one of the data sets can be equivalently used in further analysis. This content will be presented in Section 4.4.3.

4.4.1 Calculations of CCs between the different plates

The CCs on the final fitted models between the different plates are computed in the magnitudes of the velocities by running the first part of the Matlab code. Table 4.1 gives the computational results of the CCs on these models at frequencies: 208 Hz, 150 Hz and 378 Hz (on the full fitted models), respectively. The notation $\rho^2_{AcBd,f}$ in the table is defined as the same as in section 4.2. The following models are used to calculate CCs when f = 150 Hz, 208 Hz and 378 Hz respectively: (1) plate 1, test 1 to plate 2 test 1, denoted by $\rho^2_{1121,f}$; (2) plate 1 test 1 to plate 3 test 1, denoted by $\rho^2_{1131,f}$; (3) plate 2 test 1 to plate 3 test 1, denoted by $\rho^2_{2131,f}$. Figure 4.5 shows a graphic comparison of the results by a bar chart.

Table 4.1 The CCs between the different plates

Frequencies	$\rho^2_{1112,f}$	$\rho^2_{1121,f}$	$\rho^2_{1131,f}$	$\rho^2_{2131,f}$
f = 150 Hz	0.9974	0.9771	0.9531	0.9713
f = 208 Hz	0.9974	0.9769	0.9767	0.9850
f = 378 Hz	0.9977	0.9701	0.9698	0.9792

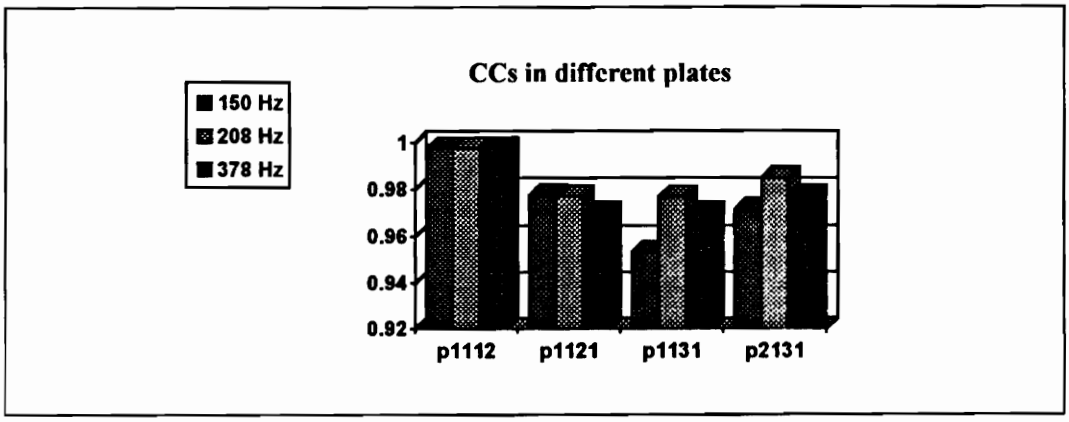

Figure 4.5 - A graphic comparison of the CCs between the different plates

4.4.2 Calculations of SCCs between the different plates

The second part of the program performs the calculations of the SCCs between the different plates on the curvature models and on the final best regression models respectively. However, the curvature models, which are given in the section 4.2, must be computed on the final best regression models before the SCCs calculations. In this section, SCCs on the final fitted models and on the curvature models at 208 Hz frequency are investigated in detail, the corresponding computational results are listed in Table 4.2 and 4.3. The values in Table 4.2 are the SCCs for the curvature models, the values in Table 4.3 are the SCCs for the final best regression models. Again, the notation $\rho^2_{AcBd,f}$ is defined as the same as in section 4.2 and all SCCs are computed in the magnitudes of the velocities.

Table 4.2 The SCCs between the different plates (On curvature models)

i,j	*1*	*2*	*3*	*4*	*5*	6	$\rho^2_{1112,208}(i,j)$
1	0.9998	0.9999	1.0000	1.0000	0.9999	0.9999	
2	1.0000	1.0000	0.9998	0.9999	1.0000	1.0000	(Plate No. 1's 1st test to the 2nd test)
3	1.0000	0.9999	1.0000	1.0000	0.9999	0.9999	
4	0.9999	1.0000	1.0000	0.9999	1.0000	1.0000	
5	1.0000	0.9998	0.9998	1.0000	0.9999	0.9999	
							$\rho^2_{1121,208}(i,j)$
1	0.9309	0.9656	0.9189	0.9507	0.9389	0.9389	(Plate No. 1 to Plate No. 2)
2	0.9963	0.9418	0.9963	0.9987	0.9326	0.9326	
3	0.9638	0.9561	0.9988	0.9971	0.9062	0.9062	
4	0.8724	0.9706	0.9981	0.9713	0.9211	0.9211	
5	0.9810	0.9723	0.9060	0.9044	0.7836	0.7836	
							$\rho^2_{1131,208}(i,j)$
1	0.9645	0.9335	0.6359	0.8808	0.9616	0.9616	(Plate No. 1 to Plate No. 3)
2	0.9897	0.7153	0.9748	0.9908	0.9508	0.9508	
3	0.9827	0.9614	0.9964	0.9976	0.9933	0.9933	
4	0.8349	0.9588	0.9874	0.9983	0.9766	0.9766	
5	0.9842	0.7705	0.3656	0.9432	0.8655	0.8655	
							$\rho^2_{2131,208}(i,j)$
1	0.9049	0.8385	0.3833	0.8897	0.9575	0.9575	(Plate No. 2 to Plate No. 3)
2	0.9875	0.8521	0.9740	0.9920	0.9588	0.9588	
3	0.9956	0.9968	0.9977	0.9899	0.8884	0.8884	
4	0.9644	0.9952	0.9946	0.9681	0.9311	0.9311	
5	0.9488	0.8287	0.6005	0.7948	0.8273	0.8273	

Table 4.3 The SCCs between the different plates (on the final best regression models)

i,j	*1*	*2*	*3*	*4*	*5*	*6*	$\rho^2_{1112,208}(i,j)$
1	1.0000	1.0000	1.0000	1.0000	0.9999	0.9999	(Plate No. 1's 1st test to the 2nd test)
2	0.9999	1.0000	1.0000	1.0000	1.0000	1.0000	
3	1.0000	1.0000	1.0000	1.0000	1.0000	1.0000	
4	1.0000	1.0000	1.0000	1.0000	1.0000	1.0000	
5	0.9999	1.0000	1.0000	1.0000	0.9999	0.9999	
							$\rho^2_{1121,208}(i,j)$
1	0.9881	0.9938	0.9915	0.9992	0.9637	0.9637	(Plate No. 1 to Plate No. 2)
2	0.9860	0.9422	0.7268	0.8376	0.9792	0.9792	
3	0.9928	0.9763	0.9969	0.9897	0.9962	0.9962	
4	0.9812	0.9960	0.9782	0.9784	0.9899	0.9899	
5	0.9983	0.9973	0.9967	0.9755	0.9822	0.9822	
							$\rho^2_{1131,208}(i,j)$
1	0.9908	0.9975	0.9952	0.9991	0.9702	0.9702	(Plate No. 1 to Plate No. 3)
2	0.9971	0.9863	0.9710	0.9810	0.9774	0.9774	
3	0.9900	0.9628	0.9918	0.9984	0.9990	0.9990	
4	0.9429	0.8954	0.9832	0.9930	0.9937	0.9937	
5	0.9975	0.9957	0.9966	0.9950	0.9922	0.9922	
							$\rho^2_{2131,208}(i,j)$
1	0.9830	0.9862	0.9816	0.9970	0.9665	0.9665	(Plate No. 2 to Plate No. 3)
2	0.9912	0.9514	0.8111	0.8408	0.9955	0.9955	
3	0.9932	0.9098	0.9862	0.9926	0.9946	0.9946	
4	0.9530	0.8777	0.9924	0.9942	0.9896	0.9896	
5	0.9983	0.9965	0.9987	0.9812	0.9905	0.9905	

4.4.3 Calculations of CCs for the same plate at the repeated tests

The CCs between the same plate's fitted regression models are calculated to analyze the consistency of the repeated test data. This is done by running the first part of code again. The difference of repeatedly running the same part of program in section A and C is to load different models. In this section, the fitted regression models from the repeated tests for the same plate are used in the calculations instead of ones from the different plates in section A. Table 4.4 lists the CCs on the fitted models of the same plates at frequencies f = 208 Hz and 378 Hz, respectively. The notation $\rho^2_{AcBd,f}$ is defined as the same as before. Here, taking plate 1 for example. The following models are used in calculating for plate 1: (1) plate 1 test 1 to plate 1 test 2, denoted by $\rho^2_{1112,f}$; (2) plate 1 test 1 to plate 1 test 3, denoted by $\rho^2_{1113,f}$; (3) plate 1 test 2 to plate 1 test 3, denoted by $\rho^2_{1213,f}$.

4.4.4 Calculations of SCCs for the same plate's repeated test models

The Calculations of SCCs for the same plate's repeated test models at 208 Hz and 378 Hz frequencies are used to investigate the data consistency of the same plate's repeated test. Table 4.5 lists the computational results of the SCCs.

4.4.5 The Matlab program

The Matlab source code consists of four parts, each part is programmed by several subroutines to finish one step computation in Sections 4.4.1, 4.4.2 and 4.4.3, receptively. Figure 4.6 gives a flow chart of the program. The first part performs computations of the CCs for section A and C, respectively. There are two subroutines to accomplish the

Table 4.4 The CCs in the same plates

Plate	f, Hz	$\rho^2_{1112,f}$	$\rho^2_{1113,f}$	$\rho^2_{1213,f}$
No. 1	208	0.9998	0.9997	0.9995
	378	0.9986	0.9988	0.9992
Plate	f, Hz	$\rho^2_{2122,f}$	$\rho^2_{2123,f}$	$\rho^2_{2223,f}$
No. 2	208	0.9998	0.9978	0.9965
	378	0.9997	0.9987	0.9982
Plate	f, Hz	$\rho^2_{3132,f}$	$\rho^2_{3133,f}$	$\rho^2_{3233,f}$
No. 3	208	0.9998	0.9996	0.9997
	378	0.9993	0.9987	0.9991

different functions. One subroutine is used to load or specify the models for CC calculations. The other subroutine is used to compute the CC values. The second part of the code computes the curvature models on the fitted regression models. There are two subroutines in this part. One is used to calculate the second partial derivatives with respect to x, the other is used to calculate the second partial derivatives with respect to y. The third part of code performs calculations of the SCCs on the curvature models obtained in part two and on the fitted regression models, respectively. There are also several subroutines to compute the two different kinds of the SCCs, respectively. And the last part performs t' statistical tests on the two means of the SCCs.

4.5 Approaches to diagnose the damaged plates and the location of the damage

To diagnose the damage in the plates, the first step is to distinguish the plate with and without the damage by analyzing the CCs between the different plate's fitted models. Then the location of the damage needs be further identified by analyzing the SCCs of the curvature models between the undamaged and damaged plates. The CCs in Table 4.1 give the numerical indications of the correlation relationships for the velocity field models

Table 4.5(a) - The SCCs of plate No.1's repeated models at 208 Hz

i,j	*1*	*2*	*3*	*4*	*5*	*6*	$\rho^2_{1112,208}(i,j)$
1	0.9992	1.0000	0.9995	1.0000	1.0000	0.9941	Test 1 to Test 2
2	0.9999	0.9999	0.9998	0.9994	0.9999	0.9999	
3	1.0000	0.9999	1.0000	0.9999	1.0000	1.0000	
4	0.9980	1.0000	1.0000	1.0000	1.0000	0.9998	
5	1.0000	0.9999	1.0000	0.9999	1.0000	0.9988	

i,j	*1*	*2*	*3*	*4*	*5*	*6*	$\rho^2_{1113,208}(i,j)$
1	0.9980	1.0000	0.9982	1.0000	1.0000	0.9959	Test 1 to Test 3
2	1.0000	1.0000	0.9998	0.9990	0.9996	1.0000	
3	1.0000	0.9996	1.0000	1.0000	1.0000	1.0000	
4	0.9985	0.9998	0.9998	1.0000	1.0000	1.0000	
5	0.9999	0.9998	1.0000	0.9990	1.0000	0.9998	

i,j	*1*	*2*	*3*	*4*	*5*	*6*	$\rho^2_{1213,208}(i,j)$
1	0.9949	0.9999	0.9963	1.0000	1.0000	0.9958	Test 2 to Test 3
2	0.9998	0.9999	0.9996	0.9996	0.9994	1.0000	
3	0.9999	0.9994	1.0000	1.0000	0.9999	0.9999	
4	0.9975	0.9999	0.9999	0.9999	0.9999	0.9997	
5	0.9999	0.9996	1.0000	0.9982	1.0000	0.9991	

Table 4.5(b) - The SCCs of plate No.2's repeated models at 208 Hz

i,j	*1*	*2*	*3*	*4*	*5*	*6*
1	0.9995	1.0000	0.9999	1.0000	0.9999	0.9964
2	1.0000	0.9999	1.0000	0.9999	0.9999	0.9999
3	1.0000	1.0000	1.0000	1.0000	1.0000	1.0000
4	1.0000	1.0000	1.0000	1.0000	1.0000	1.0000
5	1.0000	1.0000	1.0000	1.0000	1.0000	0.9999

$\rho^2_{2122,208}(i,j)$
Test 1 to Test 2

i,j	*1*	*2*	*3*	*4*	*5*	*6*
1	0.9938	0.9998	0.9985	0.9997	0.9988	0.9455
2	0.9999	0.9988	0.9997	0.9986	0.9992	0.9991
3	1.0000	0.9999	1.0000	1.0000	1.0000	1.0000
4	1.0000	1.0000	1.0000	1.0000	1.0000	1.0000
5	1.0000	1.0000	1.0000	1.0000	1.0000	0.9979

$\rho^2_{2123,208}(i,j)$
Test 1 to Test 3

i,j	*1*	*2*	*3*	*4*	*5*	*6*
1	0.9902	0.9996	0.9975	0.9996	0.9981	0.9168
2	0.9998	0.9981	0.9996	0.9979	0.9987	0.9986
3	1.0000	0.9998	1.0000	1.0000	1.0000	1.0000
4	1.0000	1.0000	1.0000	1.0000	1.0000	1.0000
5	1.0000	1.0000	1.0000	1.0000	1.0000	0.9969

$\rho^2_{2223,208}(i,j)$
Test 2 to Test 3

Table 4.5(c) - The SCCs of plate No.3's repeated models at 208 Hz

i,j	1	2	3	4	5	6	$\rho^2_{3132,208}(i,j)$
1	0.9999	1.0000	0.9996	1.0000	0.9999	0.9944	Test 1 to Test 2
2	1.0000	1.0000	1.0000	0.9999	0.9999	0.9999	
3	1.0000	1.0000	1.0000	1.0000	0.9999	1.0000	
4	0.9999	0.9994	1.0000	1.0000	1.0000	1.0000	
5	1.0000	0.9999	1.0000	0.9997	0.9999	0.9988	

i,j	1	2	3	4	5	6	$\rho^2_{3133,208}(i,j)$
1	0.9998	1.0000	0.9995	0.9999	1.0000	0.9989	Test 1 to Test 3
2	1.0000	1.0000	0.9999	0.9991	0.9987	0.9998	
3	1.0000	1.0000	1.0000	1.0000	0.9994	0.9999	
4	0.9994	0.9978	0.9997	1.0000	0.9997	0.9996	
5	1.0000	0.9999	1.0000	0.9990	0.9998	0.9991	

i,j	1	2	3	4	5	6	$\rho^2_{3233,208}(i,j)$
1	0.9999	1.0000	0.9998	1.0000	0.9999	0.9945	Test 2 to Test 3
2	1.0000	1.0000	0.9999	0.9990	0.9984	0.9998	
3	1.0000	1.0000	1.0000	0.9999	0.9997	0.9999	
4	0.9997	0.9994	0.9998	1.0000	0.9998	0.9997	
5	1.0000	1.0000	1.0000	0.9997	0.9999	0.9972	

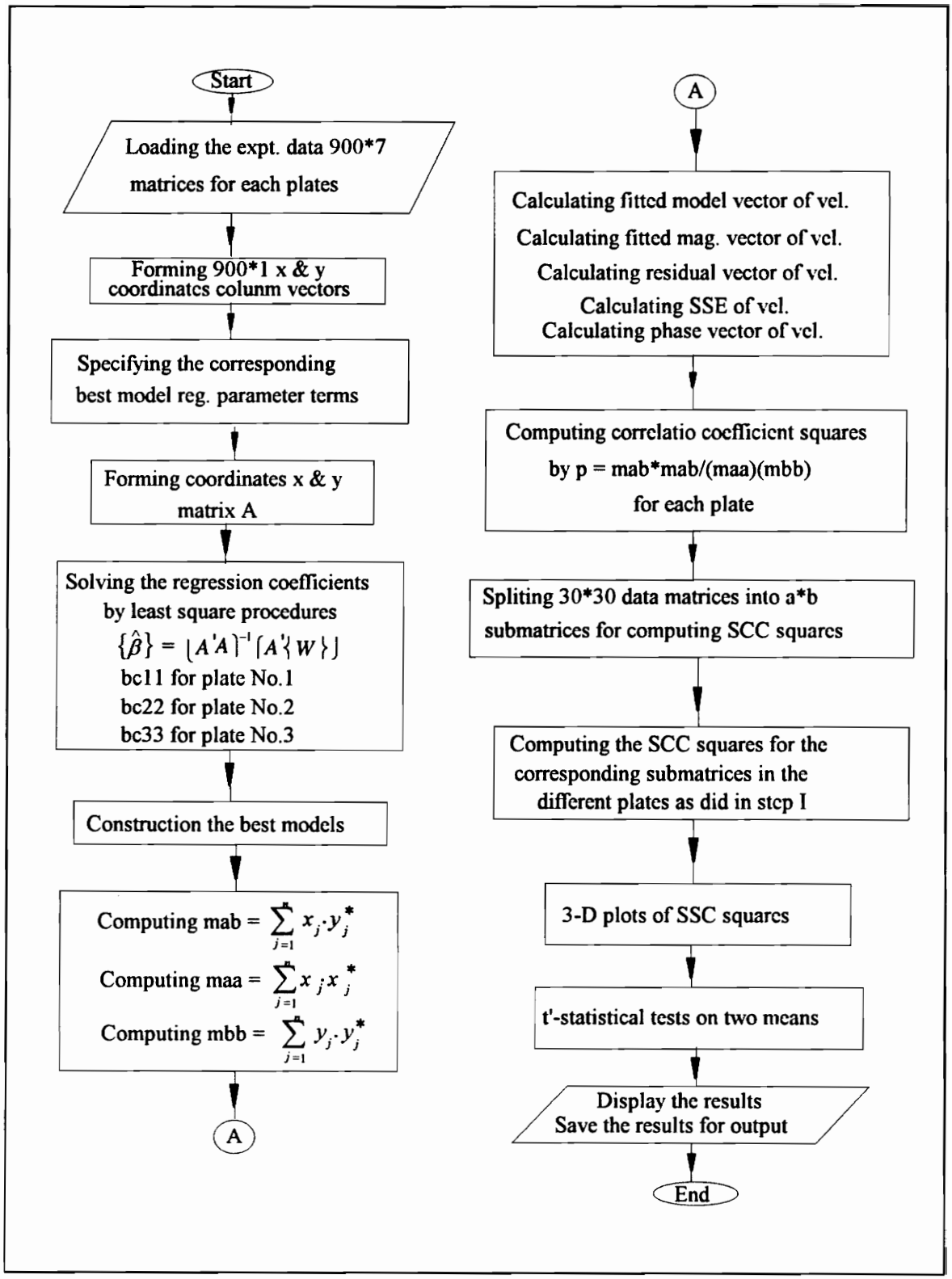

Figure 4.6 - A flow chart of the Matlab program of calculating CCs and SCCs

between the different plates, however, it is still difficult to say whether a CC value is significantly different from the others at this time, since it is not clear how far away the two compared CCs should be so that a significant difference can be determined. Therefore, we need answer that at least how much difference should appear in the two compared CC values before we can conclude that the CCs are significantly different to each other. This situation requires the setting of a criterion for the comparisons that determines how far away the compared CCs should be in order to conclude they are different. A t' statistical test on two means can be imposed as a criterion of the comparison on the means to accomplish this purpose. The significance of the criterion to compare the differences on the means of the SCCs is to identify the plates with damage. Eventually, it leads to the identification of the damage location by the analysis of the SCCs on the curvature models between the undamaged and damaged plates. The small values of the SCCs may indicate the locations where the damage appears.

4.5.1 A t' statistical test on the two means of the corresponding SCCs

Considering the SCCs (which are the CCs of the corresponding subareas in the plates), all SCCs of the each two-compared-plate make nine samples of the subarea's CCs. Based on the sample distribution, statistical parameters can be obtained to evaluate the central tendency of the data, e.g., sample means and sample standard deviation. When we want to know whether the two CCs are different, it is *reasonable* to use the mean of the SCCs as a parameter to indicate the correlation between each two-plate. Then a t'-statistic test on two means can be conducted to determine whether the two compared means are different.

Based on the thirty SCC samples of each two-plate under a specific uncertainty α or sample variations [17], the test procedures can be stated as follows: for the unknown population mean and variance (as long as the population is approximately bell-shape), a t'-test statistic on the difference of the two means, $\mu_{11} - \mu_{ij}$ can be conducted under the null hypothesis, H_0: $\mu_{11} - \mu_{ij} = 0$ against the alternative hypothesis, H_1: $\mu_{11} - \mu_{ij} \neq 0$. Where, i = 1, 2; j = 2, 3, respectively are the index numbers of the plates; μ_{11}, μ_{12}, μ_{13} and μ_{23} are the means of the SCCs between the corresponding plates. Then the T.S. is given by:

$$t'_{T.S.} = \frac{(\overline{\rho}^2{}_{AcBd,f} - \overline{\rho}^2{}_{AcBd,f}') - 0}{\frac{1}{\sqrt{n}}\sqrt{s^2_{\overline{\rho}^2} + s^2_{\overline{\rho}^2}}} \sim t_{\alpha/2,dof} \text{ under } H_0. \qquad (4\text{-}9)$$

Where, the d.o.f. is equal to $(n-1)$, $n = m1 \times n1$ as before, and the $\frac{1}{\sqrt{n}}\sqrt{s^2_{\overline{\rho}^2} + s^2_{\overline{\rho}^2}}$ is the standard error of the difference of the sample means $(\overline{\rho}^2{}_{AcBd,f} - \overline{\rho}^2{}_{AcBd,f}')$, where $s^2_{\overline{\rho}^2}$ and $s^2_{\overline{\rho}^2}$ are the sample variances of the SCC squares. It can be computed from the corresponding SCC's sample group by:

$$s^2 = \frac{1}{n-1}\sum_{k=1}^{n}(\rho^2_{k,AcBd,f} - \overline{\rho}^2{}_{AcBd,f})^2 \qquad (4\text{-}10)$$

The sample mean of the SCC squares from each thirty-sample or -subarea of the plates, denoted by, $\overline{\rho}^2{}_{AcBd,f}$, is calculated as follows:

$$\overline{\rho}^2{}_{AcBd,f} = \frac{1}{n}\sum_{k=1}^{n}\rho^2_{k,AcBd,f} \quad (i,j) \qquad (4\text{-}11)$$

According to the t' test, we will reject the null hypothesis H_0 in favor of the alternative hypothesis H_1 for $d.o.f = (n-1)$ and the specified α level, if $|t'_{T.S.}| \rangle t_{\alpha/2,n-1}$ or if the p-value = Prob.$\{|t| \rangle t'_{T.S.}\} <$ α, i.e., the two compared means are significantly different under d.o.f. = n-1 and the significant level α. Otherwise, the null hypothesis holds and the two compared means are equivalent under the α% uncertainty.

The forth part of the code performs the a t'-statistic test on the two means of the corresponding SCCs under the significant level α = 0.05. From a statistical table [17], $t_{\alpha/2,n-1} = t_{.025,29} = 2.045$. Table 4.6. gives the results of the T.S.s on the means of the SCCs between the different plates at 150 Hz, 208 Hz and 378 Hz frequencies, respectively. The two compared CCs are significantly different if the null hypothesis is rejected by the T.S. on the means of the SCCs. In this case, the damaged plates could be identified. The T.S.s on the means of the same plate repeated model's SCCs are conducted also and used to investigate the consistency of repeated data when the tests are repeated under the same test conditions. The results are given in Table 4.7 in Section 4.5.3.

Table 4.6 - Results of the T.S.s on the means of the SCCs for the different plates

For $\alpha = 0.05$ and $t_{\alpha/2,n-1} = t_{.025,29} = 2.045$, Reject H_0 in favor of H_1 if $\lvert t'_{T.S.}\rvert > t_{\alpha/2,n-1}$			
Null hypothesis H_0 Alternative hypothesis H_1	$\mu_{11} - \mu_{12} = 0$ $\mu_{11} - \mu_{12} \neq 0$	$\mu_{11} - \mu_{13} = 0$ $\mu_{11} - \mu_{13} \neq 0$	$\mu_{11} - \mu_{23} = 0$ $\mu_{11} - \mu_{23} \neq 0$
(f = 150 Hz) $t'_{T.S.}$ Conclusion	5.9240 Reject H_0	6.4153 Reject H_0	5.7345 Reject H_0
(f = 208 Hz) $t'_{T.S.}$ Conclusion	3.7999 Reject H_0	3.7807 Reject H_0	3.3405 Reject H_0
(f = 378 Hz) $t'_{T.S.}$ Conclusion	4.7791 Reject H_0	4.9711 Reject H_0	3.3931 Reject H_0

4.5.2 The criterion to identify the damaged plates

Once the differences on the means of SCCs are distinguished for the different plate's fitted velocity models, we say that the two compared CCs are significantly different if two means of the corresponding SCCs are significantly different. This implies that their

velocity fields are also statistically different with α% uncertainty. It should be pointed out that there must be a known undamaged plate as a standard objective while use this method. In our cases, the known undamaged plate's mean of the SCCs, μ_{11} (which come from the repeated test data of the undamaged plate) must be taken as the standards of the comparisons. Consequently, whenever the any other plate is compared with this known undamaged one, if the null hypothesis is rejected by the t' statistical test, the velocity field of the corresponding plate must be significantly different from the known undamaged plate. The plate with significant difference to the known undamaged one will be considered damage presented. Otherwise, if the null hypothesis holds, this plate will be considered as no difference in the velocity field as that of the undamaged plate. We conclude that the unknown plate must be undamaged too. In fact, no matter what kinds of test objects, it is possible that an initial or an original unflawed or undamaged states of the objects can always be obtained and taken as the standards of the comparisons. This is the fundamental point of the comparisons.

4.5.3 The criterion to investigate the consistency of the repeated test data

To investigate the consistency of the repeated test data, we should enable to determine whether the CCs of the same plate's velocity fitted models are significant difference, when the tests are repeated under the same test conditions and taken on the different days. Similarly, the criterion is established on the t' statistical tests on the two means of the corresponding SCCs. The null hypothesis is, H_0: $\mu_{i1,i2} - \mu_{i1,i3} = 0$, $\mu_{i1,i2} - \mu_{i2,i3} = 0$ and $\mu_{i1,i3} - \mu_{i2,i3} = 0$ against the alternative hypothesis, H_1: $\mu_{i1,i2} - \mu_{i1,i3} \neq 0$, $\mu_{i1,i2} - \mu_{i2,i3} = 0$ and $\mu_{i1,i3} - \mu_{i2,i3} = 0$, correspondingly, where, i = 1, 2 and 3 are the index numbers of the plates; the *2nd* index is the index number of the tests. For example, $\mu_{i1,i2}$ is the mean of the

SCCs between the i^{th} plate's 1*st* test and the 2*nd* test. If the p-value of the T.S. is no less than the specified α value, i.e., p-value = $\text{Prob.}\{|t| \rangle t'_{T.S.}\} \geq \alpha$, we conclude that the two means are equivalent. This indicates that there is no significant difference between the two compared velocity fields of the plates. Thus the repeated test data are consistency. Vice versa. Table 4.7 gives the T.S.s on the means of the compared SCCs between the same plate's repeated velocity models for each plate respectively at 208 Hz frequency. It should be noted that the investigation of the consistency of the same plate's repeated data are based on the initial GLP models. Since the CCs and SCCs based on the initial models already satisfy the investigations. The purpose is also to minimize the SAS running work as possible as necessary.

Table 4.7 - Results of the T.S.s on the means of the SCCs for the same plates at 208 Hz

For $\alpha = 0.05$ and $t_{\alpha/2,n-1} = t_{.025,29} = 2.045$, Reject H_0 in favor of H_1 if $\lvert t'_{T.S.} \rvert \rangle t_{\alpha/2,n-1}$			
Null hypothesis H_0 Alternative hypothesis H_1	$\mu_{11} - \mu_{12} = 0$ $\mu_{11} - \mu_{12} \neq 0$	$\mu_{11} - \mu_{13} = 0$ $\mu_{11} - \mu_{13} \neq 0$	$\mu_{11} - \mu_{23} = 0$ $\mu_{11} - \mu_{23} \neq 0$
Plate No. 1 Student $t'_{T.S.}$ Conclusion	0.1996 H_0 hold	1.0354 H_0 hold	0.9502 H_0 hold
Plate No. 2 Student $t'_{T.S.}$ Conclusion	1.2107 H_0 hold	1.2558 H_0 hold	0.3867 H_0 hold
Plate No. 3 Student $t'_{T.S.}$ Conclusion	0.3769 H_0 hold	0.6323 H_0 hold	0.4306 H_0 hold

Table 4.7 indicates that all the null hypotheses on the differences of the two compared means of the corresponding SCCs hold by the t' tests. Therefore, there are no differences between the compared means.

4.5.4 The criterion to identify the damage locations of the plates

The criterion to identify the damage locations of the plates is based on the comparisons of each corresponding SCC of the curvature models between the known undamaged plate and the damaged plates. The corresponding SCC values are given in Table 4.7. The small values of the SSCs should indicate the subareas or locations of the large strain differences in the plates. If the poor SCC are not due to the manufacture process or different geometry of the plates (because we suppose that all plates are subjected the same manufacture processes and have no geometry differences at the beginning), therefore, the differences between the compared subarea's must be theoretically due to the damage in the plate. But from Table 4.2, the small SCCs do not locate at or near the damage ranges. It can be observed that the locations of the small SCCs are not associated with the locations of the large difference in the curvature fields, i.e., the locations of damage. It is hard to identify the damage from the small SCCs. It means that the large different values in SCCs must be due to some reasons other than the damage effects. Recall the plots of the curvature models, Fig. 4.2 - 4.4, the boundary values of the curvatures of plates should be near zeros due to the free-free boundary supporting. Unfortunately, there are relative large values at the boundaries of the curvature models and obviously not equal zero. Therefore, the SCCs of the curvature models of the plates fail to identify the locations of damage.

The node line method [8] that Wolff and Richardrdson presented may have potential to identify the appearance of a large physical change in structures, such as a large change in stiffness they proposed. But in this research, the structure is not supposed to have a large physical change due to the cut of one layer laminated fiber of plates. Additionally, the node line method still faces the problem how to identify the location of the damage

according to the changes in node lines. Therefore, the node line method was not applied in this research.

CHAPTER V

CONCLUSIONS AND RECOMMENDATIONS

5.1 Conclusions

The goal of this research is to develop a systematic method for structure damage identification based on analyzing the dynamic test response data of the object. The first step of the investigation involves the study of dynamic properties of the material. A set of FRF tests under the 0-500 Hz burst random signal excitations were conducted to obtain a basic understanding of the dynamic properties of the plates while the excitation force magnitudes are changed at a small specified range. Comparing the same plate's FRFs at the three different force magnitudes, the shapes and the magnitudes of the FRFs are unchanged. Therefore, it can be concluded that the dynamic properties of the material are linearity within the investigated scope. The importance of the conclusion is to establish the linearity assumption in developing the later research methods, for instance, the least square regression method and the technique of the correlation coefficients depend on linearity. Additionally, the plots of the FRFs provide a guideline of selecting the possible excitation frequencies for the investigation.

The second step of the research involves the investigation of the initial possible regression models for the velocity fields. On the basis of the specified computational precision, the cutoff orders in polynomials are found for the initial regression models. It can be noticed that the possible cutoff orders in x and y polynomials of the initial regression models are increasing with the excitation frequencies of the velocity fields. This can be explained that

the velocity fields of the higher frequencies are more complicated than that of the lower frequencies.

On the basis of the study in the linear regression polynomial surface fitting on the velocity fields of the composite plates, the "good" fitted models are first developed by stepwise statistical analysis and then on the all-possible-regression procedure. By finding the reasonable combinations of the regression variables and getting rid of some insignificant regression variables from the initial full models, the final best fitted regression models out of the initial full models are found to satisfy the specified statistical criteria. The most significant work in this investigation is to find the best fitted regression models out of the initial full models while the numbers of the regression variables are dramatically reduced. This results the simplifications of the analytical models. Hence, the work of analyzing (the time of analyzing and the cost of running a computer) is also reduced.

The investigation on the consistency of the repeated test data for the same plate at different test days is conducted through the study of the CCs and SCCs on the initial fitted regression models. The null hypotheses on the two means of SCCs that come from the repeated models hold by the t' statistical tests. Therefore, it can be concluded that the repeated data can be well controlled and the consistency can be maintained among the data acquired at different time under the same test conditions.

The investigation of CCs on the final fitted models between the known undamaged plate and other plates indicates that the damaged plates can be well identified. All t' statistical tests reject the null hypotheses on the two means of SCCs that come from different plates. Finally, the curvature models are developed to display the local effects of change in

structures that due to the structure change in the their dynamic properties. On the basis of the computation of the second derivatives in both two dimensions of plates on the final best regression models, the curvature models are established. In order to identify the locations of the damage, the analysis of the CCs and SCCs on the curvature models are also performed to numerically demonstrate how the velocity fields are correlated at the corresponding locations. The results show that the small damage dynamic effect is still not clearly illustrated by this way. One of the possible reasons is that the effect of the changes in strains may be insensitive to the dynamic properties varying by the small damaged in structures. The curvature models on the velocity fields may not provide sufficient information in diagnosticating the locations of the small damage in structures. Another possible reason is that the curvature models are much sensitive to the boundary distortions of the higher order polynomial fitting. An example of illustrating this point will be provided later in the section 5.2. The second derivatives on the plate boundary may hind the real variations due to the changes in strains of the plates.

5.2 Recommendations and analysis of the shortcoming of the method

A systematic method based on the analysis of the velocity fields of the composite plates was developed in this thesis to accomplish the purposes of the research in an attempt of identifying structure damage. However, there are several aspects associated with further improvement of the method so that the method can be practically used in identifying the damage or difference in general structures. The following recommendations are presented for further work to fulfill this further purposes.

1. It is significant to verify the validation of the curvature method in damage identifications on the different damage strength and types, e.g., large damage intensity and multiple crack damage locations.

2. The curvature method in damage identifications is still waiting to be applied to different materials as well as structures to verify the validations of the method.

3. There is a shortcoming of the regression method that the fitted distortions are greatly enlarged at plate's corners associated with the use of the high order polynomial regression fit. Due to the sensitivity to the noise of the curvature models, the small changes in the dynamic properties of structures may be submerged or hidden when the fitted curvature models are expected to disclose any small damage information. Any small fitted distortion will be dramatically enlarged by curvature models seriously. This is a major limitation of the method. And hence, the method is restrained used in the data sets that have series boundary noise. To reduce the boundary fitted distortions in higher order polynomial fitting, other fitting function or numerical curve fitting techniques can be tried instead of the higher order polynomial regression, such as, the Taylor series or cubic Spline fitting method to improve the boundary distortions of the higher order polynomial fitted.

4. The investigation the relationship between the frequency and the cutoff orders could be conducted in future to provide a general formula to determine the cutoff orders when the excitation frequency is specified. It is also required to verify the validations of the method for higher frequencies and more excitation frequency points.

5. It should be noticed in this research that only one undamaged plate was employed for the investigation of the damage identification. To simulate the situation of multiple undamaged plates in practice, the repeated tests were used to obtain a variation bound that represented an alternative way of investigating the multiple undamaged plates. In practice, there may be a lot of undamaged plates. One of the critical points to identify damaged plates is still to establish a variation bound that is statistically different from that of the damaged plates by conducting the tests on all these undamaged plates. A $(1-\alpha)\%$ confident interval on the mean of the multiple undamaged plates could be constructed to fulfill this purpose.

REFERENCE

[1] Vary, A., 1973, *Nondestructive Evaluation Technique Guide*, U. S. National Aeronautics and Space Administration, NASA SP-3079, Scientific and Technical Information Office, Washington, D.C.

[2] Bray, Don E. and Don Mcbride, 1992, *Nondestructive Testing Techniques*, New Dimensions in Engineering, New York.

[3] Raju, P. K., 1989, *Nondestructive Evaluation of Material and Structures Using Vibration and Acoustic Techniques*, NDE-Vol.6, The American Society of Mechanical Engineers, New York.

[4] Ewins, D.J., 1984, *Model Testing: Theory and Practice*, John Wiley & Sons, New York.

[5] West, W. M., 1986, "Illustration of the Use of MAC to Detect Structure Changes in an Orbiter Test Specimen," *Proceedings of the 4th International Modal Analysis Conference*, Society for Experimental Mechanics, Inc., pp.1-6.

[6] Pandey, A.K., M. Bisvas, and M. M. Samman, 1991, "Damage Detection from Changes in Curvature Mode Shapes," *Journal of Sound and Vibration*, 145(2), pp.321-332.

[7] Rizzi, S. A., S. A. Clevenson, and E. F. Danials, 1992, "Acoustic Fatigue Characterization of Carbon/Carbon Panels," *Proceedings of SEM VII International Congress*, Las Vegas, Nevada, pp. 1348-1355.

[8] Wolff, Tom and Mark Richardson, 1989, "Fault Detection in Structures from Changes in Their Model Parameters," Proceedings of the 7th International Modal Analysis Conference, Society for Experimental Mechanics, Inc., pp. 84-94.

[9] Tenek, L. H., E. G. Henneke II, and M. D. Gunzburger, 1991, "Vibration of Delaminated Anisotropic Composite Plates," *Proceedings of the 9th International Modal Analysis Conference*, Society for Experimental Mechanics, Inc., Florence, Italy, pp. 982-987.

[10] West, W. M. Jr., 1982, "Single Point Random Model Test Technology Application to Failure Detection," *The Shock and Vibration bulletin*, pp.25-31.

[11] Al-Ansary, Mohammad, and Azayem, Kamal M., 1986, "A Modal Model for Fatigue Creek," *Proceedings of the 4th International Modal Analysis Conference*, Society for Experimental Mechanics, Inc., Los Angeles, pp. 202-208.

[12] Hoskin, B.C. and A. A. Baker, 1984, *Composite Materials for Aircraft Structure*, American Institute of Aeronautics and Astronautics, Inc., New York.

[13] Bendat, J. S. and A. G. Piersol, 1986, *Random Data Analysis and Measurement Procedures*, Second Edition, John Wiley & Sons, New York.

[14] Neter, John, William Wasserman, and Michael H. Kutner, 1989, *Applied Linear Regression Models*, Second Edition, Irwin, Homewood, IL.

[15] Draper, N.R. and H. Smith, *Applied Regression Analysis*, Second Edition, John Wiley & Sons, New York.

[16] Chatfield, C., 1978, *The Analysis of Time Series: Theory and Practice*, Chapman and Hall, London.

[17] Ott, Lyman, 1988, *An Introduction to Statistical Methods and Data Analysis*, Third Edition, PWS-KENT Publishing Company, Boston.

[18] Walpole, Ronald, E. and Raymond H. Myers, 1972, *Probability and Statistics for Engineers and Scientists*, Macmillan Publishing Co. Inc., New York.

[19] Kleibbaum, David G., and Lawernce L. Kupper, 1978, *Applied Regression Analysis and Other Multivariable Methods*, Duxbury Press, North Scituate, Massachusetts.

[20] Griffith, Daniel A., 1987, *Spatial Autocorrelation: A Primer*, Resource Publications in Geography, Pennsylvania.

[21] Cook, Robert D., David S. Malkus, and Michael E. Plesha, 1989, *Concepts and Applications of Finite Element Analysis*, Third Edition, John Wiley and Sons, New York.

[22] Timoshenko, S., 1940, *Theory of Plates and Shells*, Mcgraw-Hill Book Company, Inc., New York and London.

APPENDIX I

SAS Program Listing

```
OPTIONS LS=80;
 DATA ZIM;
 TITLE' ANALYSIS OF THE VELOCITY FIELD DATA OF THE PLATES ';
 INPUT ZIM X Y;
/* WHERE ZIM IS A 900*1 VELOCITY FIELD DATA VECTOR, X AND Y IS THE 900*1
    COORDINATES VECTORS OF THE PLATES */
;
/* DEFINITIONS OF THE REGRESSION VARIABLES */
  X2=X*X; Y2=Y*Y; XY=X*Y; X2Y=X2*Y; XY2=X*Y2; X2Y2=X2*Y2; X3=X2*X; Y3=Y2*Y;
  XY3=X*Y3; X2Y3=X2*Y3; X3Y3=X3*Y3; X3Y1=X3*Y; X3Y2=X3*Y2; X4=X3*X; Y4=Y3*Y;
  X3Y4=X3*Y4; XY4=X*Y4; X4Y=X4*Y; X2Y4=X2*Y4; X4Y2=X4*Y2; X4Y4=X4*Y4;
  X4Y3=X4*Y3; X5=X4*X; Y5=Y4*Y; X5Y4=X5*Y4; X5Y3=X5*Y3; X5Y2=X5*Y2; X5Y=X5*Y;
  X6=X5*X; X6Y=X6*Y; X6Y2=X6*Y2; Y5=Y4*Y; XY5=X*Y5; X2Y5=X2*Y5; X3Y5=X3*Y5;
  X4Y5=X4Y5; X5Y5=X5*Y5; X6Y3=X6*Y3; X6Y4=X6*Y4; X6Y5=X6*Y5; X7=X6*X; X7Y=X7*Y;
  X7Y2=X7*Y2; X7Y3=X7*Y3; X7Y4=X7*Y4; X7Y5=X7*Y5;
 ;
  CARDS;
  /* LOADING THE 900*3 DATA MATRIX */
;
 PROC STEPWISE;
 MODEL REAL = X Y X2 Y2 XY X2Y XY2 X2Y2 X3 Y3 XY3 X2Y3 X3Y3 X3Y1 X4 Y4
 XY4 X4Y X3Y2 X2Y4 X4Y2 X4Y3 X4Y4 X3Y4 X5 X5Y4 X5Y3 X5Y2 X5Y X6 X6Y
 X6Y2 X6Y3 X6Y4 X7 X7Y X7Y2 X7Y3 X7Y4 / STEPWISE;
 /* PERFORMING STEPWISE STATISTICS TO FIND THE BEST STEPWISE MODEL */
;
 PROC RSQUARE CP;
 MODEL REAL= X Y X2 Y2 XY X2Y XY2 X3 Y3 XY3 X2Y3 X3Y3 X3Y1 X4 Y4
 XY4 X4Y X2Y4 X4Y2 X4Y3 X4Y4 X3Y4 X5 X5Y4 X5Y3 X5Y2 X5Y X6 Y6 X6Y
 X6Y2 X6Y3 X6Y4 X6Y5 X7 X7Y X7Y2 X7Y3 X7Y4 X7Y5 / START=15;
 /* PERFORMING THE-ALL-POSSIBLE-REGRESSION */
 ;
 PROC REG;
 MODEL REAL= X Y X2 Y2 XY X2Y XY2 X3 Y3 XY3 X3Y1 X3Y3 Y4
 XY4 X4Y2 X3Y4 X5 X5Y3 X5Y2 X6 X6Y X6Y2 X6Y3 X7 X7Y X7Y2 X7Y3 / P;
 /* PERFORMING PRESS STATISTICS */
 ;
 OUTPUT OUT=ONE P=YHAT R=RESIDUAL;
 PROC PLOT DATA=ONE; PLOT RESIDUAL*YHAT;
 /* PLOTTING THE RESIDUAL AGAINST THE PREDICTED VALUES */
 TITLE THE STEPWISE FIT1288I.SAS MODEL;
 PROC UNIVARIATE NORMAL PLOT; VAR RESIDUAL;
  /* PLOTTING THE HISTOGRAM FOR ASSUMPTION CHECK */
```

VITA

Yu Liu was born on September 22, 1962 in Bejing, China, and was raised in Beijing, Chendo, Wuhan and Guangxi in China. She attended Nanjing Forestry University (NUF) and graduated with her Bachelor of Science in Mechanical Engineering in July 1983. After spending several years working in the university and industry in the eastern part of China, she began graduate studies and focused on the mechanical measurements and the investigation of fire protection and extinguishers at NUF. She obtained the first Masters of Science in Mechanical Engineering in September 1990. She moved to Blacksburg, Virginia to join her husband in January 1991. She started her second Masters of Science and focused on the area of signal processing and modal analysis in Mechanical Engineering at the Virginia Polytechnic Institute & State University in January 1992. She completed her second Masters of Science degree in Mechanical Engineering in December 1993.

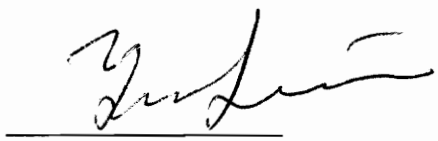

Yu Liu